Title
TURBULENCE IN THE POSITIVE COLUMN OF A GLOW DISCHARGE.

Author
Halseth, Martin W.

Publication Date
1969-02-01

UCRL-18678

eg. 2

TURBULENCE IN THE POSITIVE COLUMN OF A GLOW DISCHARGE

Martin W. Halseth
(Ph. D. Thesis)

February 1969

LAWRENCE RADIATION LABORATORY
UNIVERSITY of CALIFORNIA BERKELEY

UCRL-18678

eg. 2

DISCLAIMER

UCRL-18678

UNIVERSITY OF CALIFORNIA

Lawrence Radiation Laboratory
Berkeley, California

AEC Contract No. W-7405-eng-48

TURBULENCE IN THE POSITIVE COLUMN OF A GLOW DISCHARGE

Martin W. Halseth
(Ph. D. Thesis)

February 1969

TURBULENCE IN THE POSITIVE COLUMN OF A GLOW DISCHARGE

Contents

TURBULENCE IN THE POSITIVE COLUMN OF A GLOW DISCHARGE

Martin W. Halseth

Lawrence Radiation Laboratory
University of California
Berkeley, California

January 1969

ABSTRACT

The helical instability, which first appears in the positive column of a glow discharge at a critical magnetic field, B_c, is found to be replaced by random oscillations when the magnetic field is greater than 15 times the critical field. Measurement of the correlation of the ion density at two points along a tube diameter shows that the oscillations are out of phase with each other by more than 90 deg when the points are on opposite sides of the tube and the field is less that 15 times B_c, indicating that a helical oscillation is present. When B/B_c is greater than 15, the correlation decays exponentially with radial separation of the two points and remains positive, or nearly so, as in a turbulent plasma. The radial exponential decay length, which corresponds to the turbulent mixing length, and the radial density profile show good agreement with calculations made from a theory for turbulence in the positive column, proposed by Kadomtsev.

Measurements were made in He for various pressures up to 400 mTorr and magnetic fields up to 12 kilogauss. Mixing lengths were measured and found to be about 30% of the radius in the turbulent plasma at the highest magnetic fields. Frequency spectra were continuous, in agreement with the requirements for a strongly turbulent

plasma, and the electric field was essentially independent of magnetic field, in agreement with the theory of Kadomtsev for a strongly turbulent plasma. Turbulent radial particle transport fluxes are independent of the value of the magnetic field, and, because of the close agreement between measured and calculated radial mixing lengths and radial density profiles, agree well with empirical values of particle production rates. At lower magnetic fields, the properties of the plasma agree with those calculated from the semi-empirical theory of Sheffield based on the theory of Holter and Johnson for a large-amplitude helix in a positive column

In the positive column for magnetic fields below 15 B_c higher modes of the helical instability were temporarily produced by use of a time-dependent electric field The frequency and electric field associated with these waves were measured By use of the theory of Hölter and Johnson and the measured electric fields, calculations of the frequencies for the higher modes were made which compared favorably with the experimental values.

I. INTRODUCTION

In recent years the study of particle losses in the positive column of a glow discharge has been expanded to include anomalously large diffusion rates in high magnetic fields. Because of their similarity in nature to losses in possible thermonuclear plasmas, such particle-transport processes have major significant in the field of plasma research. The work described herein is intended to examine the change in the nature of the positive column which produces these high transport rates as the magnetic field is raised to a high value.

In the absence of a magnetic field, diffusion in the steady-state positive column is ambipolar.[1] The number of charged particles produced in the plasma depends on the value of the electric field. A particle balance relating production and loss shows that any increase in diffusion will automatically raise the electric field, provided that the current is held constant. The axial electric field dependence on distance from the cathode[2] is shown in Fig. 1. The region of steadily increasing potential is the positive column. It is possible, using a hot cathode filament, to considerably shorten the distance between the cathode and the positive column, thus yielding a longer positive column region for a given tube length.

At pressures above 300 mTorr in a positive column, with helium as the gas, striations begin to appear. These large, axially incoherent perturbations in the density of the plasma are associated with the stepwise ionization[3] resulting from the presence of metastables[4] in the discharge. In the presence of a magnetic field, these striations are weaker but do not always disappear Shaping of the electric

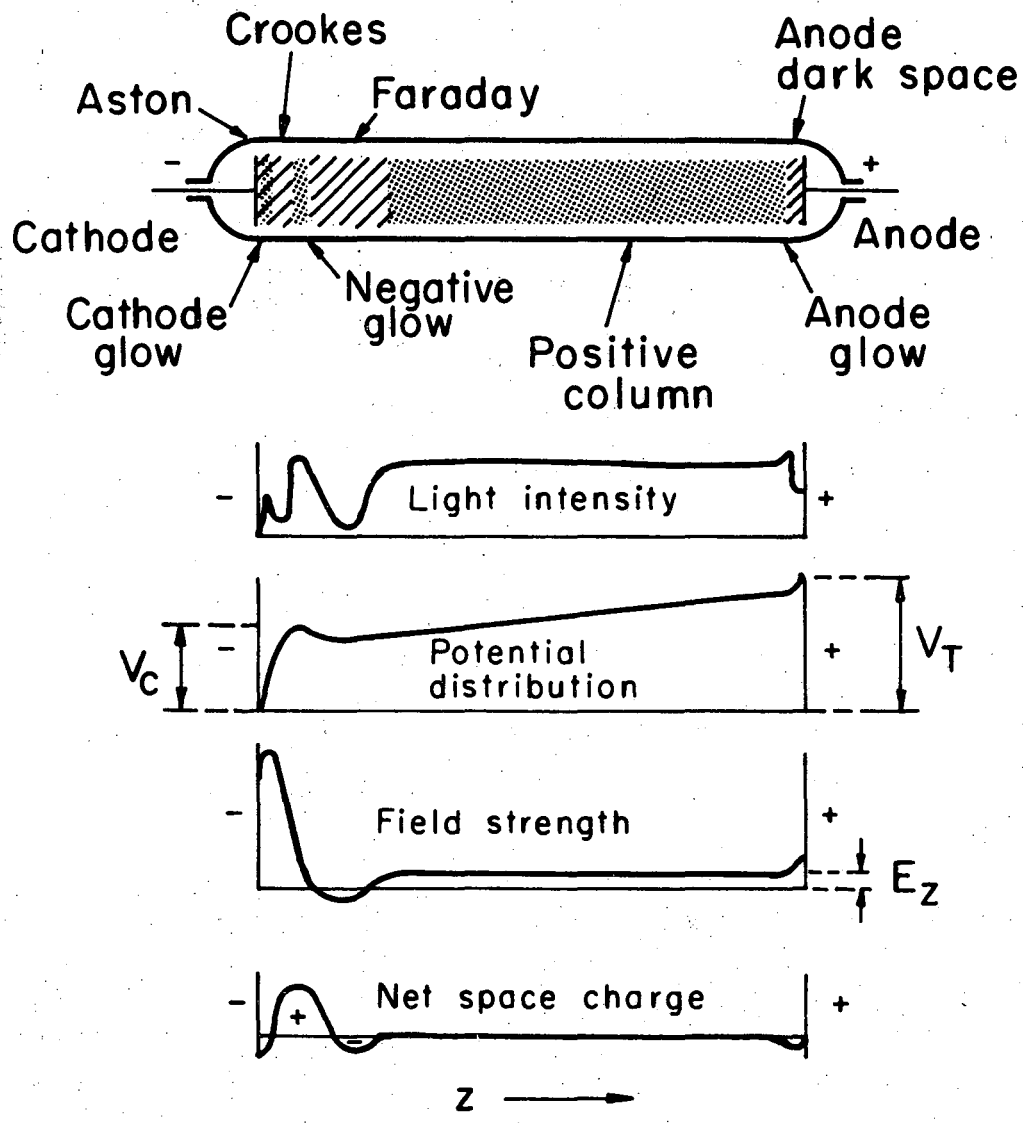

Fig. 1. Classification of the glow discharge regions, and axial distribution of some important parameters.

field at the cathode and anode has successfully prevented the appearance of these perturbations, however, when no magnetic field was applied, as described in Ref. 5.

In a typical helium positive column, densities of electrons and ions are 10^9 to 10^{11} particles per cm^3. The system is essentially neutral. The electrons are at a temperature of a few volts and the ions are near room temperature. The Debye length and electron-neutral collision length are on the order of a millimeter for the pressures used. Above a few kilogauss both the ion and electron orbits are less than a millimeter in diameter.

The positive column remains stable in the presence of a small magnetic field.[6] The magnetic field reduces the particle losses to the wall, causing the electric field to decrease in the positive column. Above a critical magnetic field, denoted by B_c, however, Lehnert and Hoh[7] observed an increase in the electric field, indicating enhanced particle loss to the walls.

It was demonstrated by Allen et al.[8] and Paulikas and Pyle[9] that this anomalous rise in the electric field was accompanied by a density perturbation of a helical nature. Using a streak camera, they were able to take photographs of the helix as it traveled along the tube. The presence of this helix and the increase in the electric field were observed with several gases with different pressures and tube radii.

A current-convective instability of a helical nature at the observed critical field was predicted theoretically by Kadomtsev and

Nedospasov,[10] using a perturbation analysis of the positive column. The result of the instability is a large convective loss of particles, which requires an increase in the axial electric field to maintain the same current. The perturbation grows rapidly until a balance is achieved between the particles lost through diffusion and convection and the particles produced by ionizing events. Hoh[11] shows that the number of particles fed into the helical instability by the perturbation azimuthal electric field is balanced by the flux of particles diffusing away when the helix has ceased to grow. Although this particular instability requires an axial current, an azimuthal drift instability triggered by a magnetic field in a long discharge tube with no applied axial current has been observed experimentally.[12] Also, though predicted in the linear theory, higher modes than the fundamental are seldom observed in the positive column unless the electric and magnetic fields are misaligned.[13]

The systematic oscillations observed in the positive column near the critical field are replaced by a broad spectrum of fluctuations at very high magnetic fields.[14] At magnetic fields below about 8 B_c Sheffield[15] observes a single broadened spectral line. In the region above B_c Holter and Johnson[16] predict a single fundamental helical density perturbation altered by its interaction with the potential perturbation. The resulting quais-linear equations were used to predict the helical frequency and wave length, and the radial plasma density profile and axial electric field for magnetic fields less than 5 B_c. Experiments such as those by Sheffield indicate that

above this region of magnetic field the positive column may be turbulent. However, he did not get far enough into this region to be sure.

In this work we use the Kadomtsev[17] definition of turbulence, and his use of the concepts of weak and strong turbulence, so it would be appropriate to quote here his definitions for the two classes of turbulence and for quasi-linear turbulence, a particularly weak form of turbulence. "At present we understand by turbulence the motion of a plasma in which a large number of collective degrees of freedom are excited. ··· The motion of the plasma in the weakly turbulent state, constituting a system of weakly correlated waves, shows greater similarity to the motion of the wavy surface of the sea or the crystal lattice than to the turbulent motion of an ordinary fluid. ··· For the case of very small amplitude, when the interaction between the oscillations can be neglected, one can use the so-called quasi-linear approximation in which only the reaction of the oscillations on the average velocity distribution function of the particles is considered." In this paper, when reference is made to the turbulent state, strong turbulence will be the condition implied unless otherwise stated.

Similar ranges of linear and nonlinear plasma instabilities in arcs have been observed by Bohm, Burhop, Massey, and Williams.[18] Granatstein, Buchsbaum, and Bugnolo[19] have studied fluctuations in a plasma which are caused by the turbulent flow of the weakly ionized host gas. In general, however, experiments in turbulent systems are rare. Moreover, often the data are ambiguous and provide little proof that the system was turbulent, because only such macroscopic quantities

as the particle loss rate were measured. The one-over-B law proposed by Bohm et al. for anomalous diffusion in their early experimental study of arcs has not fitted succeeding experiments.

Theoretical analysis of turbulent systems, particularly weak turbulence in which the various oscillation modes are only loosely coupled, has yielded more information about turbulence than experimental studies. Much of the information is taken from analogy with work in fluid hydrodynamics. The type of nonlinear equation studied by Kolmogorov,[20] Batchelor,[21] and Kraichnan[22] is quite similar to the equations of plasma dynamics.

Plasmas often are disturbed by two completely different instabilities which individually possess discrete spectra that are orders of magnitude apart in frequency and which cannot be predicted by hydrodynamic considerations. Interactions of these perturbations can result in a continuous spectrum of oscillations. Many examples of such wave-wave interactions are studied by Kadomtsev[23] and Sagdeev and Galeev.[24] It is also possible in plasmas to have a wave-number spectrum dominated by small wave numbers, unlike the Kolmogorov spectrum of turbulent hydrodynamics.

Theoretical work on the nonlinear region of the positive column has been of two types. Works by Hoh[25] and Holter and Johnson[16] have covered the quasi-linear region. In this region, the perturbations in the potential and density can still be written as single harmonic quantities, but their product terms cannot be ignored in the calculations. Hoh has also analyzed the turbulent region in Ref. 25 by

extending the quasi-linear analysis to the very-high-field region.

Kadomtsev[26] has used an analogy with hydrodynamics to derive a radial density distribution and decay length in a fully turbulent positive column. No single helix is assumed to dominate the discharge, as in quasi-linear theory.

In this report the nature of the positive column in the presence of a large axial magnetic field is explored experimentally. The axial electric field, frequency spectrum, and radial density profile are observed as a function of magnetic field, to determine at what values of field and pressure the quasi-linear theory breaks down and the positive column must be considered in a turbulent state.

The radial density correlation is of particular importance when determining the state of fluctuations in the positive column, and has been relied upon extensively here to determine the presence of turbulence. This quantity represents the degree of correlation of the density fluctuations measured at two points along a column diameter. With the two points on the opposite sides of the center of the column, if the correlation is large and negative, representing a difference in signal phases greater than 90 deg, then the system is not strongly turbulent and the quasi-linear theory is still applicable. When this correlation is positive, and one can show that no higher helical mode than the first is a dominant oscillation in the plasma, the system is turbulent and the correlation data can be compared with the predictions of Kadomtsev about turbulence.

Data are also presented describing the manner in which the plasma goes from the steady state to the unstable, quasi-linear state when

the magnetic field is above the critical field. The steady state is artificially produced with the aid of an alternating axial current. Changes in the electric field, the oscillation frequency, and the relative phase of the oscillations at several points in the plasma during the transition from a steady state to a direct-current discharge are used to demonstrate the brief presence of the higher modes which quasilinear theory and measurements in a direct current discharge show do not exist in the final state.

A. List of Symbols

a	Tube radius
B	Magnetic field
B_c	Critical magnetic field
$D_{\mp}$	Diffusion coefficients of electrons or ions
D_a	Ambipolar diffusion coefficient
e	Charge of an electron
E_z, E	Axial electric field
J_0, J_1	Bessel function of zeroth (first) order
k	Wave number
ℓ	Radial mixing length
$\ell_{\parallel}$	Axial mixing length
m	Azimuthal mode number
$m_{\mp}$	Electron or ion masses
$n_{\mp}$, n	Particle densities of electrons or ions
n', $\tilde{n}$	Fluctuating component of the density
p	Pressure

q	Particle flux
R_{AB}	Correlation coefficient
T_+	Electron or ion temperature
u_+	Ion thermal velocity
$\mathbf{v}'$	Fluctuating component of the velocity
$v_\mp$	Electron or ion drift velocities
V	Electric potential
V_i	Ionization potential
y_0	Turbulent radial density profile as predicted by theory
Z	Ionization rate per second per electron
β_0	First zero of the J_0 Bessel function
γ	Growth rate
κ	Boltzmann constant
λ	Wavelength
$\lambda_\mp$	Mean free path of electrons or ions
$\mu_\mp$	Electron or ion mobilities
$\tau_\mp$	Mean time between collisions of electrons or ions with neutral particles
ϕ	Calculated quantity representative of the convective particle losses
ω	Angular frequency
$\Omega_\mp$	Electron or ion cyclotron frequencies

II. THEORY

A. Classical Theory

The physical characteristics of the stable, classical positive column in the absence of a magnetic field are determined by the particle and energy balances which occur in the system. Since the percentage of ionized particles is low in this quasi-neutral plasma, only single-charged-particle collisions with neutrals are important in the temperature range under consideration. The major particle-loss mechanism in a stable column, ignoring striations, is diffusion along and across the tube. If the cylinder is sufficiently long, radial ambipolar diffusion is dominant. The particle-balance equation is

$$\nabla^2 n(r) + \frac{Z}{D_a} n(r) = 0, \tag{II-1}$$

where Z is the number of ion pairs produced per second per electron and the ambipolar diffusion coefficient is

$$D_a = \frac{D_+\mu_- + D_-\mu_+}{\mu_+ + \mu_-} \approx \frac{D_+T_-}{T_+} \tag{II-2}$$

$$= \frac{\mu_+T_-}{e} \propto \frac{T_-}{p}$$

for a noble gas. Since n(0) is bounded, the solution to (II-1) is

$$n(r) = n(0)J_0(\alpha r/a), \tag{II-3}$$

with $\alpha = a(Z/D_a)^{1/2}$ and J_0 the zero-order Bessel function of the

first kind. When the ratio of the ion density at the wall to that on the axis is small (Schottky theory),[27] so that n(a) may be set equal to zero, then

$$\alpha = \beta_0 \equiv 2.405 \qquad \text{(II-4a)}$$

for an average ion mean free path $\lambda_+ \ll a$. If $\lambda_+ \approx a$, then the modified Schottky theory applies,

$$\frac{4D_a}{au_+} = \frac{1}{\alpha}\frac{J_0(\alpha)}{J_1(\alpha)}, \qquad \text{(II-4b)}$$

in order to satisfy the new boundary condition that the ion flux at the wall is $n(a)u_+/4$.

An expression relating the ionization rate per second per electron, the pressure in Torr, and the electron temperature can be found either empirically or theoretically. Considering the electron distribution to be Maxwellian, von Engel[28] found that

$$Z = \frac{600ApV_i}{\pi^{1/2}} \frac{2kT_-}{m_-} \left(1 + \frac{2kT_-}{eV_i}\right) \exp(-eV_i/kT_-) \qquad \text{(II-5)}$$

(A is a constant representative of the gas).

Either Eq. (II-4a) or (II-4b), when coupled with (II-2) and (II-5), yields a relationship between the electron temperature and the product of the tube radius and pressure, with the additional requirement that T_+ be known when (II-4b) is used.

From an energy balance equating the average energy gain of an

electron in the field E_z between two collisions to the average electron energy loss during a collision, the equation relating E_z/p to the electron temperature may be obtained:

$$E_z = \left(\frac{64}{\pi}\right)^{1/4} \left[\chi(T_-)\right]^{1/2} \kappa T_-/e\lambda_-, \qquad \text{(II-6)}$$

where $\chi(T_-)$ is the mean fraction of its random energy that is lost by an electron in a collision and λ_- is the electron mean free path. Since the electron temperature is a function of ap, the quantity E_z/p is also a function of ap; the experimental curve is plotted in Fig. 2.

When there is an applied magnetic field less than the critical value for the onset of the helical instability, then the diffusion is still ambipolar, with D_a replaced by

$$D_a' = D_a/(1 + y),$$

where $y = \mu_-\mu_+B^2$. If $\lambda_+ \ll a$ then E_z/p is now a function of ap', where $p' = p\sqrt{1 + y}$ and $\alpha = ap'f(E/p)$. Figure 2, with ap' replacing ap, can be used to find the electric field. If the modified Schottky theory applies, however, the Eqs. (II-4b), (II-5), and (II-6) must be used, since Eq. (II-4b) involves functions of E/p, ap', and p'^2/p.

B. Instability Theory

Although several solutions--such as Hoh's analysis in Ref. 29, for example--were originally proposed to explain the observed anomalous rise in electric field when the magnetic field was above a critical value, the Kadomtsev and Nedospasov approach has been generally accepted in preference to the other theories, which failed to

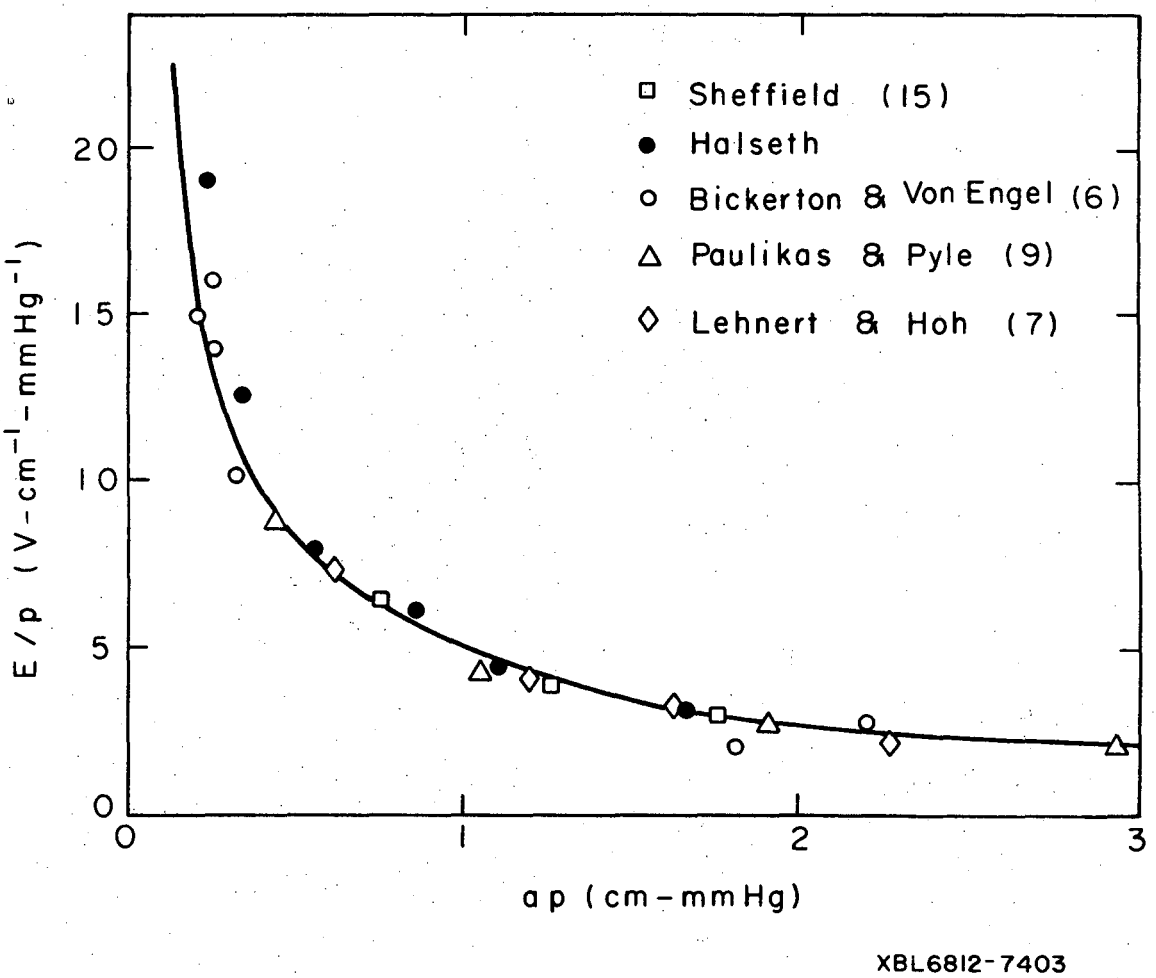

Fig. 2. E/p as a function of ap, He gas. □, Sheffield, Ref. 15; ●, present experiment; o, Bickerton and von Engel, Ref. 6; △, Paulikas and Pyle, Ref. 9; and ◇, Lehnert and Hoh, Ref. 7.

fit the experimental results. Subsequent works[16,30] attempted to improve the mathematical basis for the theory. A resumé of the theory of Kadomtsev and Nedospasov and the improvements by Holter and Johnson is given below.

The equations describing momentum transfer in the positive column when $\Omega_-\tau_- \gg 1 \gg \Omega_+\tau_+$ and $\omega\tau_+ \ll 1$ are

$$n\vec{v}_\pm + D_\pm \vec{\nabla}n + \mu_\pm n\left[\vec{E} + v_\pm \times B\right] = 0. \qquad \text{(II-7)}$$

The equations of continuity are

$$\frac{\partial n}{\partial t} + \vec{\nabla}\cdot n\vec{v}_\pm = nZ. \qquad \text{(II-8)}$$

Kadomtsev and Nedospasov assumed first-order perturbations of the form

$$n(\vec{r},t) = n_0(r) + n_1 J_1(3.83\ r/a)\ \exp\left[i(m\theta + kz - wt)\right] \qquad \text{(II-9)}$$

and

$$V(\vec{r},t) = V_0(r) + V_1 J_1(3.83\ r/a)\ \exp\left[i(m\theta + kz - wt)\right] \qquad \text{(II-10)}$$

where $V_0(r)$, $n_0(r)$ are the solutions to the unperturbed equations. They substituted these solutions into the equations of momentum and continuity and linearized and combined the resulting equations. They set the density at the wall to zero (Schottky condition) and applied the approximative method of Galerkin,[31,32] multiplying the combined equations by $J_1(3.83r/a)$ and integrating over r, to obtain a dispersion equation in ω and $k = 2\pi/\lambda$. For stability $\mathrm{Im}(\omega) < 0$, where

$$\mathrm{Im}(\omega) = (3.83/a)^2 \frac{5D_-}{4(\Omega_-\tau_-)^2}\left\{\frac{1}{\left(\frac{0.33m\mu_-}{\Omega_-\tau_-\mu_+}\right)^2 + \left[\frac{1+y}{y} + \frac{k^2}{0.79}\frac{\mu_-}{\mu_+}\left(\frac{R}{3.83}\right)^2\right]}\right\}$$

$$\times\left(-KX^4 - FX^2 - G_2 - G_1 + 0.16mXv^*\frac{\mu_-}{\mu_+}\right). \qquad \text{(II-11)}$$

The requirement for stability can be written as

$$KX^4 + FX^2 + G_1 + G_2 > 0.16mXv^*\frac{\mu_-}{\mu_+}\ , \qquad \text{(II-12)}$$

since the first term in square brackets is always positive. Here $v^* = \mu_-E/\beta_0 D_-$ and $X = k\Omega_-\tau a/3.83$, where

$$\begin{aligned} K &\equiv (1.28 + y)/\left[y(y+1)\right]\ , \\ F &\equiv 0.8(y+2)/y\ , \\ G_1 &\equiv 0.48(1+y)/y\ , \\ G_2 &\equiv 0.1(\mu_-/\mu_+)m^2/(1+y)\ . \end{aligned} \qquad \text{(II-13)}$$

At the critical field the inequality (II-12) becomes an equation and $\partial \mathrm{Im}(\omega)/\partial k = 0$, which is apparent from Fig. 3. Hence B_c and k can be found from

$$\begin{aligned} X^2 &= \left\{-F + \left[F^2 + 12K(G_1+G_2)\right]^{1/2}\right\}/6K, \\ 0.08v^* &= \frac{\mu_+}{m\mu_-}(2KX^2 + F)X \end{aligned} \qquad \text{(II-14)}$$

if the temperature, pressure, and electric field are known.

Johnson and Jerde solved the differential equations of momentum and continuity [(II-7) and (II-8)] without any assumption about the

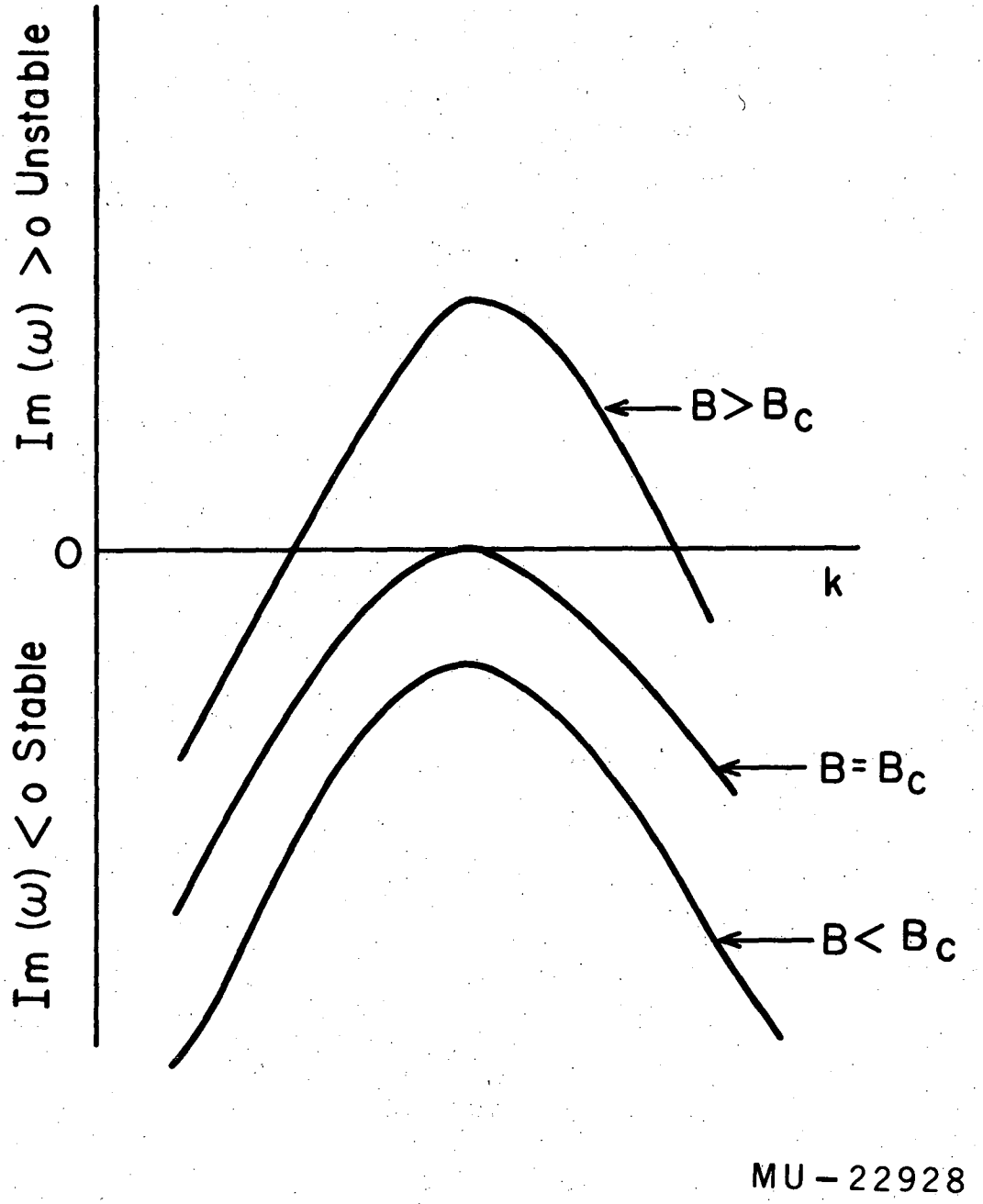

Fig 3. The general from of Eq. (II-11); Im (ω) vs k for several values of B.

form of the radial dependence of the perturbations. The result is an infinite determinant of eigenvalues, $\omega_j(k)$, and a weighted set of Bessel functions of the first kind $J_1(\beta_j \frac{r}{a})$. The value of the perturbed wall potential is no longer zero. Although they give no proof that the solution provided by the full determinant converges, they do show that the first term (identical to the density perturbation of Kadomtsev) yields results which differ by only 6% from those obtained if the first two terms are used.

When the magnetic field has been increased above the critical value, the interaction between the potential and density perturbations causes a change in the mean density profile in the plasma. For small perturbations, the new "anomalous" diffusion can be calculated by using the previous forms for the density and potential fluctuations with a phase shift between the two included. Kadomtsev and Nedospasov, performing a quasi-linear calculation in the same paper,[10] used the old form, $J_0(\beta_0 \frac{r}{a})$, for the mean density profile, and arrived at the same Eq. (II-14) with new values:

$$\begin{aligned} K &\equiv (1 + y + 0.78S - 0.5\phi)/\left[y(1 + y)\right] , \\ F &\equiv (0.8y + 1.8 + 0.6S - 0.8\phi)/y , \\ G_1 &\equiv 0.8(1 - 0.4\phi)/\left[y(1 + y)\right] , \\ G_2 &\equiv 0.1m^2(\mu_-/\mu_+)(1.3s - 0.3\phi)/(1 + y) . \end{aligned} \qquad \text{(II-13a)}$$

The quantity S is a constant introduced in the equation for the average potential

$$\frac{dV_0}{dr} = \frac{1}{n_0}\frac{dn_0}{dr}\frac{D_-}{\mu_-(1+y)}S \ . \qquad \text{(II-15)}$$

The quantity ϕ is related to S through

$$S = \phi(1.3 + X^2 - 0.7\phi)/(1.5 + X^2 - 0.9\phi) \ , \qquad \text{(II-16)}$$

and ϕ is a measure of the total particle loss, including enhanced diffusion. Its value is unity at the critical field.

Since the equation involves two unknowns, ϕ and E_z, a second equation is required. This equation comes from a knowledge of the new number of ionization events per electron per unit time derived from above,

$$Z = \frac{\mu_+}{\mu_-}\frac{D_-\beta_0^2}{(1+y)a^2}\phi \ , \qquad \text{(II-17)}$$

and the energy balance requirement [from (II-5),(II-6)],

$$Z = p\, f(E/p), \qquad \text{(II-18)}$$

resulting in a functional dependence of E/p on ap^* [where $p^* = p\sqrt{(1+y)/\phi}$] identical to the old dependence on ap when B = 0. This relationship assumes that the Schottky condition applies.

Holter and Johnson have improved upon this analysis by discarding the assumption that the average density profile remains a zeroth-order Bessel function. The results are very similar to those of Kadomtsev, but hysteresis can occur near the critical field because the electric field is found to be double-valued in this region for a certain range of pressures. Holter and Johnson also rely upon Schottky theory and

the energy balance equation to complete the set of equations necessary for a solution. Their electron temperature also comes from these equations.

Sheffield[15] has attempted to improve upon the model of Holter and Johnson by including some data from experiments in the calculations. The fundamental helical mode is allowed a nonzero growth rate to be calculated from the theory implying that, at some time, the helix will break up and a new helix will start to grow. He was then forced to use experimental values for one unknown quantity, which he chose to be the electric field. He found that the density profiles predicted by Holter and Johnson differed considerably from measured values, so he also used an empirical form for his radial profile. He then obtained reasonable agreement with measured wavelengths, frequencies, and particle transport rates.

C. Turbulence

In later articles[26,33] Kadomtsev has extended the theory of the unstable positive column to include the case of the very high magnetic field, in which many oscillations of different wavelength and frequency may exist.

Plane geometry is used here on the assumption, which must be proven by the results of the theory, that any characteristic lengths derived will be small compared with the radius. For electrons, collisions can be ignored in the momentum equation for particles moving in the plane transverse to the column axis, so one has only

$$\vec{v}_{-\perp} = \frac{1}{B^2}\vec{B} \times \vec{\nabla}v_- - \frac{D_-}{\mu_-}\vec{B} \times \vec{\nabla}n/n \ . \qquad \text{(II-19)}$$

The one other change from the equations at lower magnetic fields is the elimination of the extremely small ion-diffusion term. Again, there is an equilibrium state, represented by the single equation and a set of equations which, combined with the equation of continuity, yields solutions for the density and potential perturbations which are of the same general form as in Eq. (II-9). These in turn yield a dispersion equation which can be solved for the frequency of small-amplitude oscillations. The imaginary part of the frequency when $(\Omega_+\tau_+)^2 \gg 1$ (which is true for the highest field used in this experiment) is

$$\gamma = \left[\left(\frac{\mu_+ E}{\Omega_+\tau_+}\right)\frac{d \ln n}{dx}\frac{k_y}{k_z} - D_-\frac{\mu_+}{\mu_-}\frac{k_\perp^2}{(\Omega_+\tau_+)^2}\right]\frac{1}{1 + \frac{\mu_+}{\mu_-}\frac{k_\perp^2}{(\Omega_+\tau_+ k_z)^2}}, \qquad \text{(II-20)}$$

where $k_\perp^2 = k_x^2 + k_y^2$. The largest growth rate exists for that perturbation for which $k_\perp$ is so small that the second term in Eq. (II-20) can be ignored, and $(k_\perp/\Omega_+\tau_+ k_z)^2\mu_+/\mu_- \equiv X' = 1$ and $k_y \approx k_\perp$. Then $\gamma = U\, d \ln n/dx$, where

$$U = \frac{1}{2} E_z \sqrt{\mu_+\mu_-}. \qquad \text{(II-21)}$$

An analogy with hydrodynamics was drawn at this point by Kadomtsev to associate these perturbations with measurable quantities in a chaotic plasma. Because of the spectral continuum of wavelengths

in the plasma, coherent oscillations are impossible outside a small region or cell in the plasma. This cell can be characterized by an effective mixing length, ℓ, as in ordinary turbulence Similarly, the density fluctuation can be written as $n' = \ell\, dn/dr$, and its speed would be $v' = Un'/n$. Kadomtsev assumed that, for insulating walls which have no stabilizing effect on the fluctuations, ℓ may be taken as constant for a given tube.

In a turbulent system, turbulent diffusion is the dominant loss mechanism. The flux of particles in a cylindrical system can then be written as[17]

$$q = n'v' = D\, dn/dr, \qquad \text{(II-22)}$$

where $D = v'\ell = \gamma\ell^2$. Here the value of γ calculated in the Cartesian system can be used on the basis of the previous hypothesis. The equation of continuity, $1/r\ d/dr(rq) = nZ$, can be solved for n with the boundary conditions $n(0) = n_0$, $n'(0) = 0$ and $n(a) = 0$. The result is a density profile $y_0(rx_0/a)$, where the root is

$$x_0 = 3.40 = (Za^3/\ell^2 U)^{1/3}. \qquad \text{(II-23)}$$

This equation may be simplified if one considers a second column of radius a_1 at the same pressure and electric field but without an applied magnetic field. In this tube, the ionization rate and electron temperature are the same as in the tube of radius a if one ignores turbulent heating, which depends on the value of ℓ/a, as will be seen. In the stable column,

$$Z = (\mu_+/\mu_-)T_-\mu_-\beta_0^2/ea_1^2. \qquad \text{(II-24)}$$

Then

$$\ell^2 = \frac{a^3\mu_+T_-\beta_0^2}{x_0^3ea_1^2u} = \frac{2a^3T_-\beta_0^2}{x_0^3ea_1^2E_z}\left(\frac{\mu_+}{\mu_-}\right)^{1/2}. \qquad \text{(II-25)}$$

Using the results of previous experiments which measured E_z when $B \gg B_c$, Kadomtsev calculated typical values of ℓ/a which were of the order of 0.15. Kadomtsev has shown also that the fluctuations of the total electric field, which measure the heating of the electrons by the oscillations, are of the order of $(\ell/a)E_z$, so that turbulent heating has very little effect on the electron temperature and can be ignored.

Another boundary condition, based upon an experiment by Artsimovich and Nedospasov,[34] was proposed by Kadomtsev in his book on turbulence.[17] Since, in all experiments, the density in the turbulent column is nonzero near the wall, Kadomtsev suggests that the extrapolated boundary-length condition be imposed. That is, q/U = density at the wall and the extrapolated boundary length $\ell' = 1/(d \ln n/dr)$ at the wall. This leads to the relation $\ell' = \ell$ and a new value for a to be used in Eq. (II-25): a = a + L, where L is the distance between the radius of the tube and the new position were n = 0, which is to be found by an iterative method using the known form of y_0. In this work a will be taken as the tube radius in Eq. (II-25), but the curves y_0 will be drawn so that $n(a) = \ell(dn/dr)\big|_{r=a}$.

Sato[35] extended Kadomtsev's analysis to derive the axial correlation length, $\ell_\parallel$. For the system considered by Kadomtsev, Sato found

that, assuming $k_\perp/k_z = \ell_\parallel/\ell$ and $X' = 1$,

$$\ell_\parallel = \ell \sqrt{\mu_- \mu_+} \cdot B. \qquad \text{(II-26)}$$

Sato then noted that, in Eq. (II-20), if the restriction that $X' = 1$ is removed, and if $\ell_\parallel/\ell$ is considered to be a constant, then γ is a function of B^{-1} and the diffusion coefficient should also vary as B^{-1}. Then the electric field should decrease as the magnetic field is increased.

In his paper, Hoh[25] suggests that the single helix of the quasi-linear region will break up into many high-frequency helical modes, all of which possess the same growth rate, when the magnetic field is many times B_c. The many modes will result in a plasma that is in a turbulent state.

Equation (II-25) and the density profile from Kadomtsev's theory of turbulence $y_0(x_0 r/a)$ provide numerical results which can be easily compared with experiment. The best experimental test for the absence of the helical $m = 1$ mode is a check, by use of correlation techniques, of Eq. (II-9). If no dominant oscillation is present, but the spectrum is a broad continuum of frequencies, the system is turbulent. Then one can check to find out if results compare with the predictions by Kadomtsev about turbulence.

When the helical oscillations are present, the results of the theory of Holter and Johnson and the theory of Kadomtsev and Nedospasov [(II-13a), (II-14)] can both be compared with the electric fields measured in the experiment. Holter and Johnson's results were also

compared with the frequencies of the higher modes measured here. Sheffield's semi-empirical theory, which depends upon the theory of Holter and Johnson, predicts wavelengths for the first helical mode. Finally, growth rates calculated from the works of Johnson and Jerde and Kadomtsev and Nedospasov (II-11) were compared with experimentally measured growth rates.

III. EXPERIMENTAL EQUIPMENT AND PROCEDURE

A. Apparatus

The basic arrangement used throughout this experiment is shown in Fig. 4. The Pyrex discharge tube used had a length of 300 cm and radius of 2.75 cm. Two easily removed electrodes with tungsten filaments were attached to the ends of the tube by means of ground glass joints sealed with Apiezon wax. In some cases, with a direct current discharge in the tube, a flat plate was used in place of a filament as the anode. Neither filament was emission-limited during operation. At low pressures, the length of the tube was increased 2 m to reduce the effects of the ends on the conditions in the central axial region of the plasma, where most experiments were performed.

A power supply with the capacity to supply up to 1 A of discharge current in either an alternating-square-wave mode or a direct mode was used in the study. A schematic diagram of the electrical system is shown in Fig. 5. The synchronous, gated pulser in conjunction with the signal generator allowed the operator to switch from the alternating to the direct mode within the driver preamp at any point in the cycle. Simultaneously, the capacitor from the final amplifying stage was shorted out by the thyratron. In practice, the change was triggered to occur on the leading edge of the positive cycle. The range of the signal generator was 0 to 50 kHz. In those instances when the discharge was being operated only in the direct mode the current was stabilized to within less than 1% deviation by a separate regulating device.

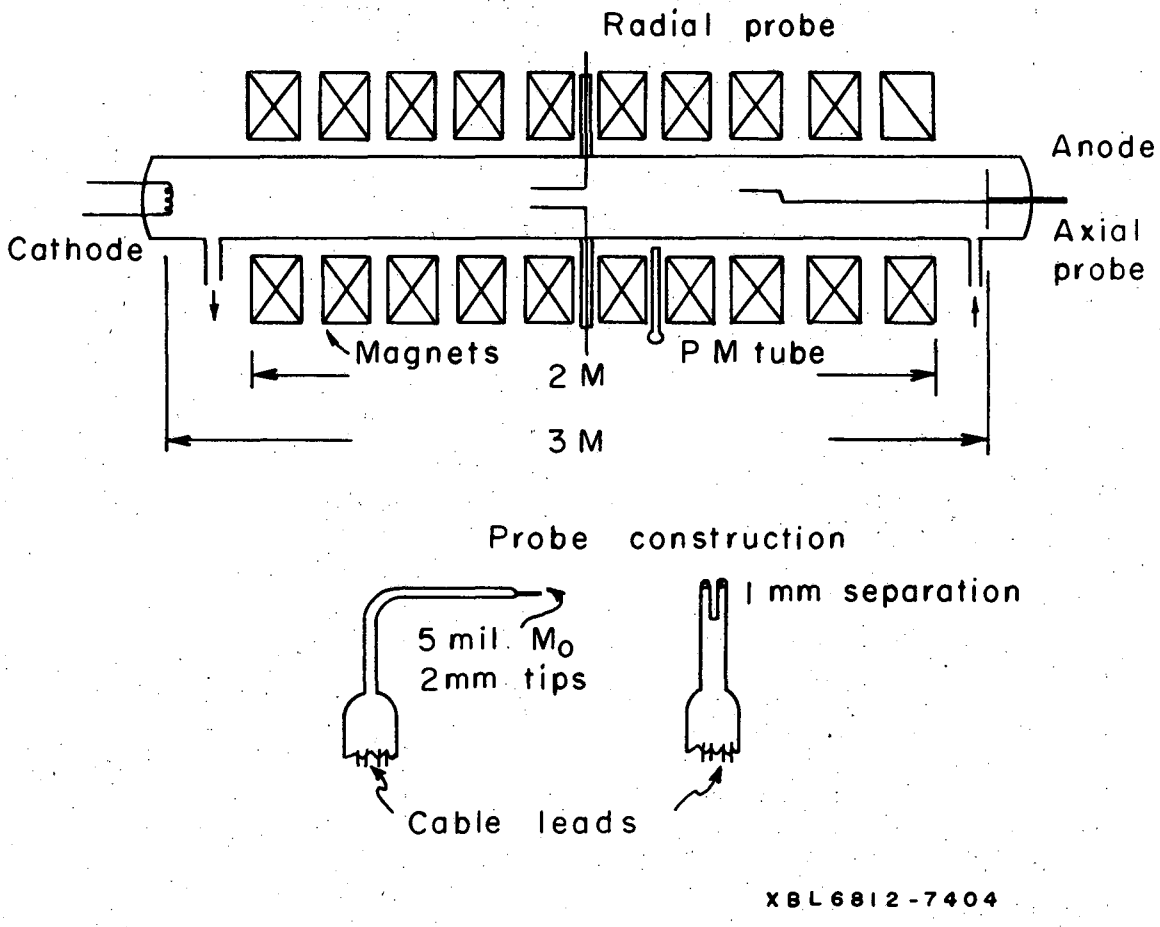

Fig. 4. Schematic of positive column experiment and probe construction.

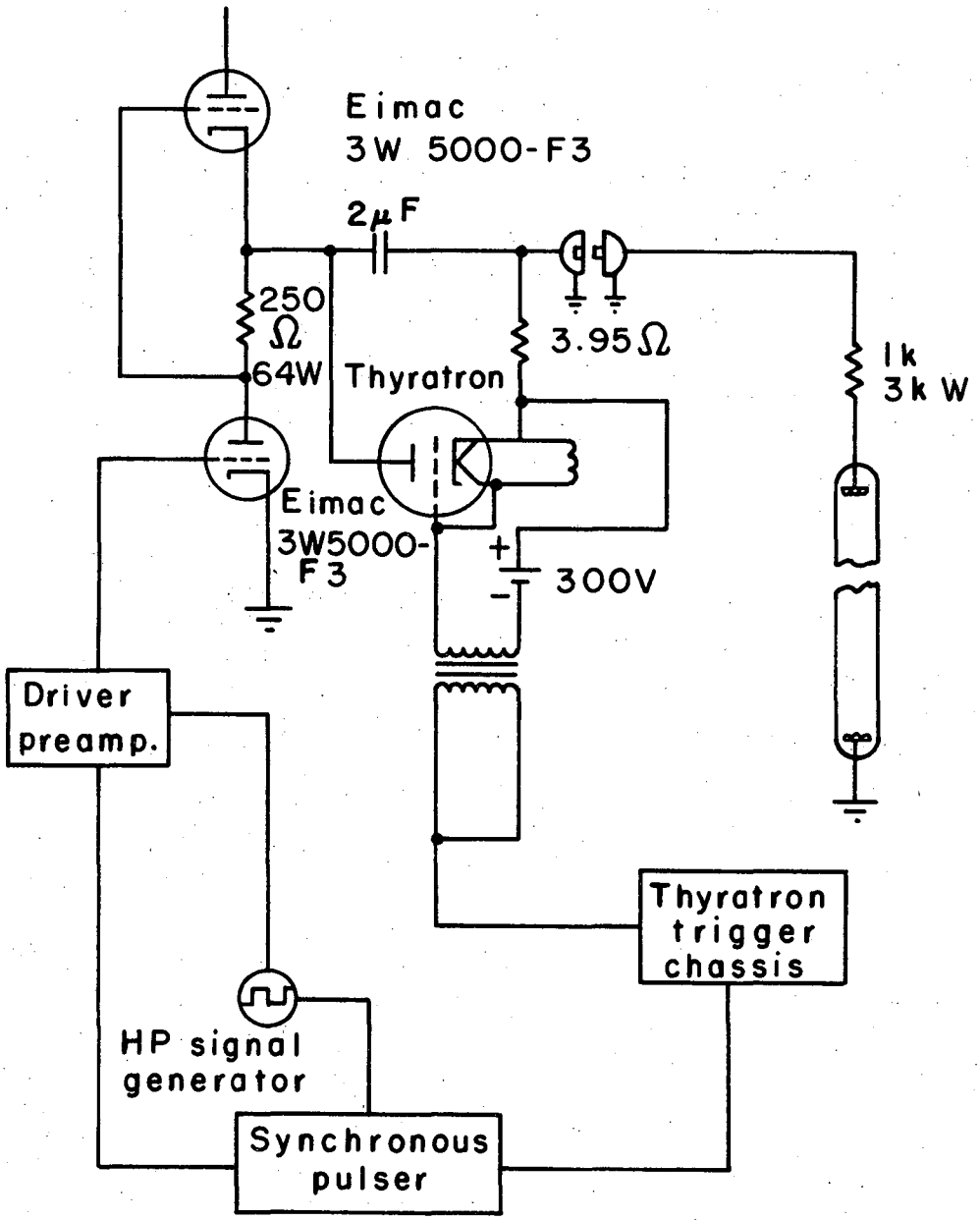

Fig. 5. Schematic of ac-dc control system.

The magnetic field was provided by ten 9-in. i.d. water-cooled coils 6 in. wide and spaced 2.25 in. apart. Photomultiplier monitoring and probe insertion took place between the coils. With one power supply of the type available, the maximum axial field was 7 kG. Fields of up to 12 kG were obtained by splitting the coils into three groups of three and using three power supplies.

The vacuum was provided by a 4-in. oil diffusion pump in conjunction with a refrigerated baffle system and liquid nitrogen cold trap. The base pressure of this system was 10^{-7} mm Hg. Control of the helium pressure inside the tube was maintained by regulation of the exit valve near the grounded electrode and of the bleed valve through which the gas was continuously fed. Any significant impurities in the system were flushed out by running the discharge for an hour before data were recorded. Satisfactory purity was signified by a deep pink glow throughout the column. The neutral gas pressure was measured with an Autovac gauge.

B. Diagnostics

The discharge current and the total axial potential drop, V_t, were continuously monitored on a Tektronix 551 oscilloscope. The rms value of the alternating potential was displayed on an rms voltmeter. In all experiments wherein the mode of the discharge current was changed the peak current of the alternating mode was set equal to the final current of the direct mode.

At various times several movable double Langmuir probes[36,37] were inserted in the plasma. Their locations are shown in Fig. 4.

The axial probe was a dogleg probe which rested on the bottom of the column, except for the 8-cm-long double bend, and reached from the anode to slightly past the center of the tube. Except when axial correlations were being measured, the radial probes were bent parallel to the axis of the discharge tube several centimeters before the probe tips. Continuous frequency spectra were taken on a Panoramic Analyzer or on a Nelson-Ross spectrum analyzer unit built for a 551 Tektronix oscilloscope. Both the azimuthal electric field and the ion saturation current were analyzed. The ion current was recorded on 35-mm film during mode switching of the plasma.

The two probe wires were covered by separated slender glass sleeves for 3 cm, terminating at the tips in 2-mm-long bare wires separated by 1 mm (Fig. 4). The wires of 5-mil-diameter molybdenum were protected by a larger single glass sleeve after the separate sleeves. This joined to a 6-mm glass tube which could be moved by means of a calibrated gear mechanism, in the case of the radial probe.

The system used to measure the current between the two ends of a double probe is shown in Fig. 6 The 1-MΩ resistors were replaced with resistors of larger value when ac-dc measurements were made. A differential voltmeter, separated from the probe ends by 500-MΩ chains of resistors, measured the dc current across a 5×10^4-ohm resistor.

All normalized correlations are defined as a time average of the product of two probe signals divided by the rms values of the two signals. If the two signals are the same, the correlation is 100%. If they are sinusoidal and differ in phase, or possess some degree

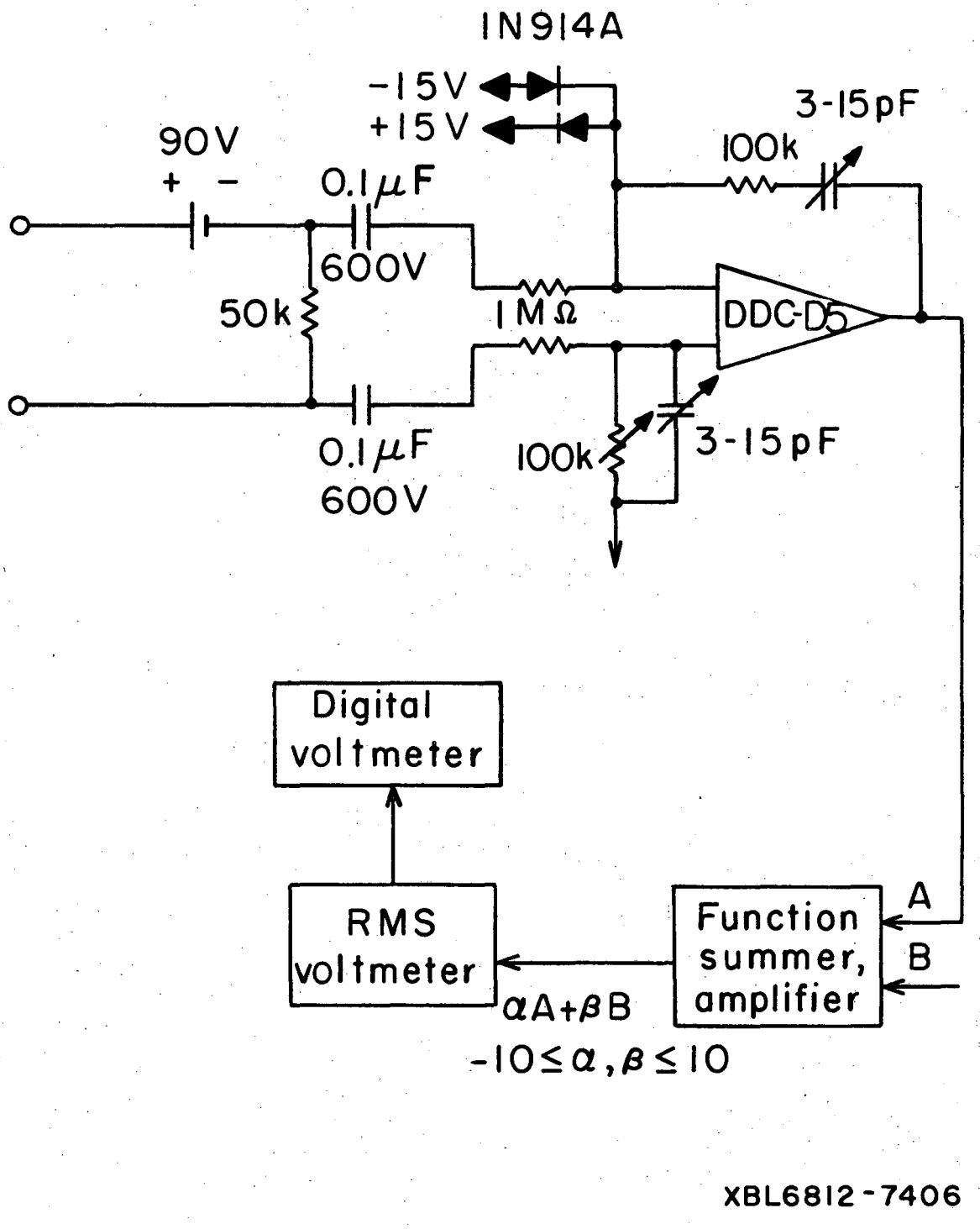

Fig. 6. Schematic of double-probe diagnostic system.

of randomness with respect to each other, then the value is less.

Radial spatial correlation measurements were made with two probes entering radially from opposite sides of the tube. Signals from the two probes were amplified to a common rms value and then put into a special-function summer, shown in Fig. 6, which provided the rms values of the sum and difference of the two signals. The difference of the squares of these two values divided by the sum of the squares provides the normalized correlation of the two signals. The equation for finding the correlation is

$$R_{AB} \equiv 2\langle(\tilde{f}_A\tilde{f}_B)\rangle/(\langle\tilde{f}_A^{\,2}\rangle + \langle\tilde{f}_B^{\,2}\rangle)$$

$$= \frac{\langle(\tilde{f}_A + \tilde{f}_B)^2\rangle - \langle(\tilde{f}_A - \tilde{f}_B)^2\rangle}{\langle(f_A + f_B)^2\rangle + \langle(f_A - f_B)^2\rangle} \quad ,$$

where $\tilde{f}$ is the fluctuating part of the quantity f.

Photomultiplier tubes were used to measure the time-dependent light intensity. They provided a check of the signals from the Langmuir probes. The radial bank of tubes was also used to detect azimuthal phase shifts necessarily present if the oscillations are helical.

IV. RESULTS

A. Electric Field in a dc Discharge

The axial electric field in the positive column was measured in two independent ways. The potential difference between the two electrodes and the potential difference measured by a movable probe between two axial positions on the same field line were both used as sources of axial electric field values. Results of the measurements are shown in Figs. 7 through 11.

By the theory of Kadomtsev, the electric field should no longer be affected by the magnetic field when the plasma is strongly turbulent. The results indicate agreement with this theory when the ratio of B to B_c is large.

Neither measuring technique is without error. The total potential drop across the length of the tube is not an accurate measure of the electric field because there is a different axial electric field at the ends of the tube, and this varies in its own way with magnetic field. The average field represents the larger electric field at the ends and the smaller value in the center, where the magnetic field lines are straight.

An axially movable probe was used to record the potential at several positions along the tube, providing a second method of measuring E_z. The probe was observed to affect the plasma potential and there was difficulty in keeping the probe on the same field line during the measurements, resulting in errors in the calculated electric field. Since the radial variation in potential near the center of

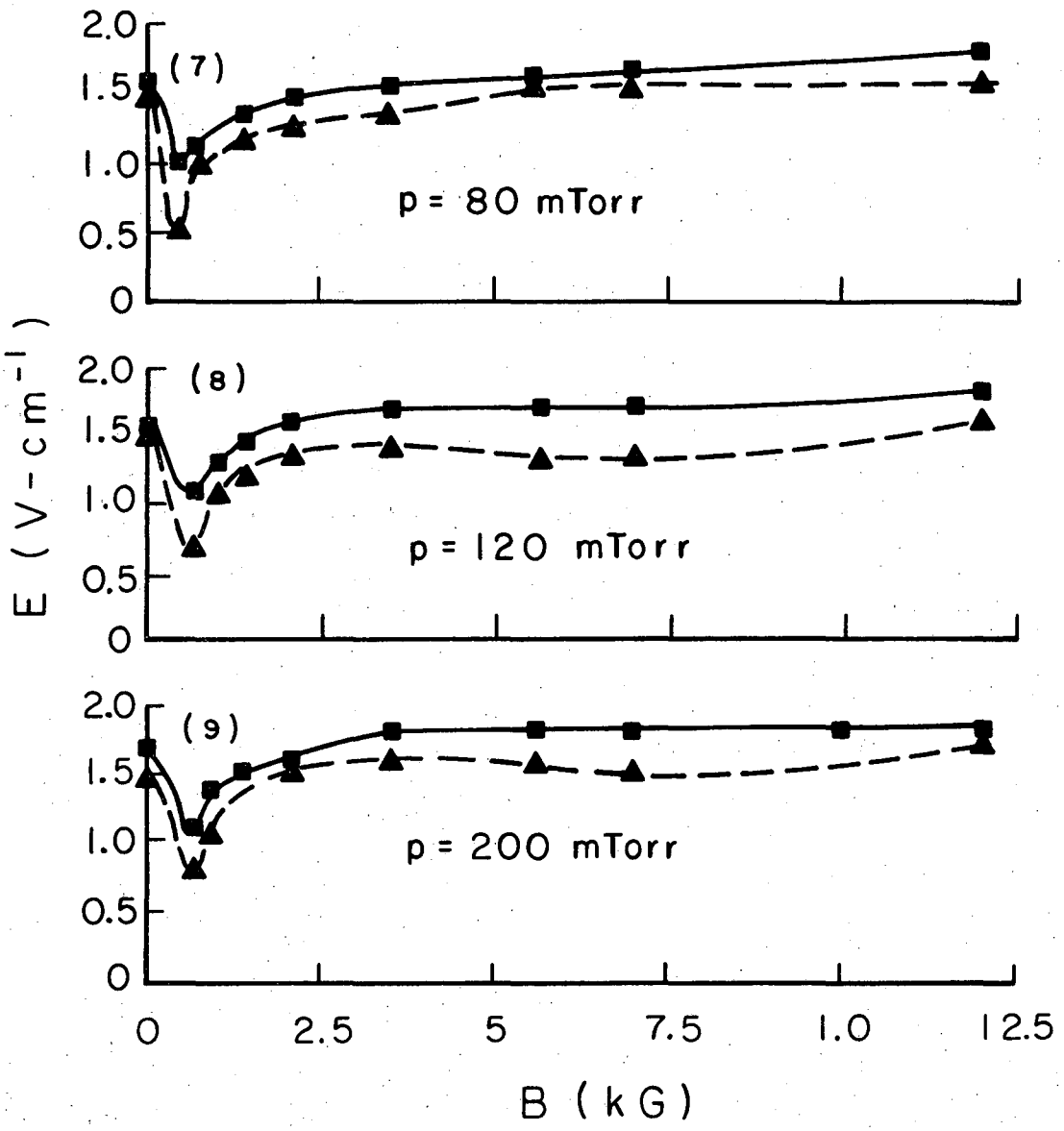

XBL691-1879

Figs. 7 to 9. Electric field as measured by a probe (▲) and as measured from the interelectrode potential (■). Fig. 7, p = 80 mTorr; Fig. 8, p = 120 mTorr; Fig. 9, p = 200 mTorr.

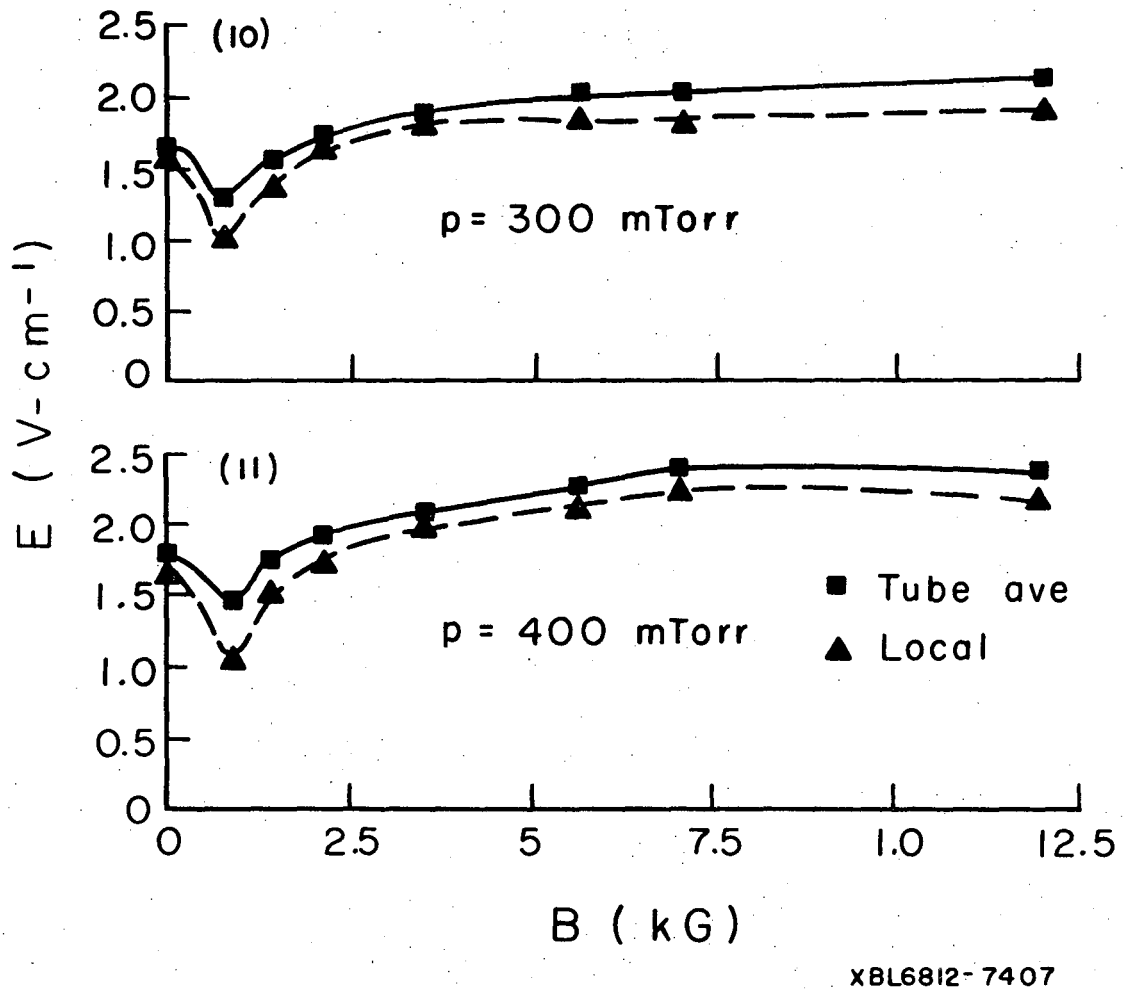

Figs. 10 and 11. Electric field as measured by a probe (▲) and as measured from the interelectrode potential (■). Fig. 10, p = 300 mTorr; Fig. 11, p = 400 mTorr.

the tube was about 10 V or less, the error caused by the failure of the probe to remain on a field line was estimated to be no more than 2 V for each measurement of potential. This is an error of 10% at most if the electric field is measured over a distance of 30 cm.

These probable errors lead to some uncertainty in the shape of $E_z(B)$, particularly at high magnetic fields where E_z changes slowly with B. Since the axial probe data were taken near the center of the tube, these were the measurements used in calculations of the turbulent decay length in Section IV D.

B. Radial Density Profiles

Measurements of the relative ion density as a function of radius have been made in the positive column in the pressure range from p = 20 to p = 400 mTorr. Results are shown in Figs. 12 through 17 for magnetic fields up to B = 12 kG in a constant discharge current of 400 mA. In Fig. 15 results are included for a different current, I = 200 mA, when B is 12 kG. For the sake of comparison, the J_0 Bessel function and the function $y_0(x_0 r/a)$ of Kadomtsev's turbulence theory are included.

The data were obtained with a double probe which had probe tips several centimeters axially removed from the point of entry of the probe into the plasma. The measured profiles were symmetric about the center of the plasma, which was always within 2 or 3 mm of the geometric center of the tube. Densities were measured from about 0.5 cm from the near wall to about 0.5 cm from the far wall. No more than 50 μA was ever drawn between the two probe tips.

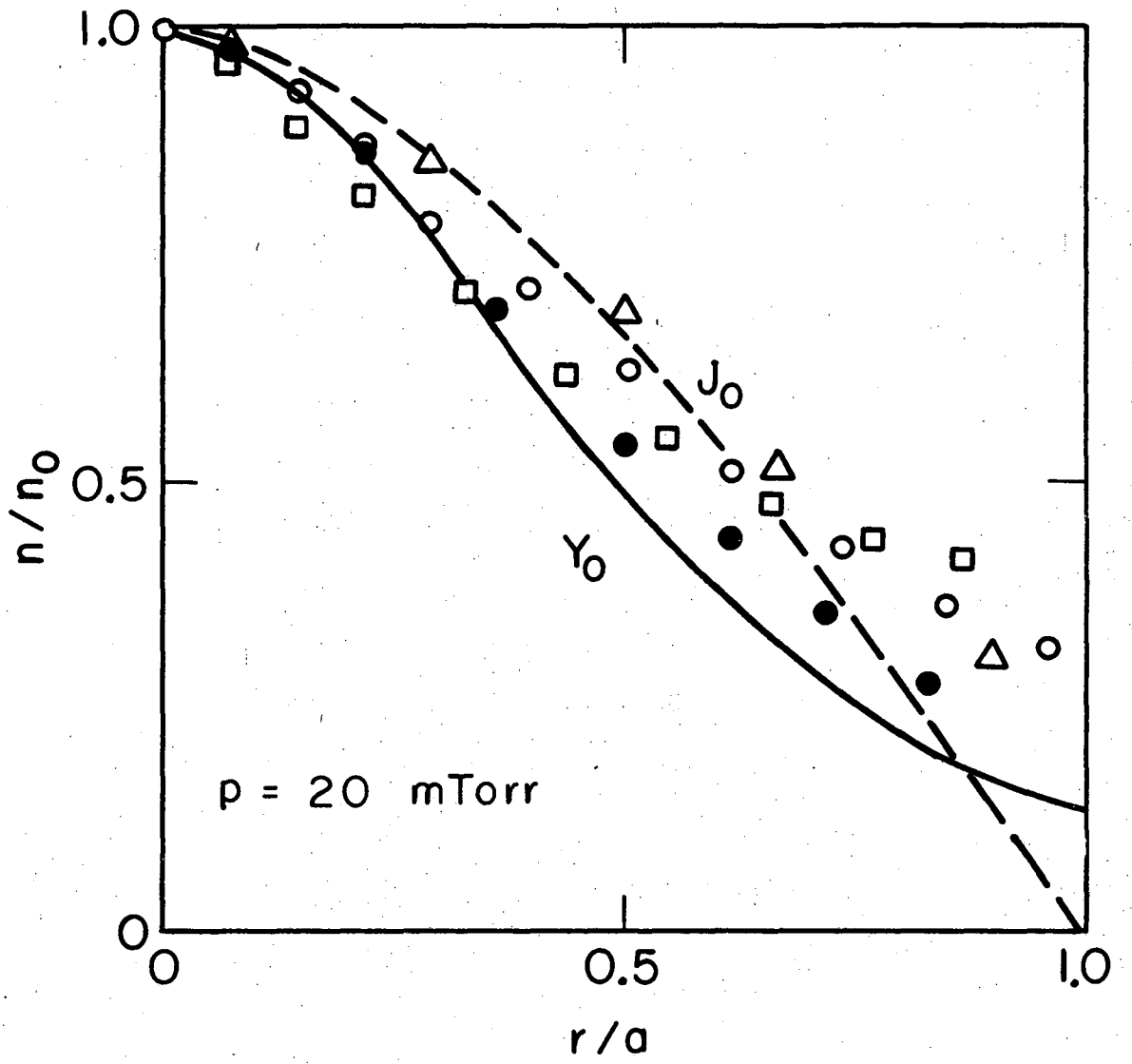

Fig. 12. Normalized density profile. p = 20 mTorr. ●, B = 2.1 kG, tube 5 m long; □, B = 1 kG, tube 5 m long; o, B = 1 kG, tube 3 m long; Δ, B = 0, tube 3 m long.

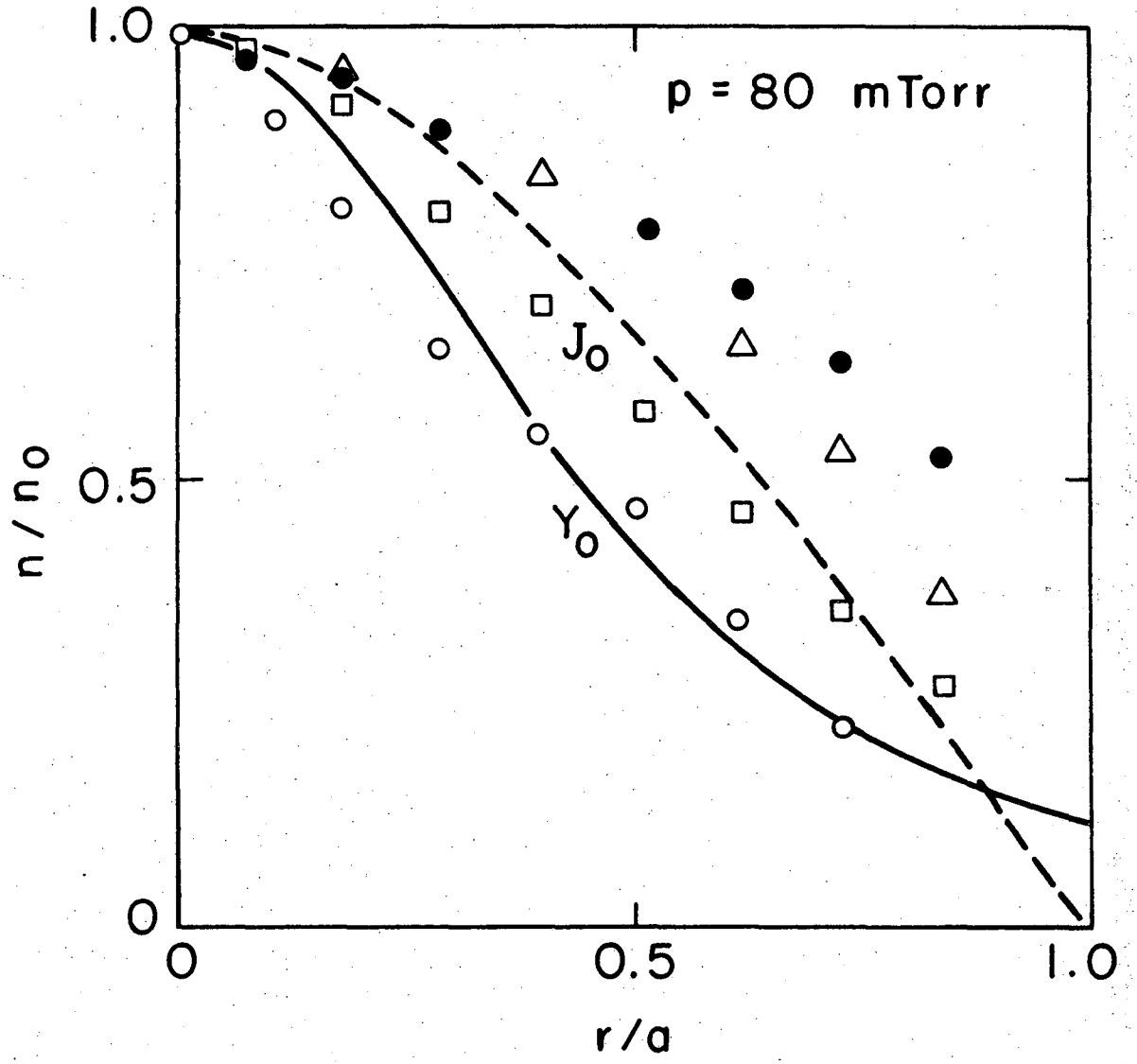

Fig. 13. Normalized density profile. p = 80 mTorr. △, B = 0 kG; •, B = 2.1 kG; □, B = 3.5 kG; o, B = 12 kG.

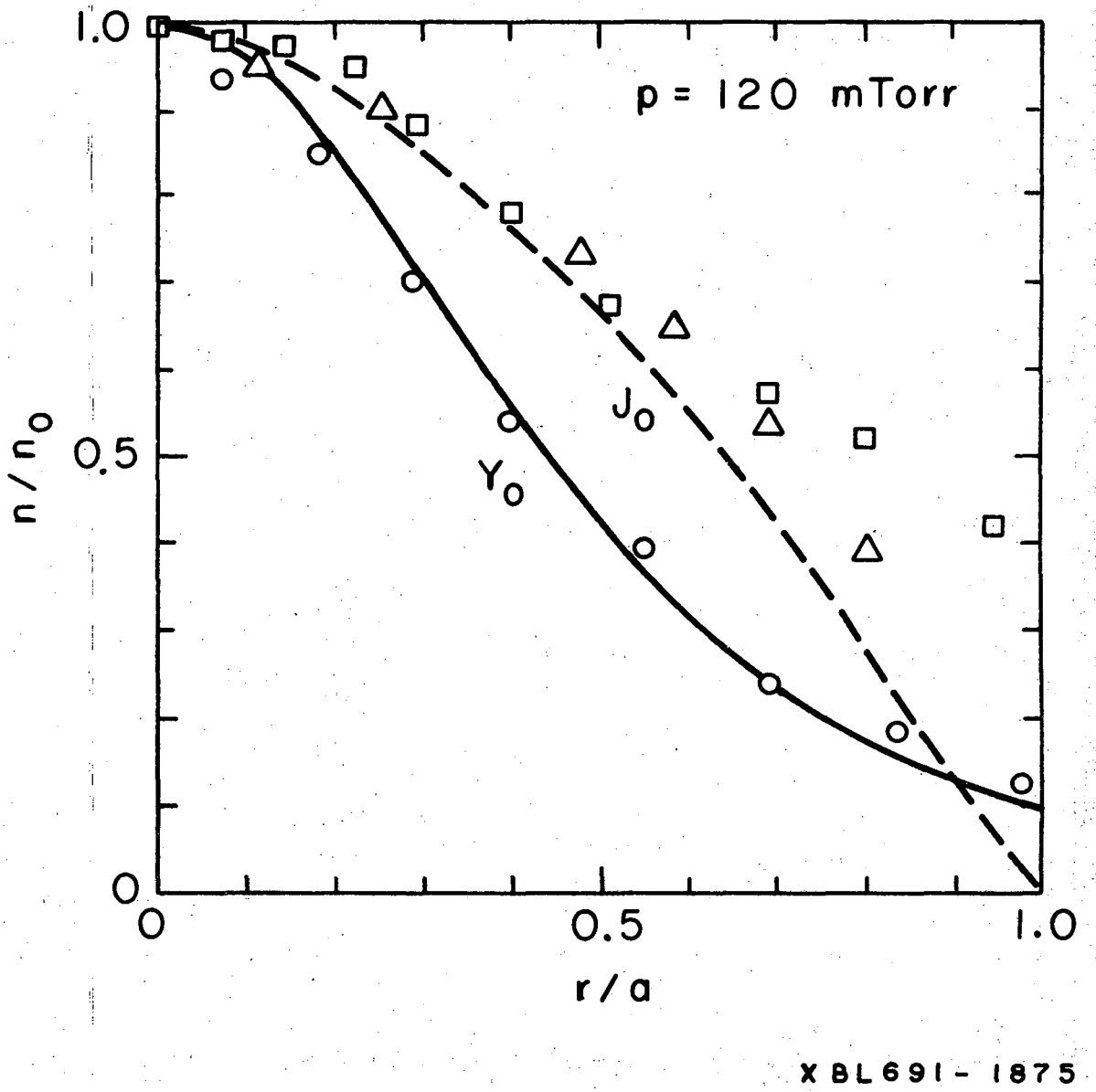

Fig. 14. Normalized density profile. p = 120 mTorr. △, B = 0 kG; □, B = 3.5 kG; o, B = 12 kG.

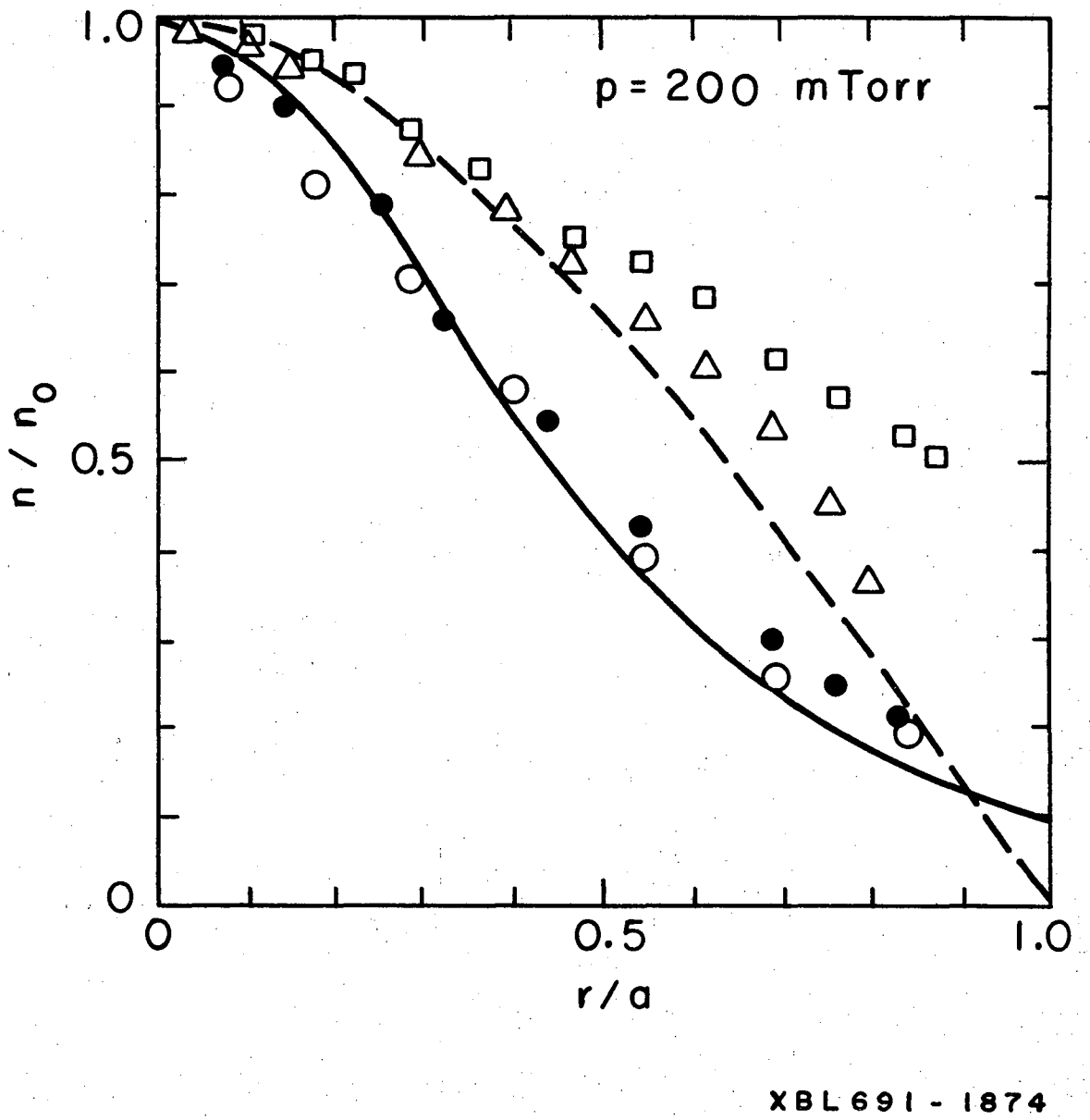

Fig. 15. Normalized density profile. p = 200 mTorr. △, B = 0 kG; □, B = 3.5 kG; o, B = 12 kG; ●, B = 12 kG, I = 200 mA.

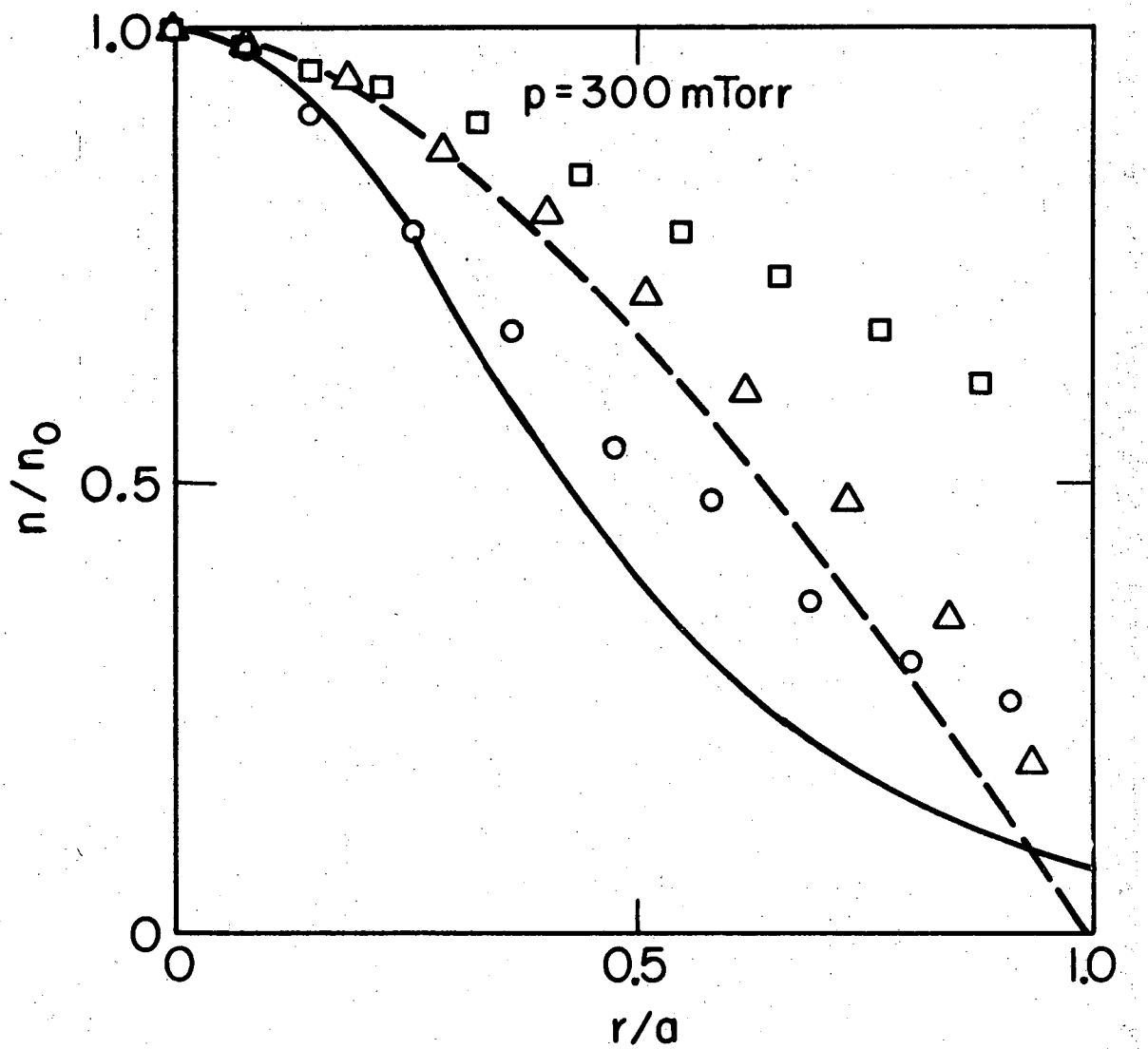

Fig. 16. Normalized density profile. p = 300 mTorr. △, B = 0 kG; □, B = 3.5 kG; o, B = 12 kG.

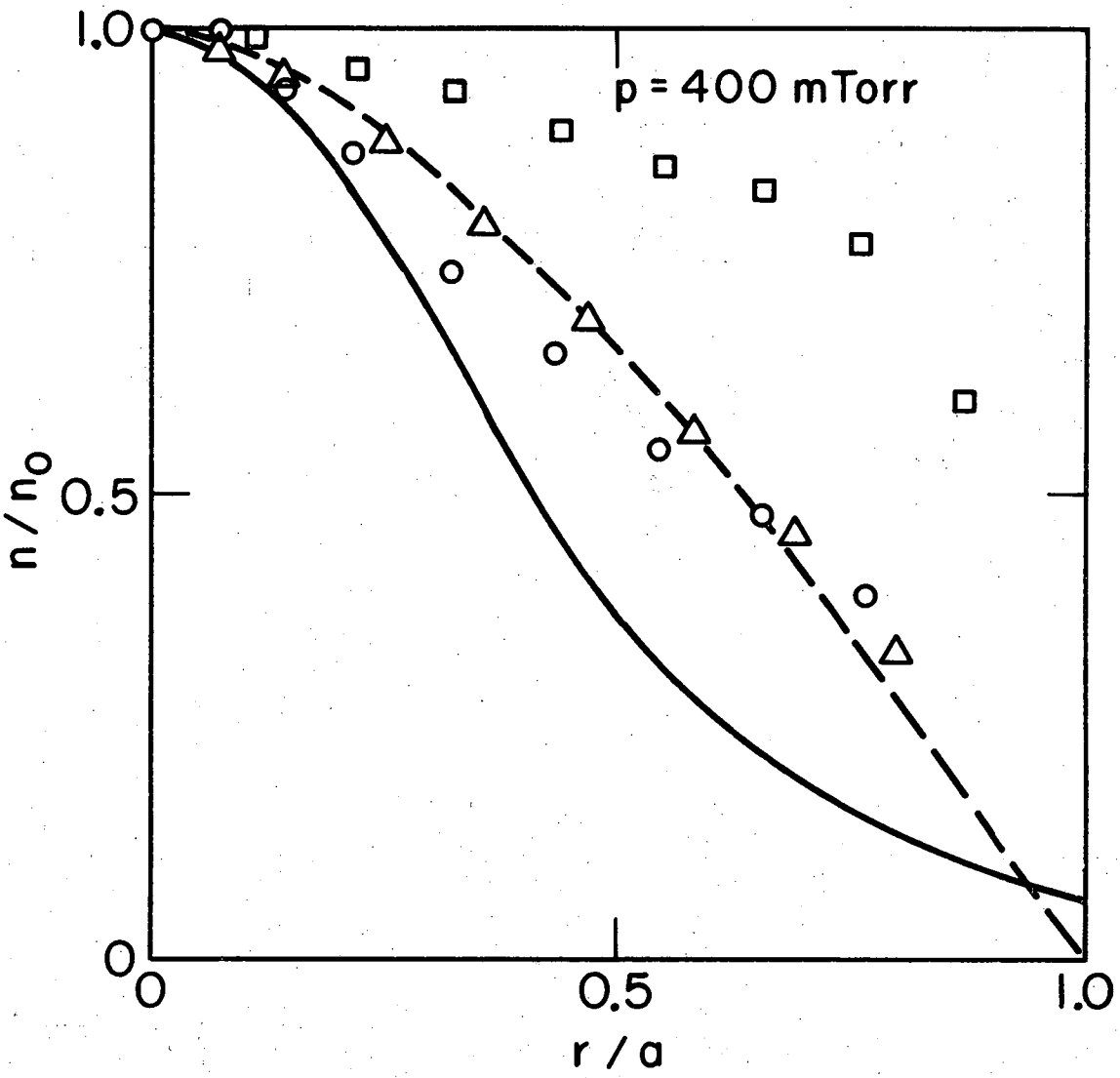

Fig. 17. Normalized density profile. p = 400 mTorr. △, B = 0 kG; □, B = 3.5 kG; o, B = 12 kG.

The data at the higher magnetic fields agree with the Kadomtsev profile $y_0(x_0 r/a)$, even in some cases in which the correlations would indicate that the plasma is not in a highly turbulent state. The flattening of the profile at the intermediate magnetic fields is in agreement with the theory that assumes the presence of a dominant helical instability at such fields.

The conditions here are quite similar to those in an experiment by Nedospasov and Artsimovich[34] in which, from the close correspondence of their radial profile to that of the theory, they deduced that agreement was obtained with the turbulence theory of Kadomtsev. Since the criterion of Simon[38] for ambipolar diffusion is violated by the relatively small ratio of length to radius for this pressure and magnetic field, it was felt that the results of Nedospasov might not reflect turbulence.

A longer tube, with two meters of the cathode end extending outside the field, was also used in the experiment presented here. Although this added length does not prevent the region outside the field from affecting the magnetized plasma if the field region is too short to satisfy the Simon criterion, it does eliminate cathode effects in the field region. Density profiles shown in Fig. 12 imply that these effects are absent in the shorter tube.

C. Oscillation Spectra and Fluctuation Level

The spectrum of azimuthal electric field oscillations and spectrum of density oscillations were recorded with the spectrum analyzer when the radial double probe was located 1.5 cm from the center. This

position was always near the maximum in the helical fluctuation intensity. The results are shown in Figs. 18 through 23. No fluctuations, including striations, were found when the field was lower than the critical field, provided the pressure was not greater than 400 mTorr.

An m = 0--i.e., azimuthally symmetric--mode (not a striation) is observed in the positive column when the magnetic field is greater than the critical value. This oscillation, Huchital and Holt[39] discovered experimentally, is associated with any small transverse magnetic field that may be present, perhaps because of a slight misalignment between the electric and magnetic fields. It is measured along with the helical oscillation when density fluctuations are observed. Azimuthal electric field fluctuations are associated with the helical instability, and do not measure any azimuthally symmetric oscillation. Hence any peaks in the E_θ spectrum signify the presence of helical oscillations.

At 12 kG, for all pressures except 400 mTorr, the spectra give no indication that they are dominated by any single oscillation. The spectra are continuous, implying the presence of turbulent fluctuations. At lower fields, the spectra are dominated by a single oscillation at the frequency of the first helical mode. The frequency spectrum is particularly sharp when B is near B_c. At intermediate fields some of the m = 0 mode is present because of imperfect common-mode rejections by the electrical system.

The relative level of density fluctuations with respect to the

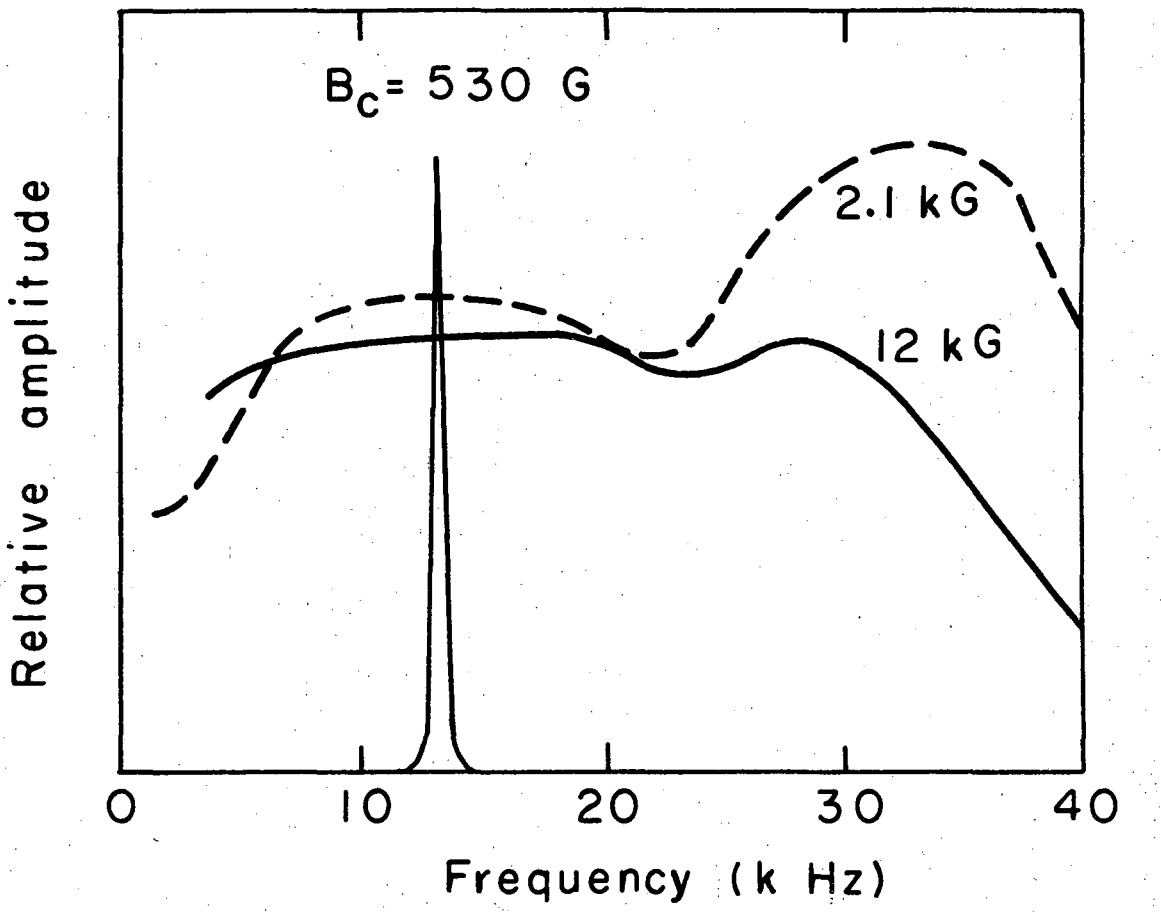

XBL 691-1880

Fig. 18. Fluctuating azimuthal electric field spectra. p = 80 mTorr.

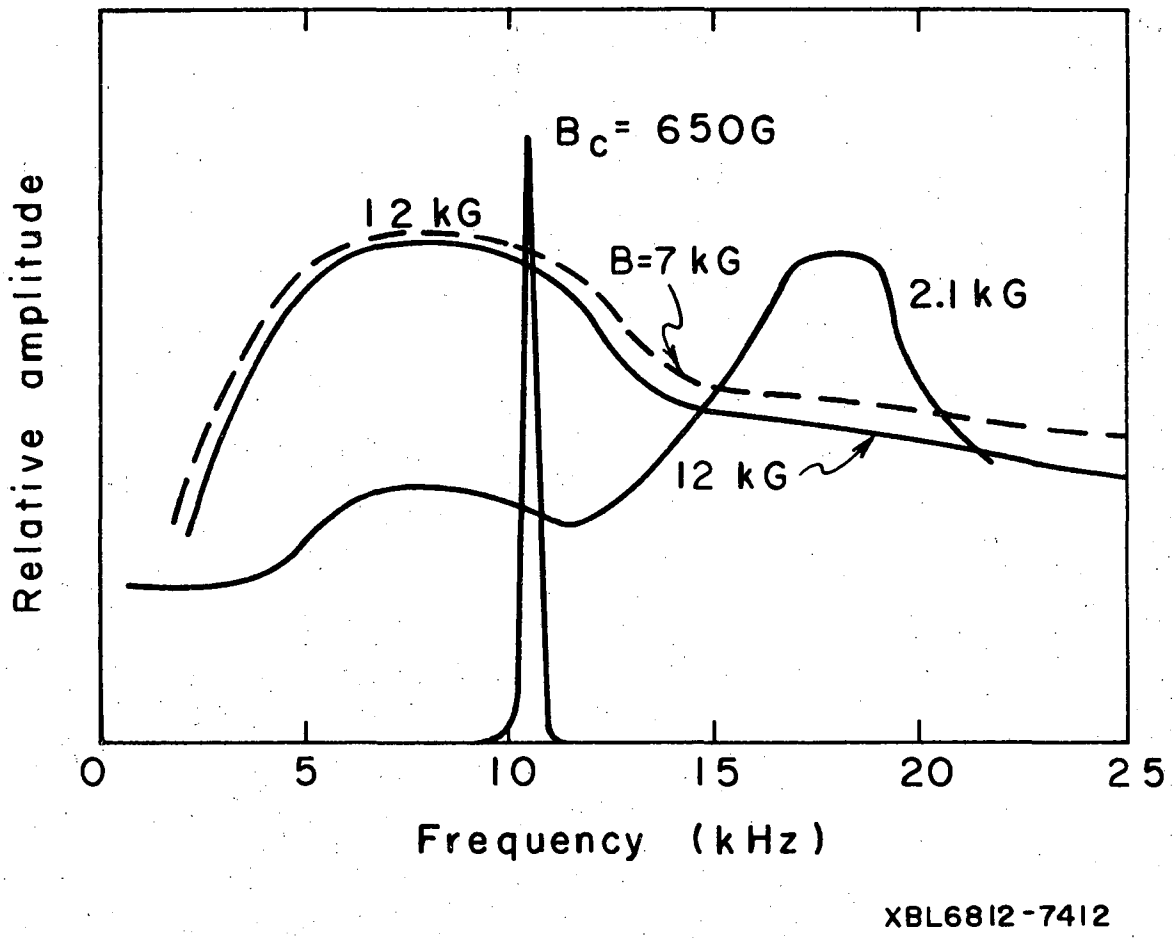

Fig. 19. Fluctuating azimuthal electric field spectra. p = 120 mTorr.

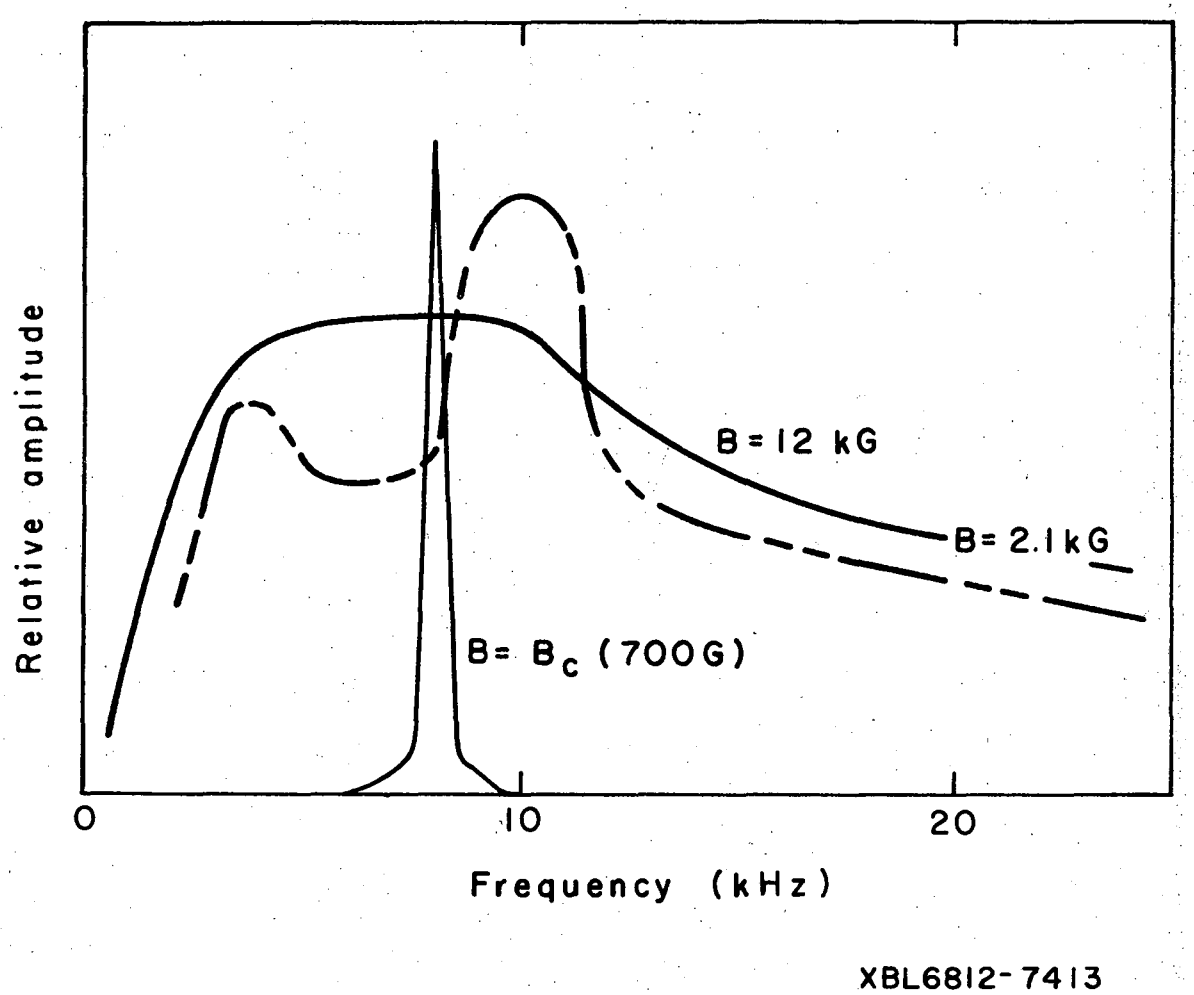

Fig. 20. Fluctuating azimuthal electric field spectra. p = 200 mTorr.

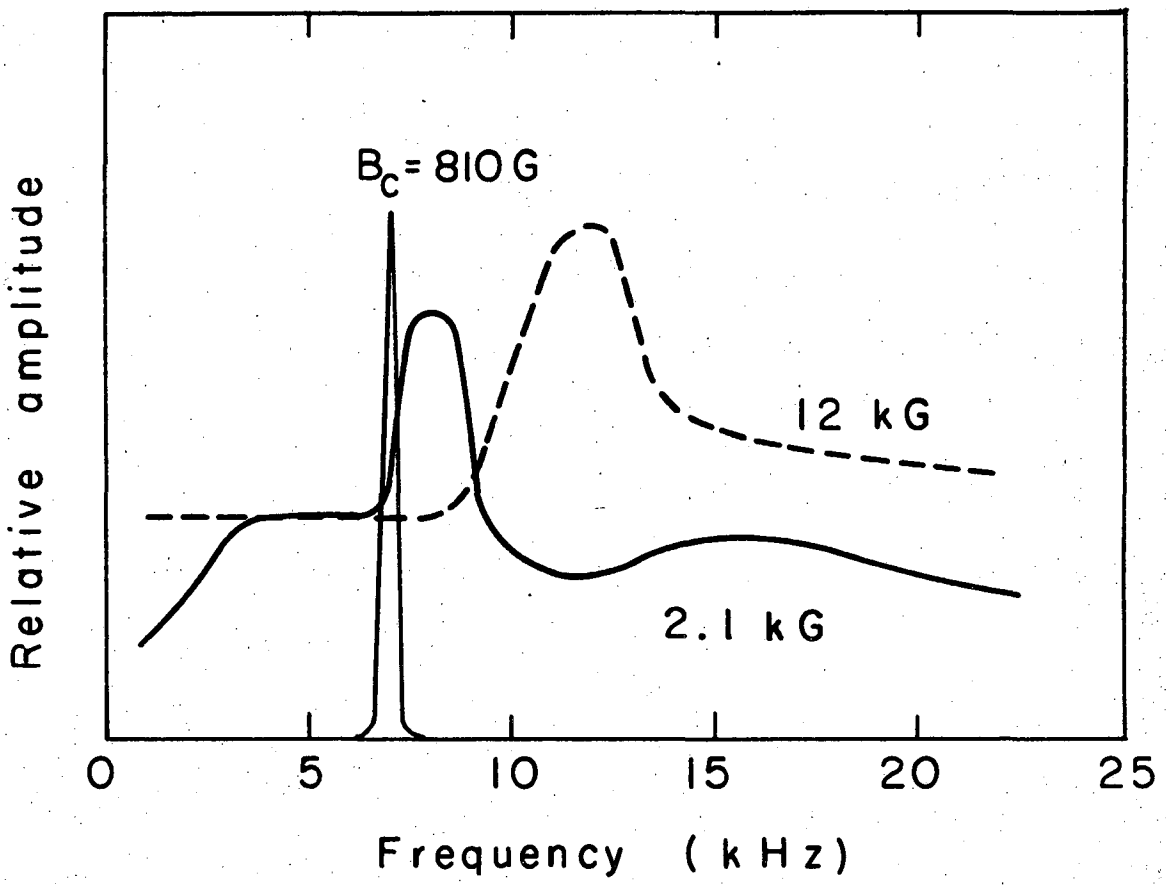

Fig. 21. Fluctuating azimuthal electric field spectra. p = 300 mTorr.

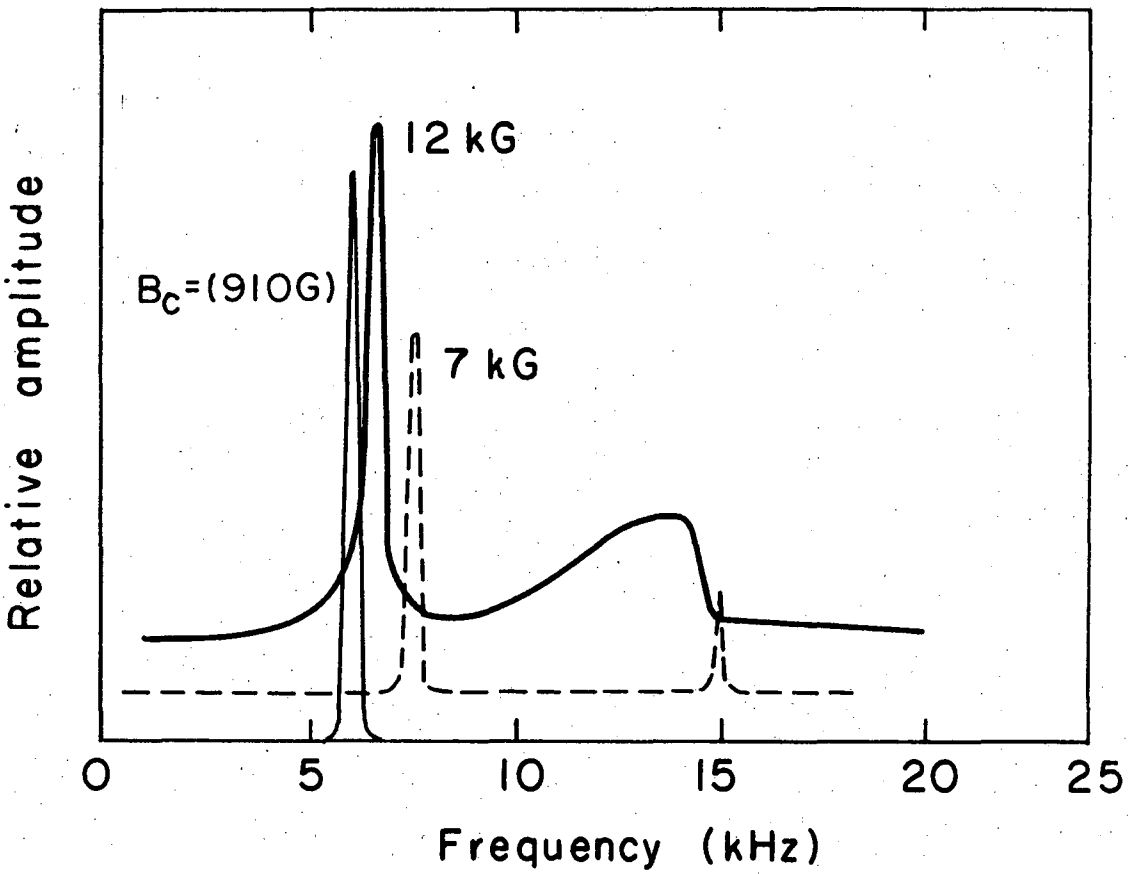

XBL6812-7415

Fig. 22. Fluctuating azimuthal electric field spectra. p = 400 mTorr.

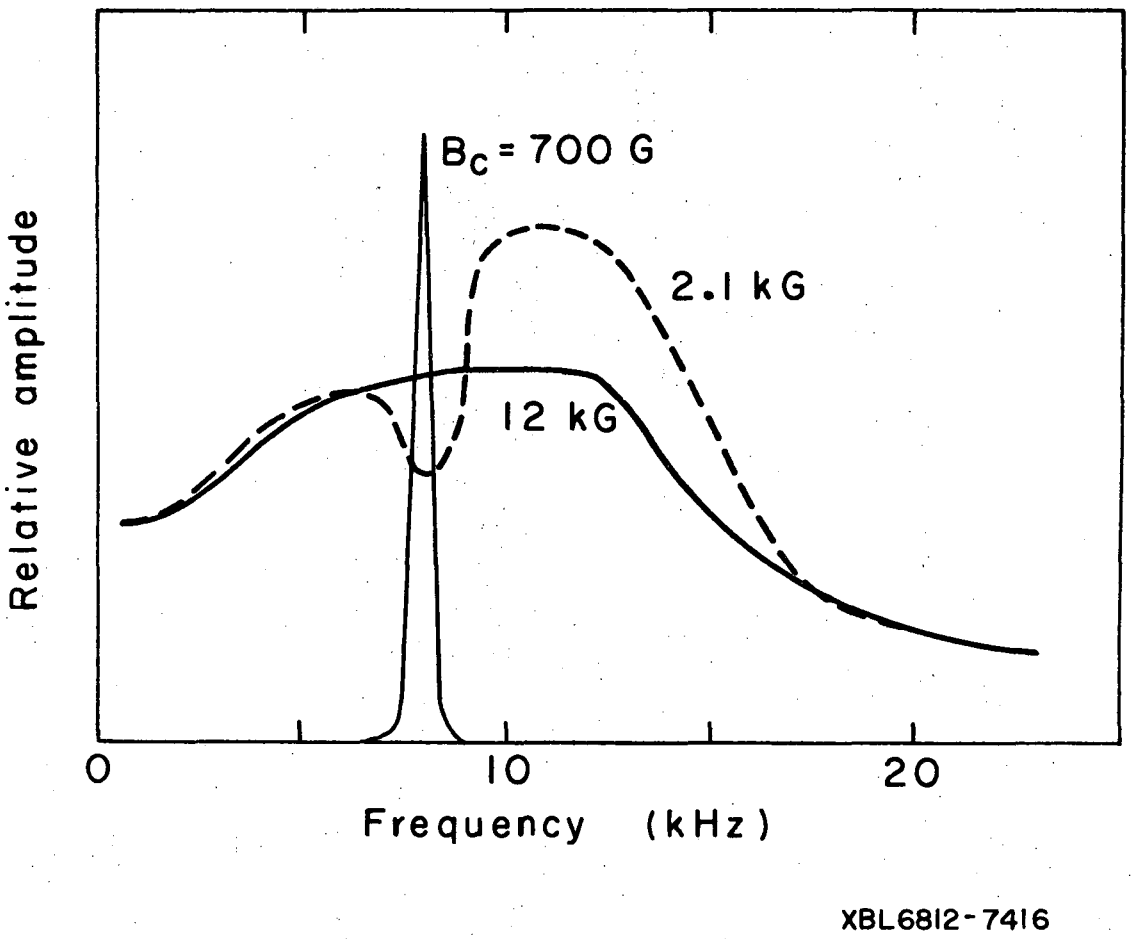

Fig. 23. Fluctuating density spectra. p = 200 mTorr.

average density was measured at r = 1.5 cm as a function of pressure and magnetic field. The radial variation of this quantity for a pressure of 200 mTorr as a function of magnetic field was also measured. Results are shown in Figs. 24 and 25.

D. Correlations

Both radial and azimuthal correlations were obtained at magnetic fields up to 12 kG in the positive column. Earler data,[15] taken at lower magnetic fields, have indicated only the presence of an m = 1 helical mode accompanied by a regular oscillation with no azimuthal variation.

Radial density correlations ($R_\perp$) taken for pressures ranging from 80 to 400 mTorr and a current of 400 mA are shown in Figs. 26 through 30. The points were taken with the fixed probe located 1 cm into the plasma. This permitted data to be taken with the movable probe on the opposite side of the axis. If the m = 1 mode is dominant, it will appear as a significant negative correlation when the probes are on opposite sides of the column axis. The presence of higher modes can be discounted in most cases because the higher frequencies associated with these modes are not observed in the frequency spectra.

For a different axial current, I = 200 mA, and for B = 7 and B = 12 kG when the pressure is 200 mTorr, the radial correlations are shown in Fig. 31. The results are essentially identical to those obtained for a current of 400 mA.

Small negative correlations are observed at 12 kG when the probes are 180 deg apart. These may be attributable to experimental error,

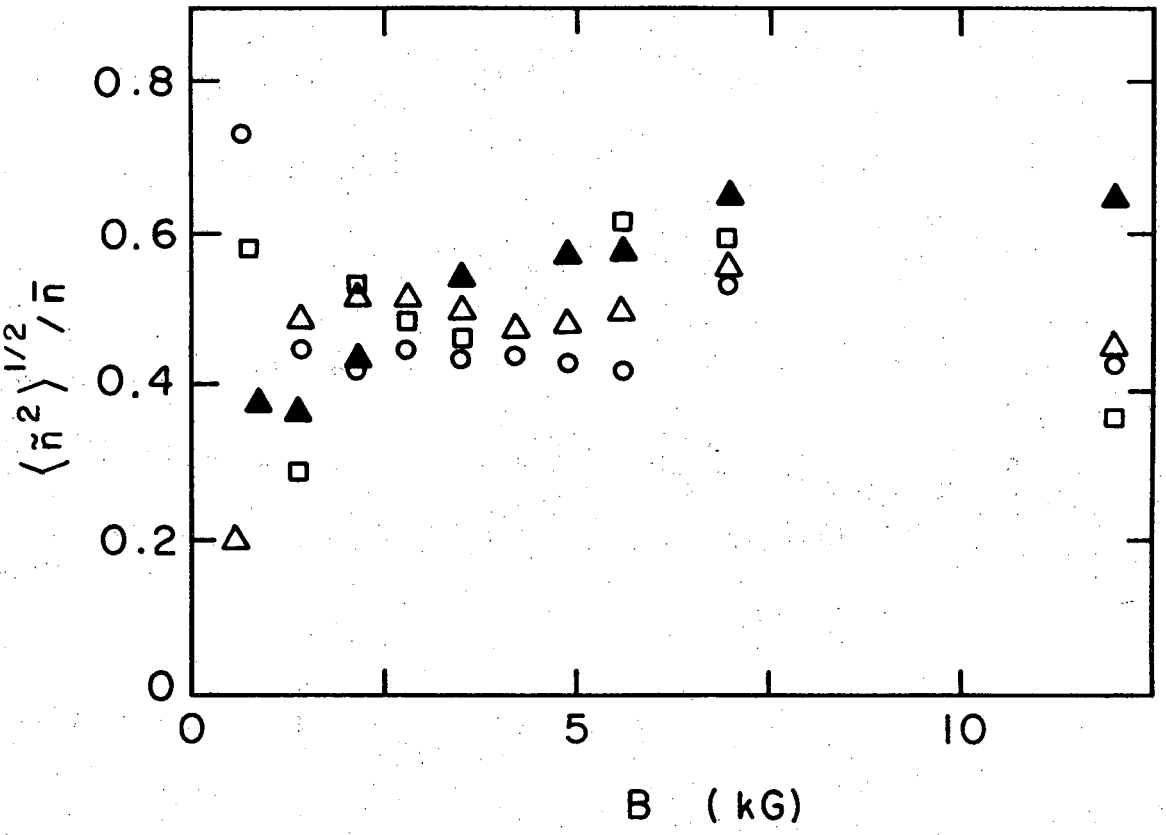

XBL6812-7417

Fig. 24. Relative level of density fluctuations vs magnetic field. △, p = 80 mTorr; o, p = 120 mTorr; □, p = 200 mTorr; ▲, p = 400 mTorr.

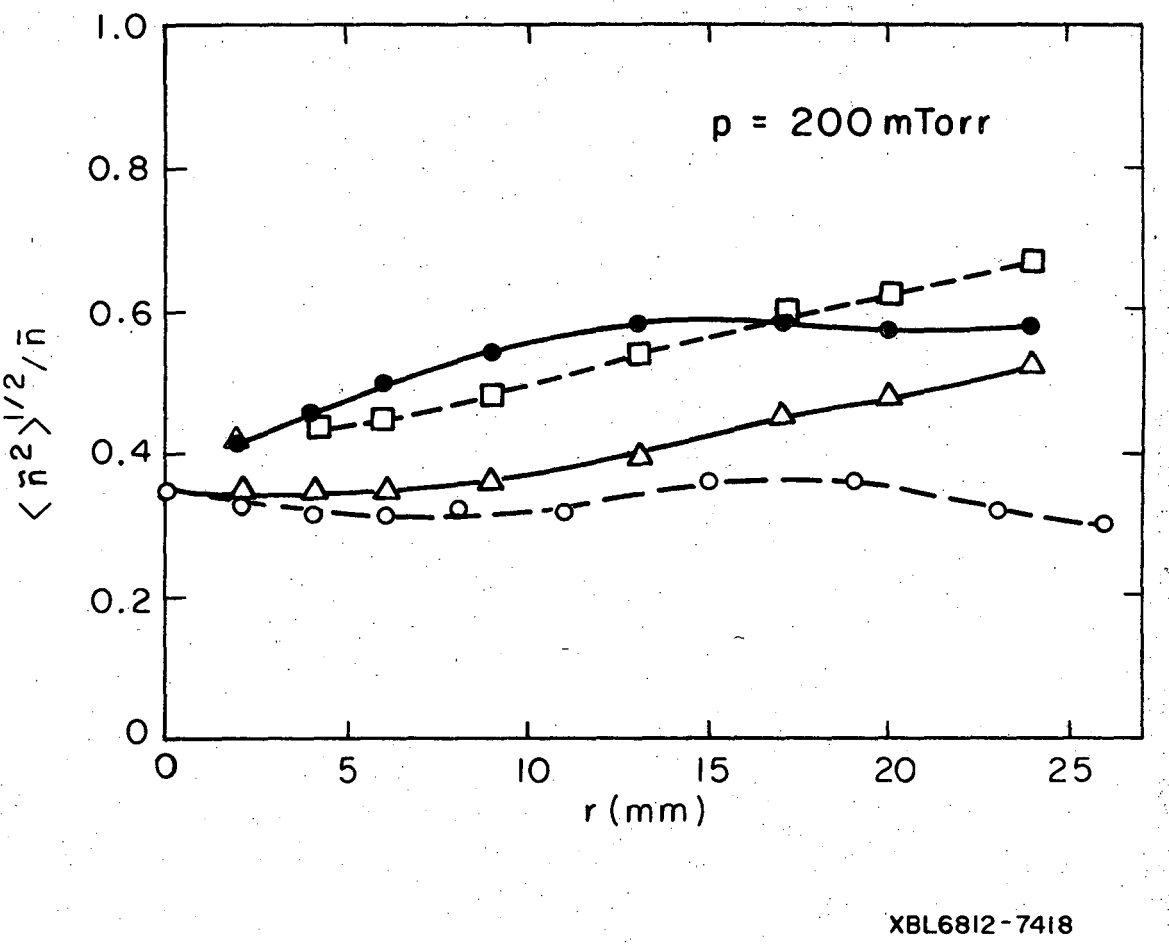

Fig. 25. Relative level of density fluctuations vs radius.

●, B = B_c (700 G); △, B = 3.5 kG; □, B = 7 kG; ○, B = 12 kG.

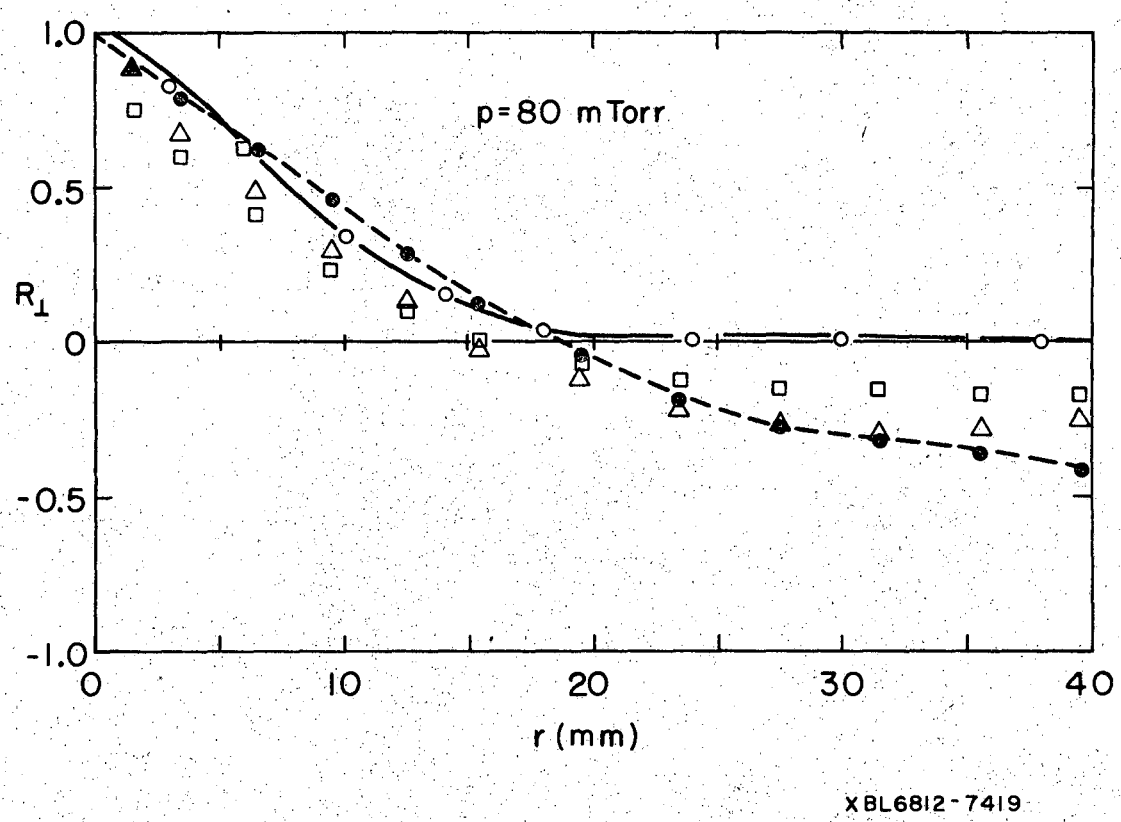

Fig. 26. Radial density correlation vs radial separation. p = 80 mTorr. ●, B = 2.1 kG; △, B = 3.5 kG; □, B = 7 kG; o, B = 12 kG.

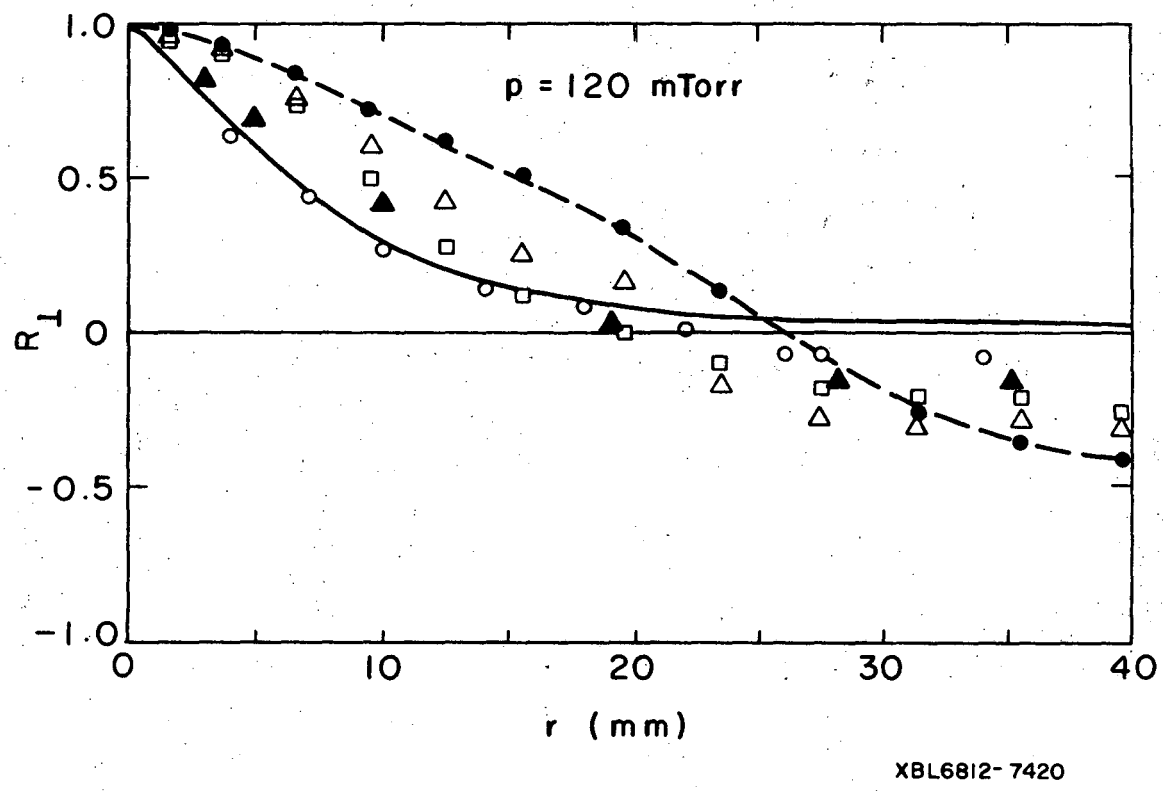

Fig. 27. Radial density correlation vs radial separation. p = 120 mTorr. ●, B = 2.1 kG; △, B = 3.5 kG; □, B = 7 kG; ▲, B = 10 kG; o, B = 12 kG.

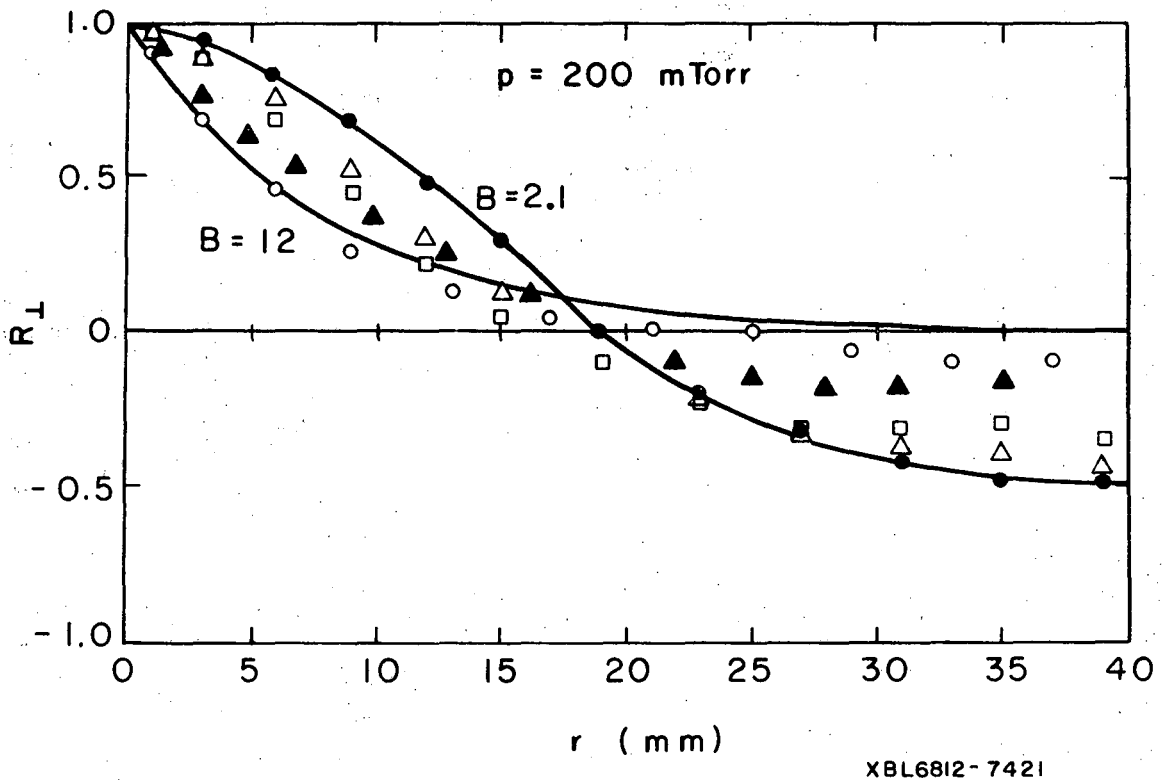

Fig. 28. Radial density correlation vs radial separation. p = 200 mTorr. ●, B = 2.1 kG; △, B = 3.5 kG; □, B = 7 kG; ▲, B = 10 kG; ○, B = 12 kG.

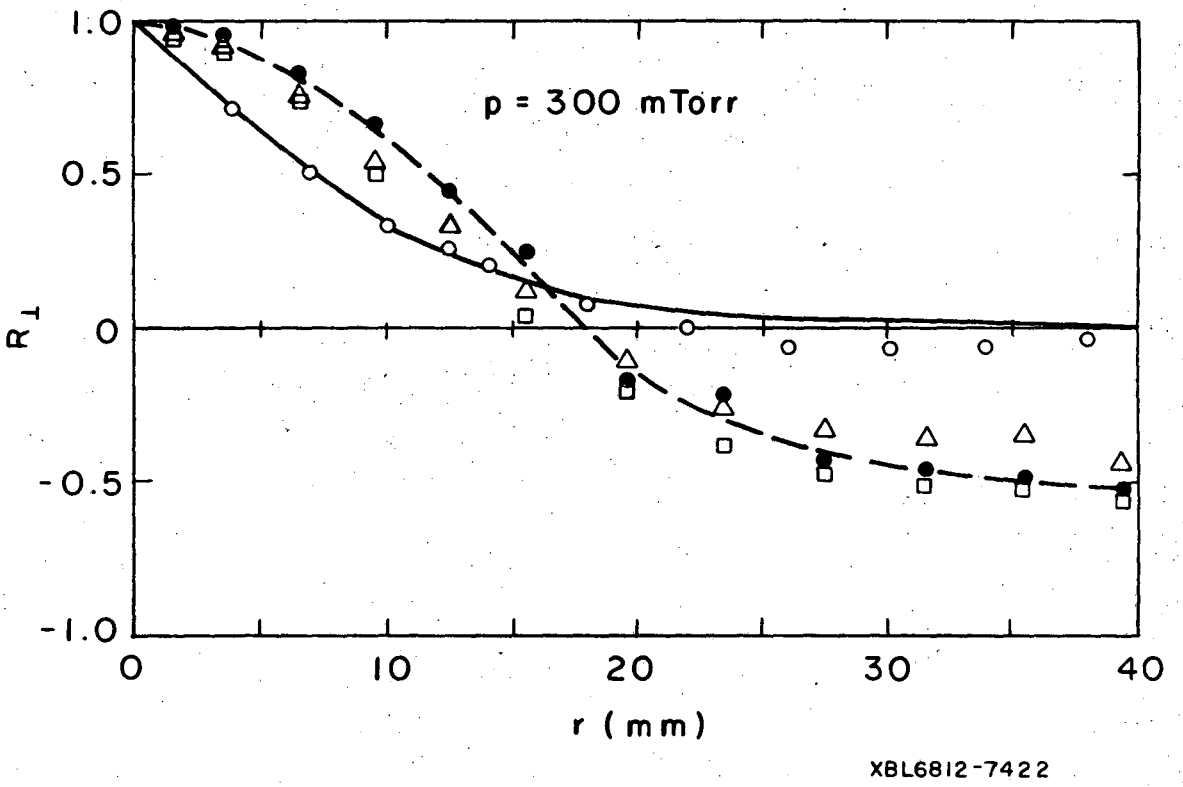

Fig. 29. Radial density correlation vs radial separation. p = 300 mTorr. ●, B = 2.1 kG; △, B = 3.5 kG; □, B = 7 kG; o, B = 12 kG.

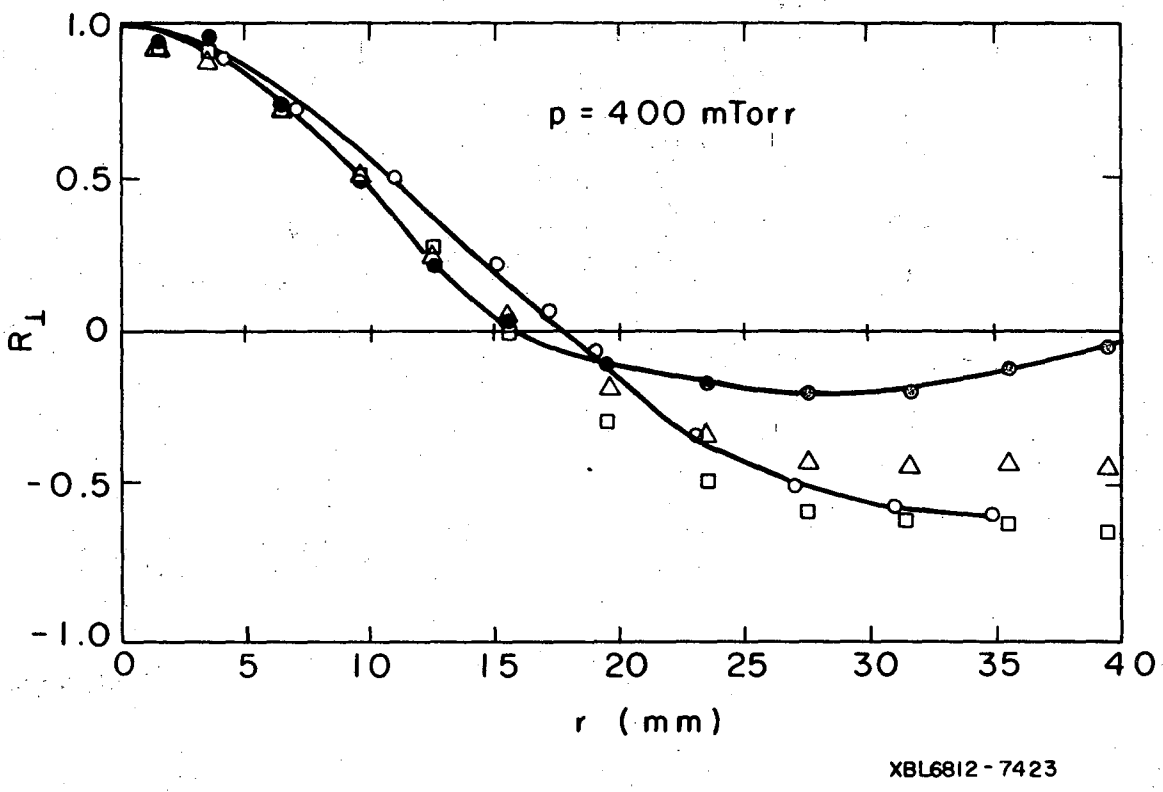

Fig. 30. Radial density correlation vs radial separation. p = 400 mTorr. ●, B = 2.1 kG; △, B = 3.5 kG; □, B = 7 kG; ○, B = 12 kG.

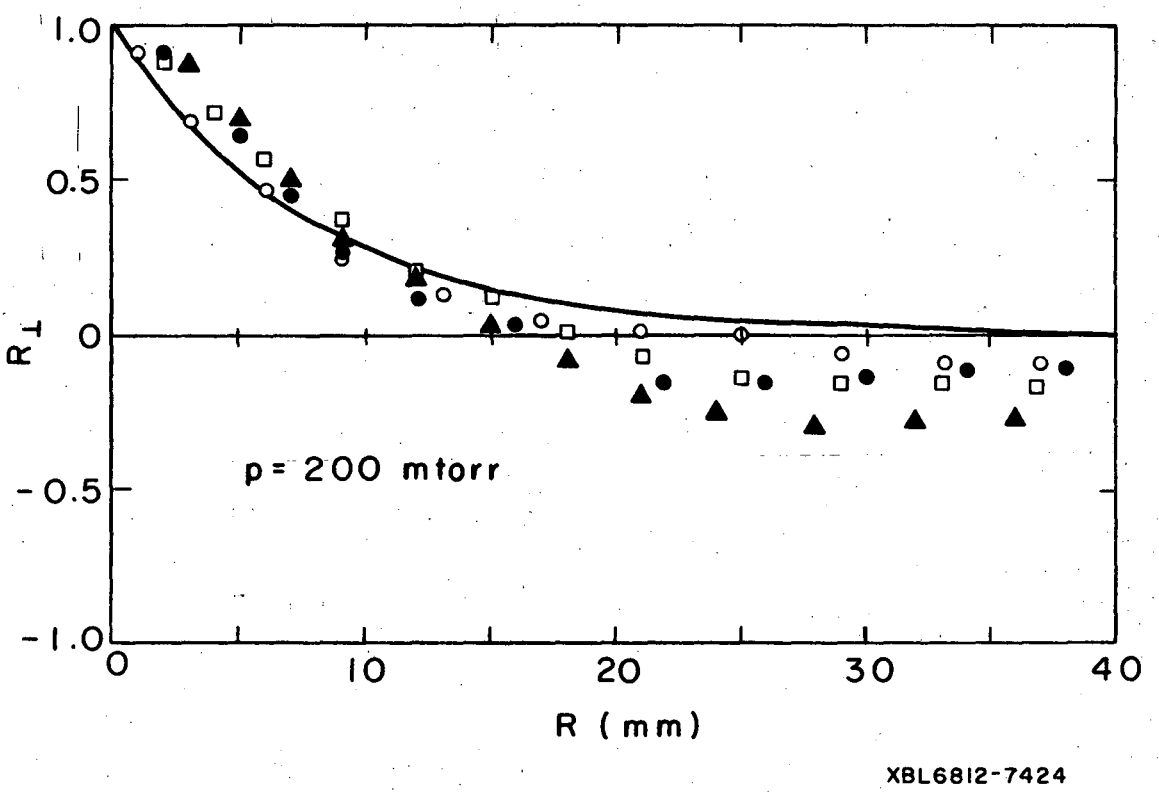

Fig. 31. Radial density correlation vs radial separation. p = 200 mTorr. □, B = 7 kG, I = 200 mA; o, B = 12 kG, I = 400 mA; ●, B = 12 kG, I = 200 mA; Δ, B = 12 kG, I = 400 mA, probe tip diameter = 2 mil.

since the possible error in the correlating electronics is about 10%. The fact that all results are similar, however, would indicate that a small portion of the fundamental helix does not decay.

At lower magnetic fields than 12 kG, the helical mode is clearly dominant. The signals would be 180 deg out of phase on the two probes when the probes are on opposite sides of the axis except for the presence of the m = 0 mode. The shape of the radial correlation at 7 kG suggests that there is turbulence in the plasma, but a comparison with the correlation at 12 kG when the probes are in radial positions such that the helical portions of the two signals are out of phase shows that the fundamental helical mode is stronger at 7 kG.

Radial correlation of the azimuthal electric field and the ion density when the two probes, located equidistant from the axis on a diameter, were 35 mm apart, was made (Fig. 32) to check the density correlation measurements. If the ion density correlation at 12 kG is in error because of the influence of the azimuthally symmetric mode, this error will be apparent here. Only the helical portions of the electric field and density signals provide a nonzero correlation, which in this case will be negative if the helix is present.

In order to determine the relative amounts of m = 0 and m = 1 fluctuation, density correlation measurements were made between a radial probe and an axial probe separated by 90 deg and both located at the same axial position and 1.5 cm from the center. Unless the system is turbulent, the positive value of the signal is the fraction of the oscillations in the plasma that are azimuthally symmetric. In

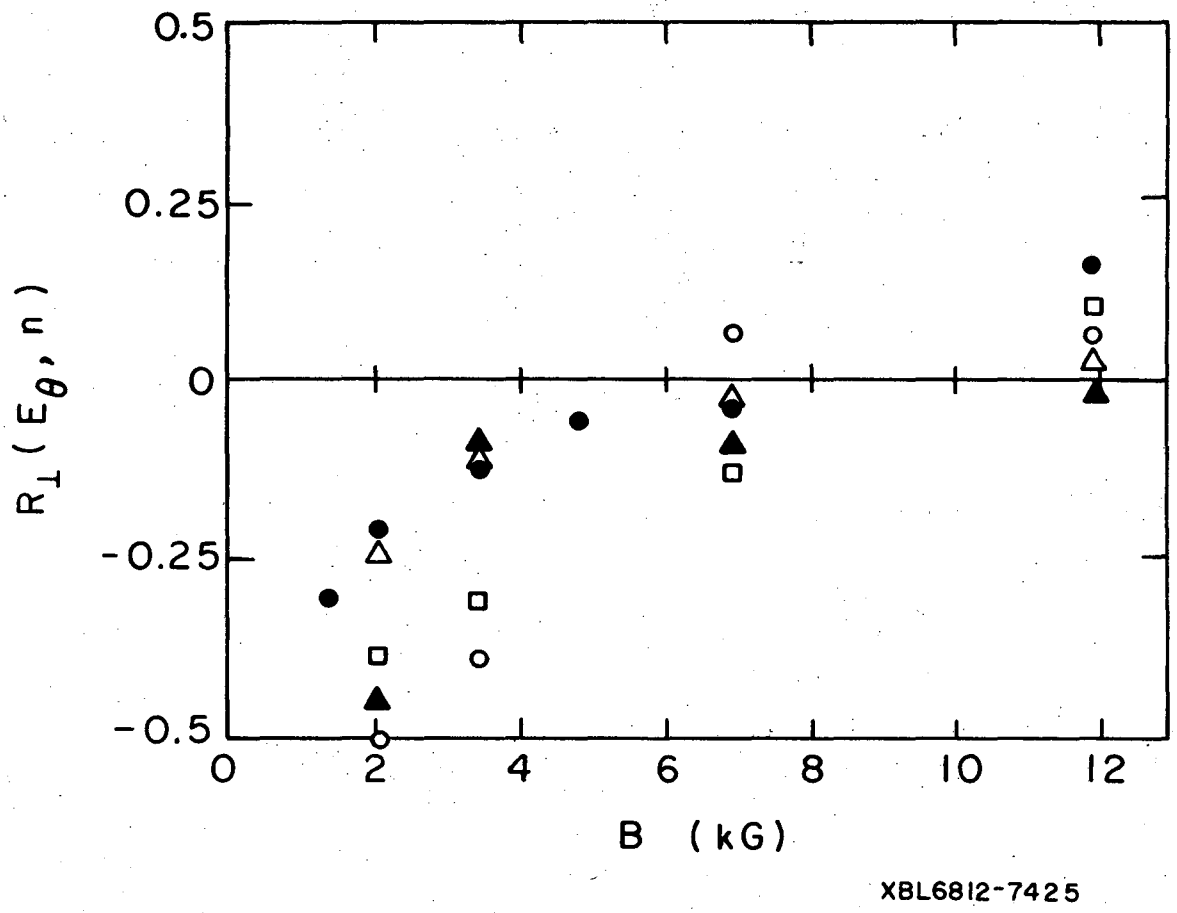

Fig. 32. Radial correlation of $\langle \tilde{E}_\theta \tilde{n} \rangle_\perp$ vs magnetic field--probes 180 deg apart and 1.5 cm from center. ●, p = 80 mTorr; Δ, p = 120 mTorr; o, p = 200 mTorr; □, p = 300 mTorr; ▲, p = 400 mTorr.

the case of turbulence, the signal is a measure of the transverse decay in the spatial correlation between fluctuations. Results are given in Table I.

Table I. Fraction of signal that is azimuthally symmetric.

B (kG) \ P (mTorr)	80	120	200	300	400
1.4	0.16	0.21	0.38	0.59	0.48
3.5	0.07	0.25	0.32	0.03	0.14
7.0	0.05	0.11	0.09	0.03	0.21
12	0.04	0.07	0.05	0.07	0.04

The degree of homogeneity of the plasma turbulence was determined by comparing the results taken when the fixed probe was 1 cm from the wall nearest its entrance port with measurements of the radial correlation with the fixed probe located 3 mm from the center on the same side as the movable probe. Results for a pressure of 200 mTorr are Shown in Fig. 33. The results at 12 kG in Fig. 33 differ only slightly from the results of Fig. 28 taken with the fixed probe 1 cm from the side, indicating that the turbulence is homogeneous in the region within 2 cm of the tube center. Results at lower fields differ because the helix is present.

The difference in results obtained when straight double probes are used in correlation measurement instead of the bent probes, which

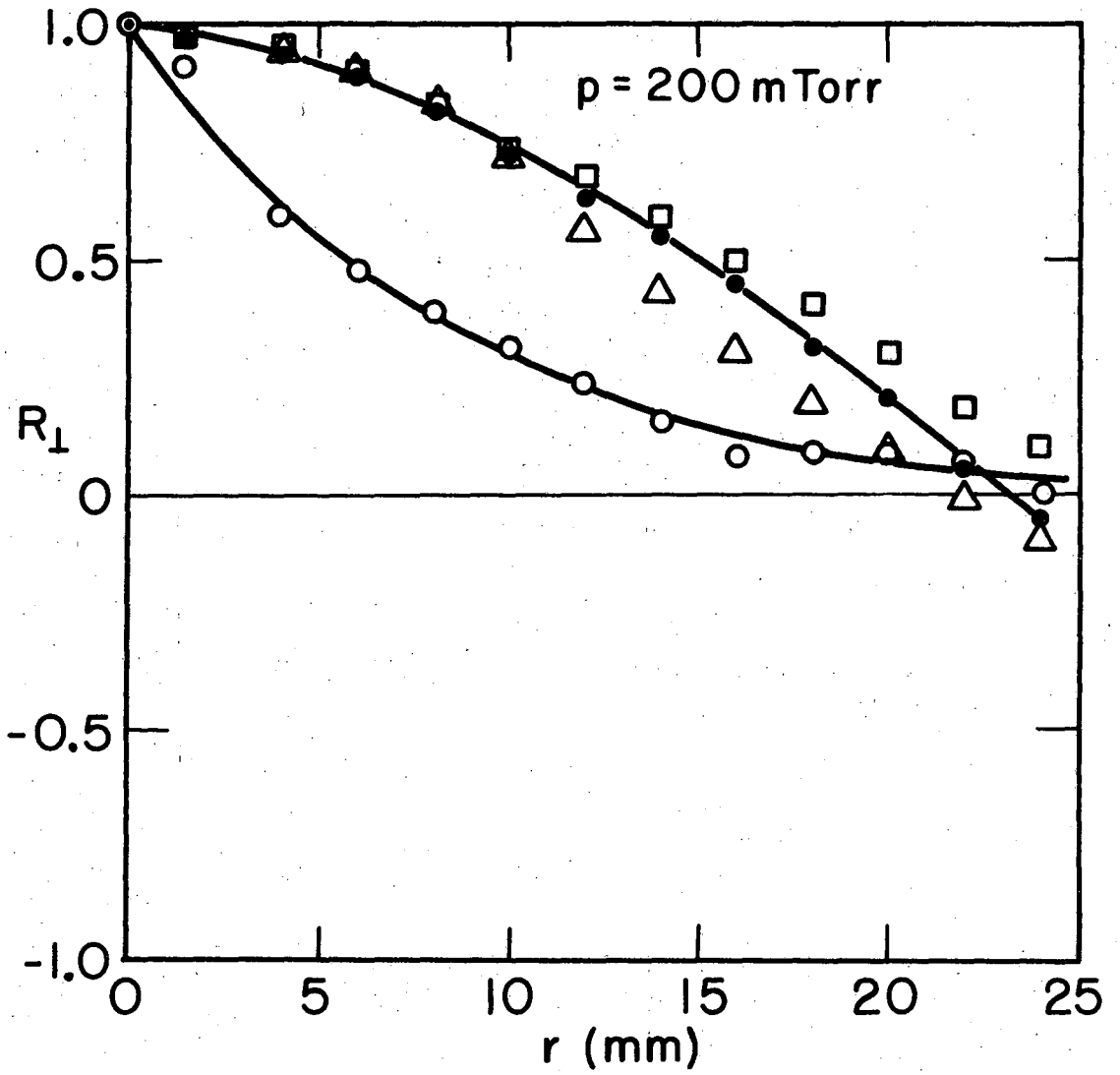

XBL6812-7426

Fig. 33. Radial density correlation vs radial separation; fixed probe 3 mm from center on same side as movable probe. p = 200 mTorr. ●, B = 2.1 kG; △, B = 3.5 kG; □, B = 7 kG; o, B = 12 kG.

isolate the data-gathering probe tips from the bulky entrance segments of the probes, is shown in Fig. 34. The increase in correlation is quite probably a result of the interference between the two entrance lengths, which are at the same axial positions as the probe tips.

At 12 kG the ion cyclotron radius is 2 mils for an ion at room temperature. This is approximately equal to the radius of a probe tip, and there may be interference effects because of the ions that are removed from the plasma by the probe. To determine the magnitude of this effect, a radial correlation was made with 2-mil-diam probe tips on the usual bent probes. Results, seen in Fig. 31, indicate that interference effects are not serious for the 5-mil probe tips.

Turbulent fluctuations have a cell size associated with their wave length beyond which there is no interaction with other fluctuations. The mixing length defined by Prandtl[40] for hydrodynamic turbulence is essentially the integral of the correlation integrated over the path of separation, i.e., the average cell size. Since to a good approximation a correlation curve in fluid turbulence is an exponentially decreasing function, the mixing length can be taken as the decay length of the correlation function.

Figure 35 shows the calculated length at 12 kG, obtained by fitting the data to a decaying exponential and ignoring the region of negative correlations. Also included is the mixing-length curve predicted in Kadomtsev's theory for the turbulent positive column and obtained with the aid of the measured electric field at 12 kG.

If the m = 1 mode is still strong at high pressures, at which

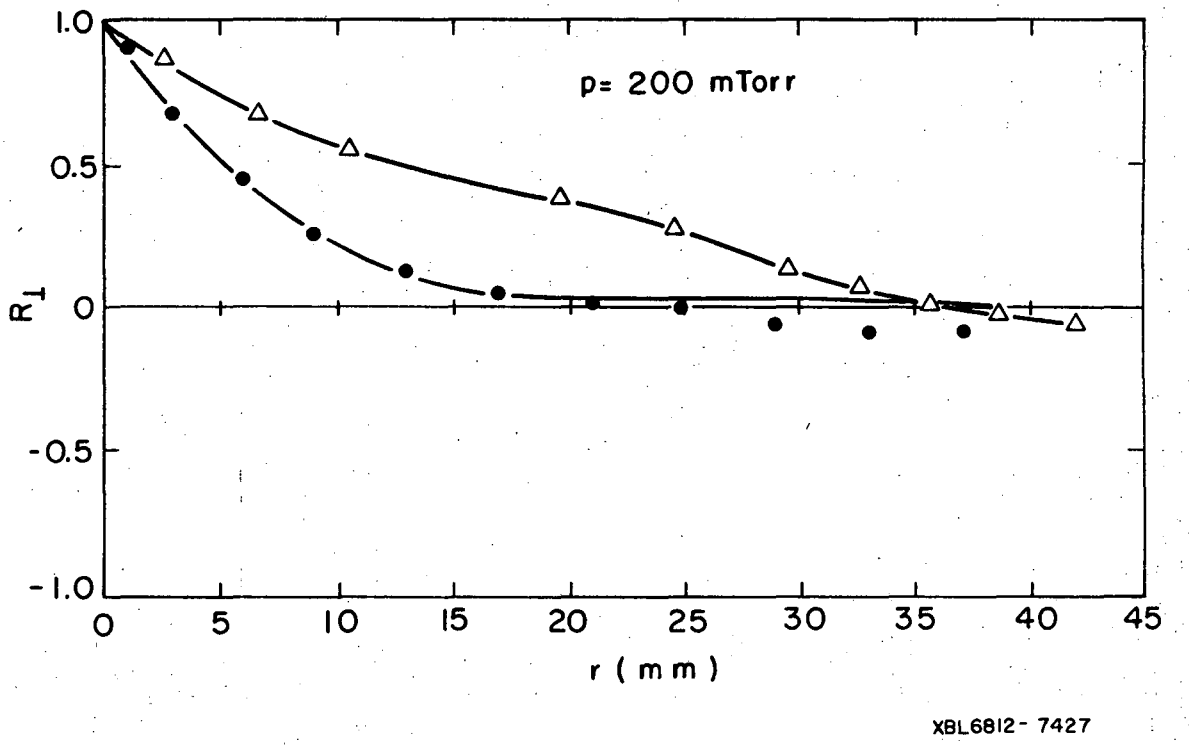

Fig. 34. Radial density correlation vs radial separation. p = 200 mTorr. ●, bent probe (standard configuration used in experiment); △, straight probe.

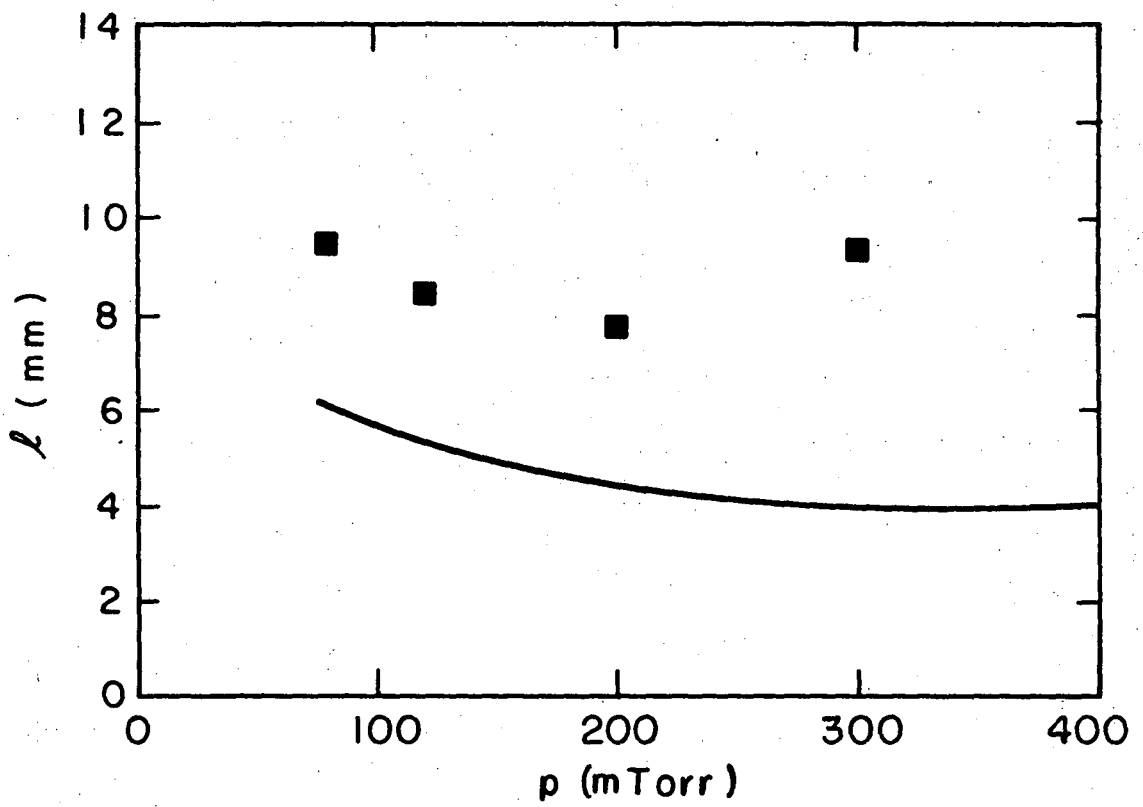

Fig. 35. A comparison between the radial mixing length as a function of pressure as calculated from Kadomtsev's theory of turbulence and the radial correlation length as measured in this experiment.

B over B_c is less for a given B, the radial correlation is dominated by the helical oscillation rather than the random oscillations also present. The mixing length taken from the data is then increased because the effect of the helix is to increase the value of the correlation when the two probes are on the same side of the axis. Then the mixing length should increase with pressure for high pressures, in opposition to the predicted trend.

Axial correlation measurements were obtain in the same manner as were the radial data. Results are shown in Figs. 36 through 41. The axially mobile probes were built with a double bend in the shape of a dogleg in order to reduce the distortion induced by the probe arm. The fixed probe was straight with only the tips bent along the field lines. With the fixed probe in place, the axial probe could be rotated to read the signal on or near the field lines passing by the fixed probe tips or the signal at the same radial positions 180 deg away from the fixed probe.

Results of axial density correlations may be ambiguous because there are two types of oscillations present, one of which, the m = 0, is azimuthally symmetric. However, if data are taken with the axial probe separated azimuthally by 180 deg from the fixed probe's field line as well as being taken with the probe near the field line, the two modes can be separated. The correlation between one signal and a second signal at another axial position is independent of the azimuthal separation in the case of the m = 0 wave, and proportional to the cosine of the azimuthal separation for the m = 1 wave. The

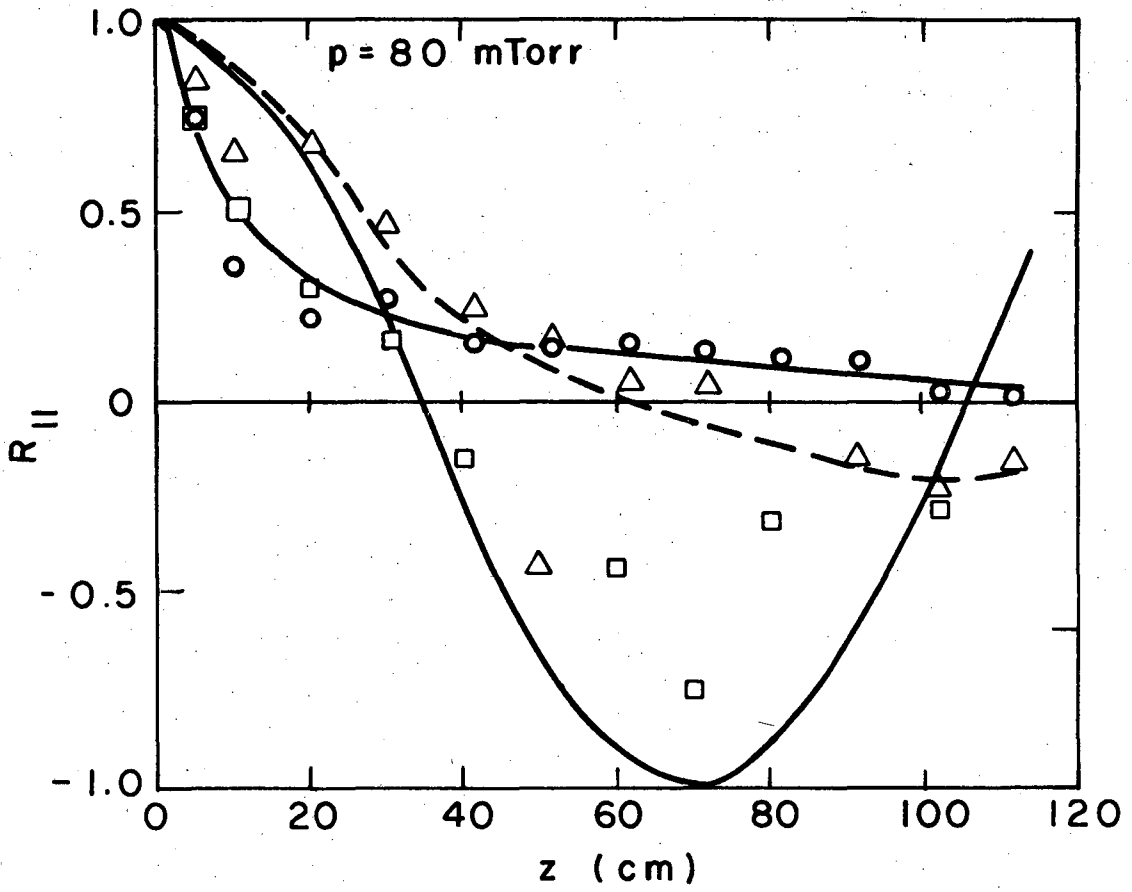

Fig. 36. Axial m = 1 density correlation vs axial separations p = 80 mTorr. All curves drawn to fit data, except for the curve for B = B_c which is fit to a cosine shape. □, B = B_c (560 G); △, B = 5.6 kG; o, B = 12 kG.

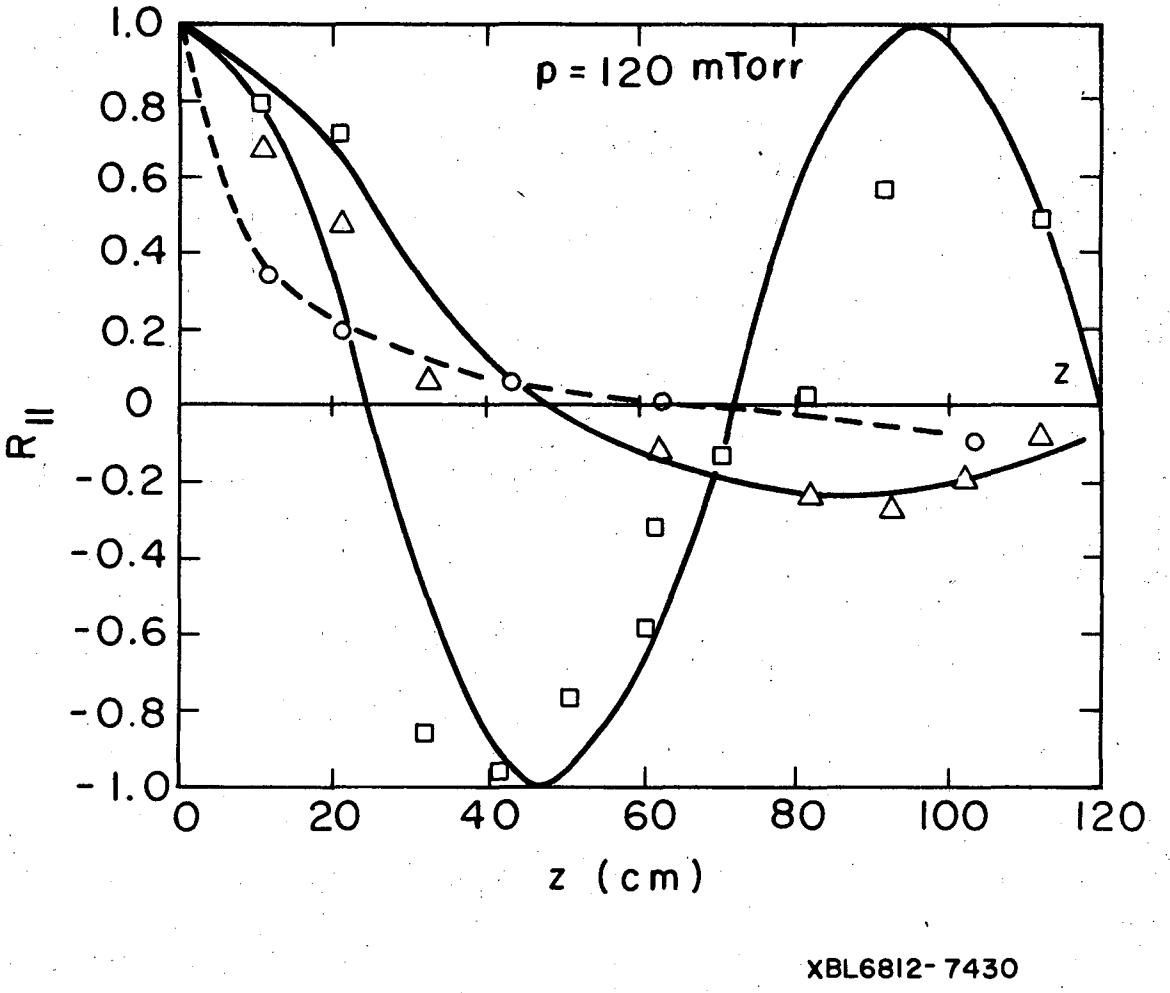

Fig. 37. Axial m = 1 density correlation vs axial separation. p = 120 mTorr. □, B = B_c (630 G); Δ, B = 5.6 kG; o, B = 12 kG.

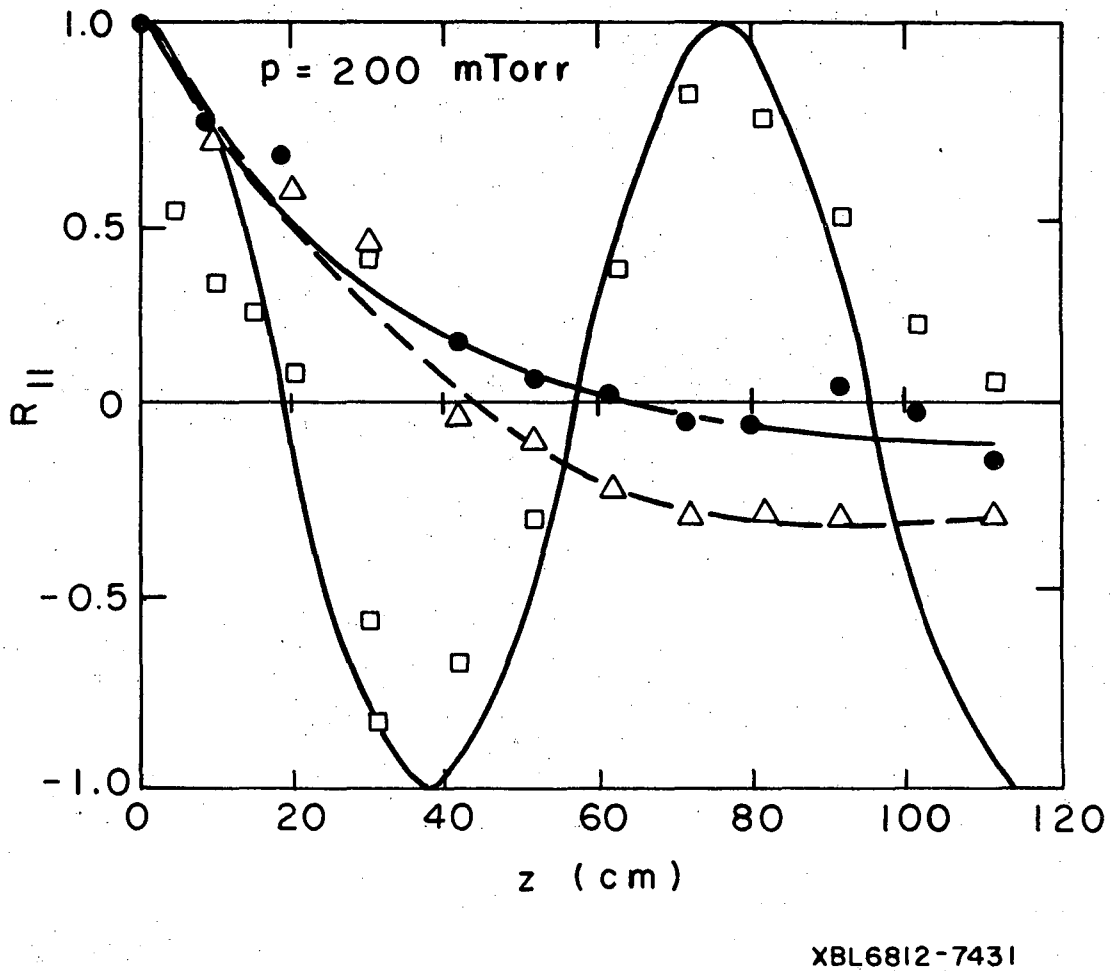

Fig. 38. Axial m = 1 density correlation vs axial separation. p = 200 mTorr. All curves drawn to fit data, except for the curve for $B = B_c$ which is fit to a cosine shape. □, $B = B_c$ (700 G); △, B = 5.6 kG; o, B = 12 kG.

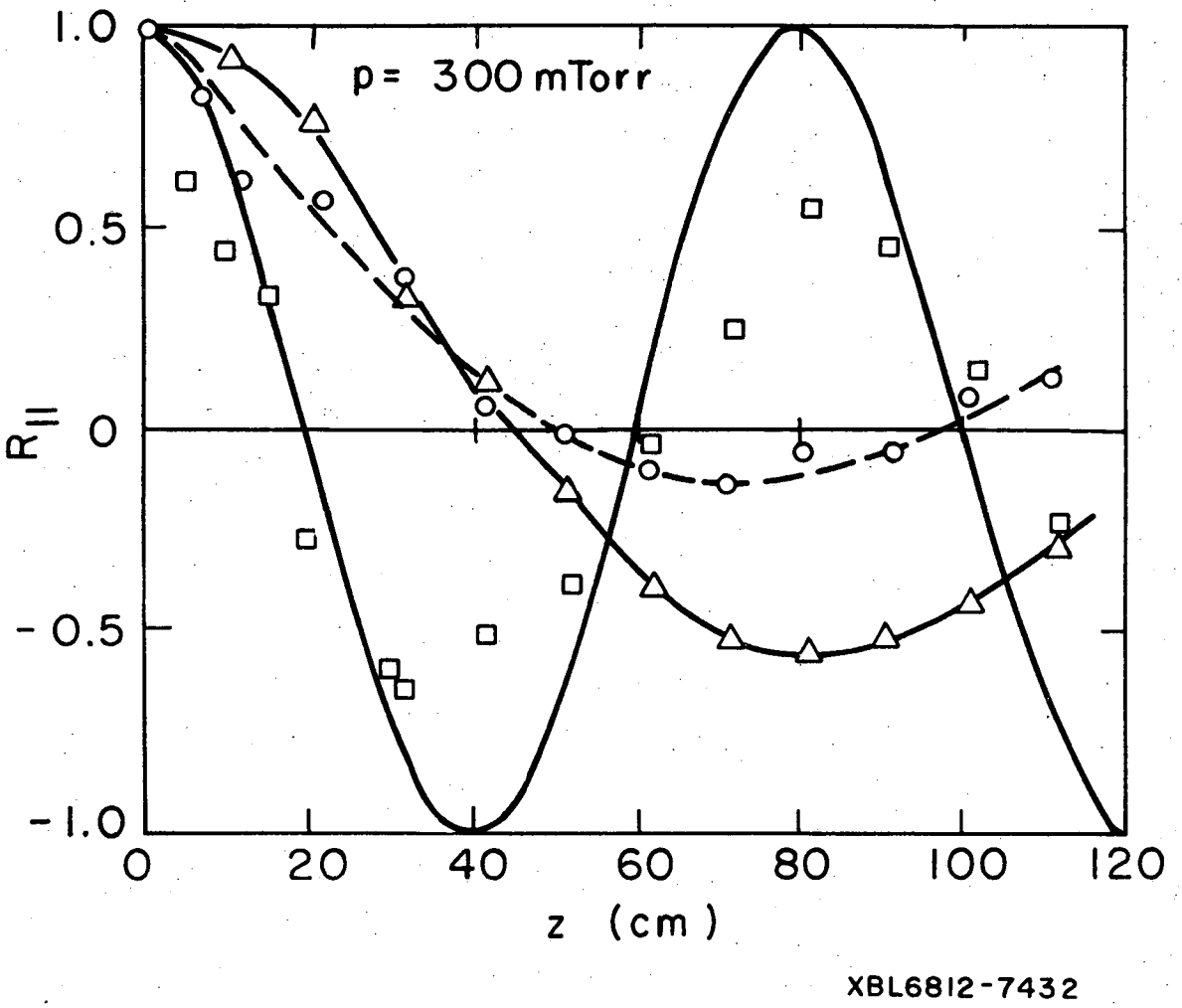

Fig. 39. Axial m = 1 density correlation vs axial separation. p = 300 mTorr. All curves drawn to fit data, except for the curve for B = B_c which is fit to a cosine shape. □, B = B_c (805 G); △, B = 5.6 kG; o, B = 12 kG.

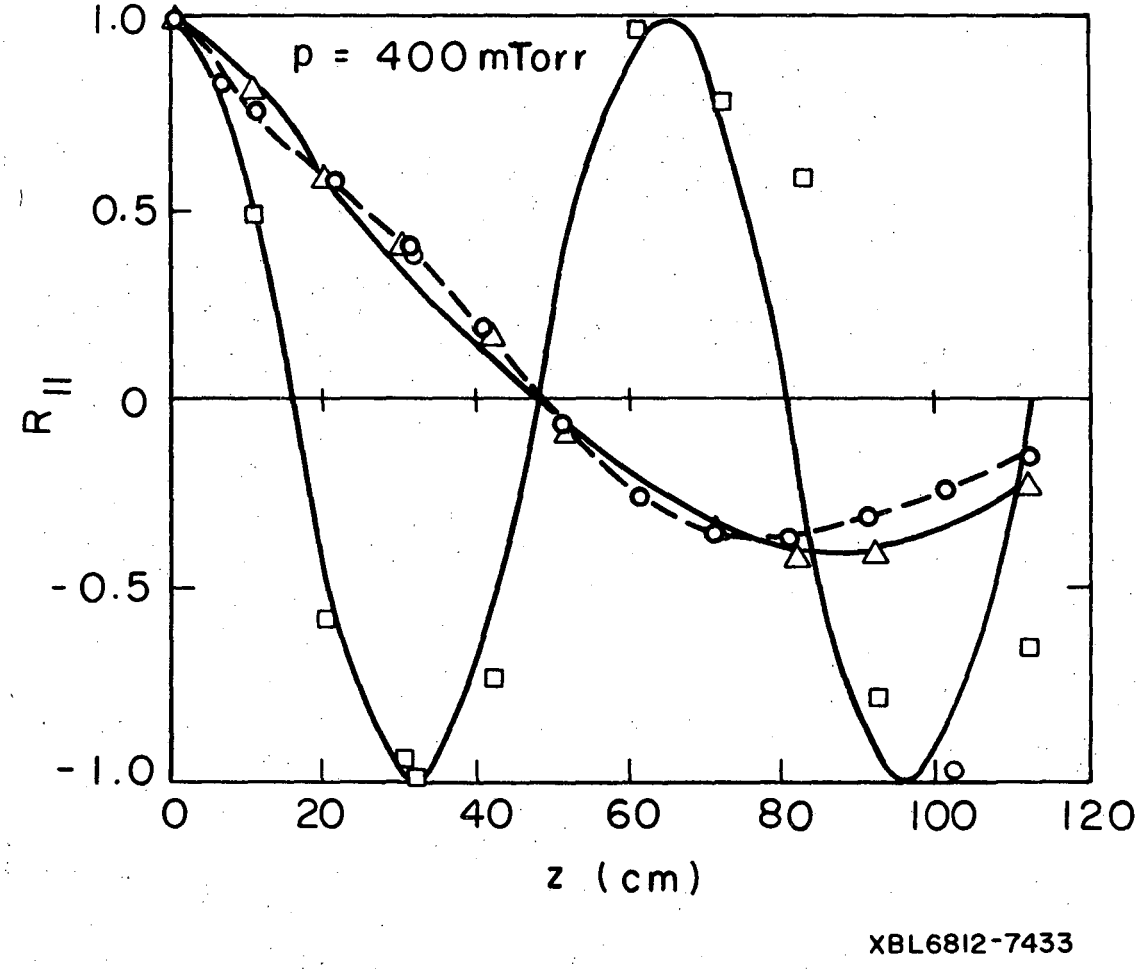

Fig. 40. Axial m = 1 density correlation vs axial separation. p = 400 mTorr. All curves drawn to fit data, except for the curve for B = B_c which is fit to a cosine shape. □, B = B_c (910 G); △, B = 5.6 kG; o, B = 12 kG.

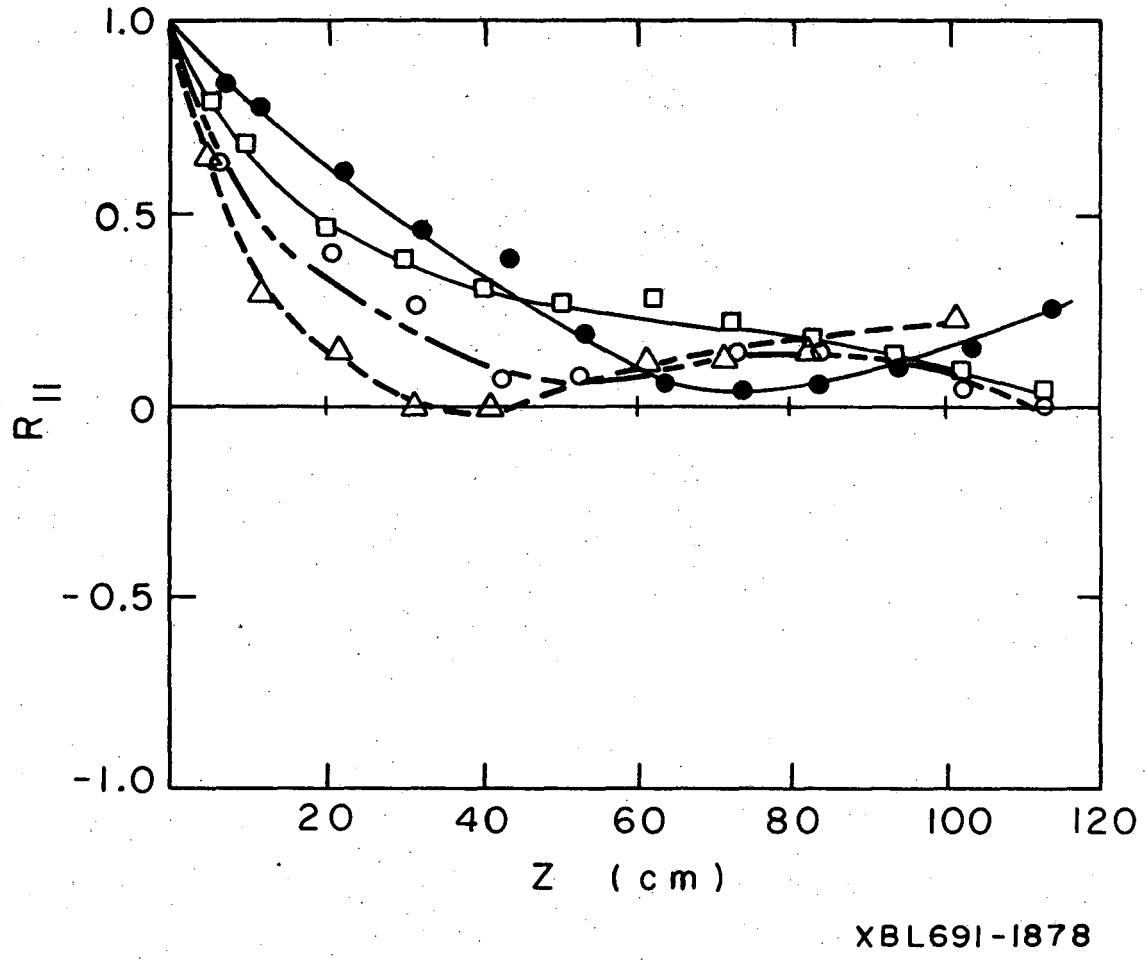

Fig. 41. Axial density correlation vs axial separation. B = 12 kG, curves drawn to fit data. o, p = 80 mTorr; Δ, p = 120 mTorr; □, p = 200 mTorr; ●, p = 400 mTorr.

weighted difference between the two correlations, assuming that no higher modes exist and assuming that the m = 0 mode is perfectly correlated radially, gives the shape of the fundamental helix:

$$R_{m=1}(z_1,z_2,\theta = 0^\circ) = \frac{R(z_1,z_2,\theta = 0^\circ) - R(z_1,z_2,\theta = 180^\circ)}{R(z_1,z_1,\theta = 0^\circ) - R(z_1,z_1,\theta = 180^\circ)}$$

From this, the wavelength and the amount of axial decay of the helix can be found. Results are shown in Table II.

Included in Table II are calculations of the axial wavelength found by using the linear theory of Johnson and Jerde when $B = B_c$ and the quasi-linear semi-empirical theory of Sheffield when the m = 1 mode was dominant. The temperature of the electrons was calculated from the experimental curve on page 474 of Ref. 6. It was assumed that the electron temperature was a unique function of E_z/p, but not a unique function of ap.

When the magnetic field is at 12 kG both the correlation along the field line (Fig. 41) and the correlation used in Figs. 36 through 40 are important. Both show no sinusoidal variation. This fact and their rapid decay, except in the 400-mTorr case, indicate absence of both the helix and the azimuthally symmetric oscillation. Decay lengths measured by fitting exponential curves to the data in Figs. 36 through 41 were included in Table II (an average value of the results from Figs. 36 through 40 and from Fig. 41 was used), and the results were compared with the calculations of $\ell_{||}$ made with Eq. (II-26) from Ref. 35.

Table II. Axial wavelength and correlation length.

p (mm Hg)	B (kG)	λ(cm) measured	λ(cm) computed	ℓ(cm) measured	ℓ(cm) computed
80	B_c = 0.560	140	170	--	--
	3.5	256	153	--	--
	12	---	---	23	71
120	B_c = 0.630	96	132	--	--
	5.6	185	224	--	--
	12	---	---	12	42
200	B_c = 0.710	76	96	--	--
	5.6	175	134	--	--
	12	---	---	30	21
300	B_c = 0.805	80	76	--	--
	7	172	109	--	--
	12	---	---	28	13
400	B_c = 0.910	65	66	--	--
	7	195	78	--	--
	12	195	75	--	11

Presence of the helix at lower magnetic fields is observable in all the data taken. To check the appropriateness of the procedure for separating out the helical portion of the correlation, wavelengths were also measured at the critical field. The results agree with the theory (Table II), and the signal shows little decay even in the presence of a large m = 0 mode, indicating that separation of the two modes was obtained.

No measurements were made in the dc plasma at pressures above 400 mTorr because of the presence of striations and the low value of B_{max}/B_c.

E. Properties of the Electric Field During Transition from an ac to a dc Discharge

As a further inspection of the properties of the positive column when B is much larger than the critical field, the discharge was operated in an ac mode and measurements were made as the discharge was switched to a direct current. The discharge, which is stable in the ac mode,[41,42] develops a helical instability when the current is direct. Any higher modes generated should affect the behavior of the electric field during the time taken by the plasma to reach its final state.

Figure 42 illustrates the effects of the square wave on the electric field. Note that, although the magnetic field is much greater than the critical field in the dc case, the electric field is much lower than the value when B = 0. Also shown is the transition in electric field and current when B = 0. When a frequency less than

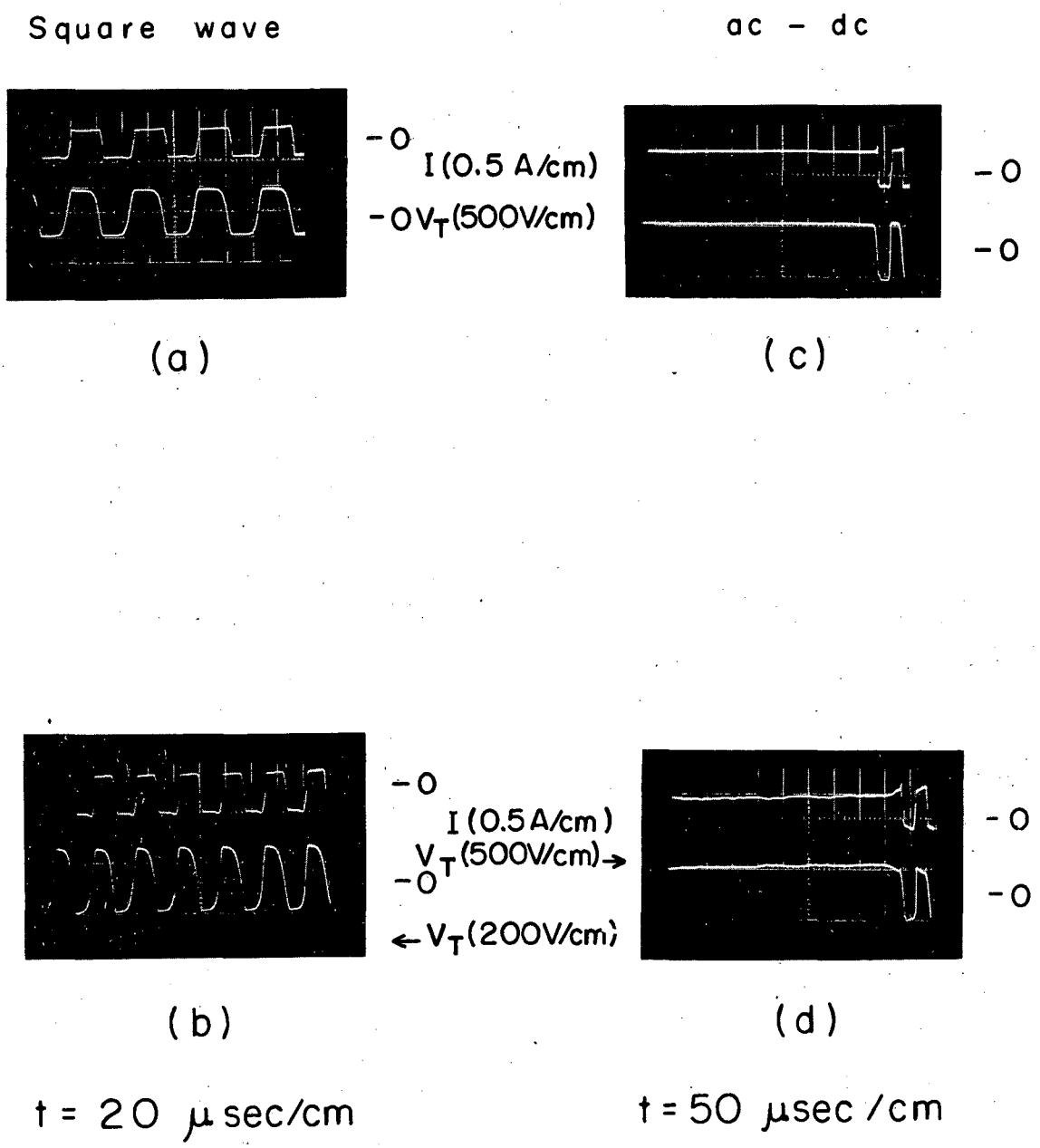

Fig. 42. Tube voltage and current vs time. p = 200 mTorr. I(dc) = I(ac, rms) = 400 mA. (a) B = 0, f = 20 kc; (b) B = 2.8 kG, f = 30 kc; (c) B = 0, f = 20 kc; (d) B = 3.5 kG, f = 20 kc < critical frequency.

the frequency necessary to prevent the growth of the instability is used in a high magnetic field, the transition to dc will be uninformative because of the disruptive effect the previous half cycle had on the plasma. This is also shown in Fig. 42.

Figure 43 shows a typical transition in the electric field when the frequency is greater than the critical frequency. The time-dependent voltage observed after the transition to a direct current represents the modes that are dominant in the plasma. Theory predicts that the electric field increases with mode number, and that the growth rate for the highest mode is largest. This agrees with the observed maximum in the electric field, which occurs about 50 μsec after the electric field changes direction.

Two hundred microseconds after the onset of instability, the final state is reached. This state corresponds in detail to that situation which exists if the magnetic field is raised from zero to the same value as in the transitional plasma. In both cases, no higher modes than m = 1 are found.

In Figs. 44 through 53 the measured peaks in the electric fields and their final values are plotted. Quasi-linear calculations corresponding to the Kadomtsev-Nedospasov theory and the Holter and Johnson theory were made for the first three modes. These are shown in the figures. The agreement between experimental and theoretical values as shown in the figures is not good except near the critical field. A mobility ratio of 100, an electron temperature of 3 eV, and an electron mobility of $76.0/p\ m^2/V\text{-sec}$ were used in the calculations. The electron temperature is not a strong function of pressure in this

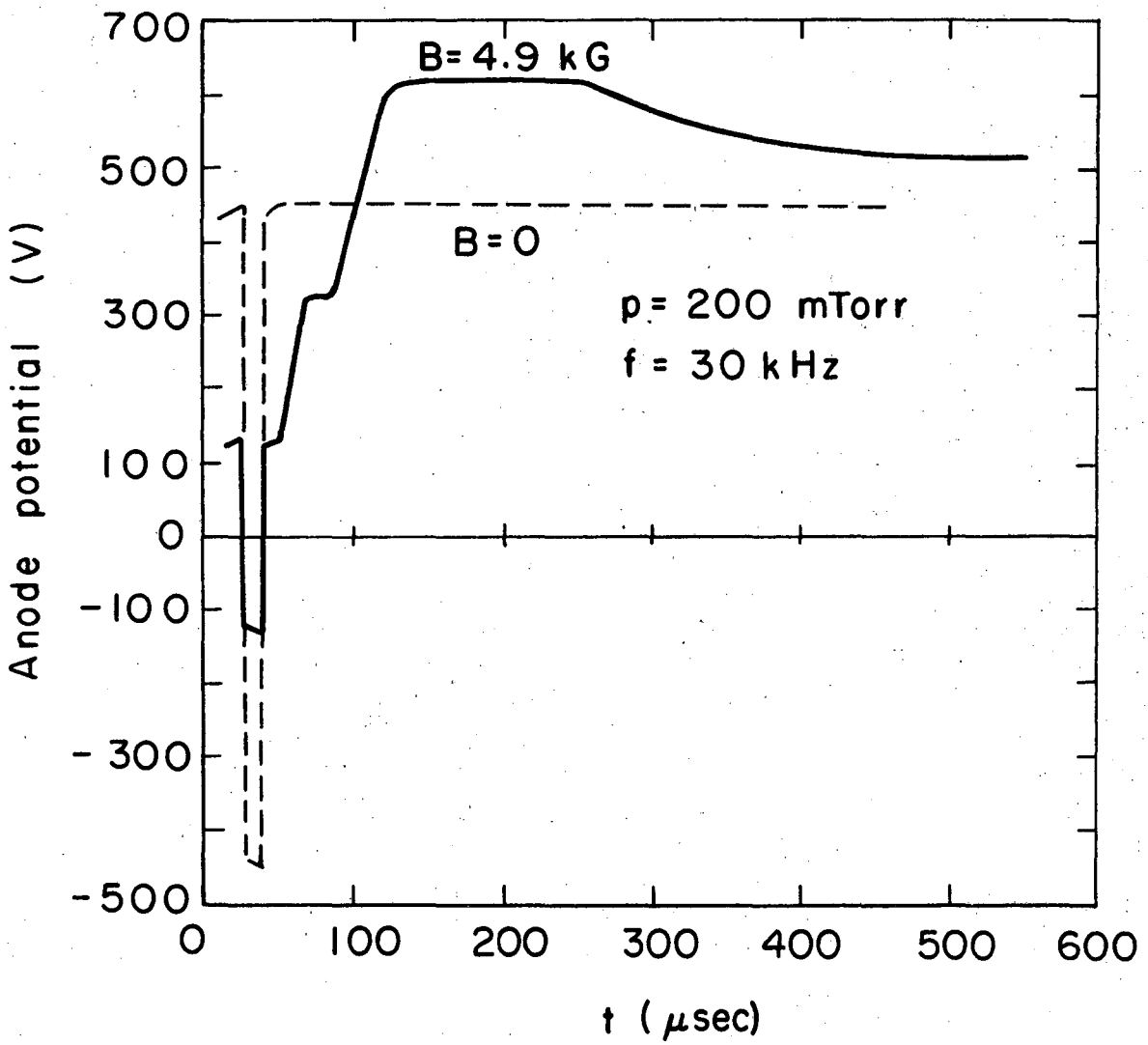

Fig. 43. Tube voltage vs time during transition from ac to dc. p = 200 mTorr, f = 30 kc.

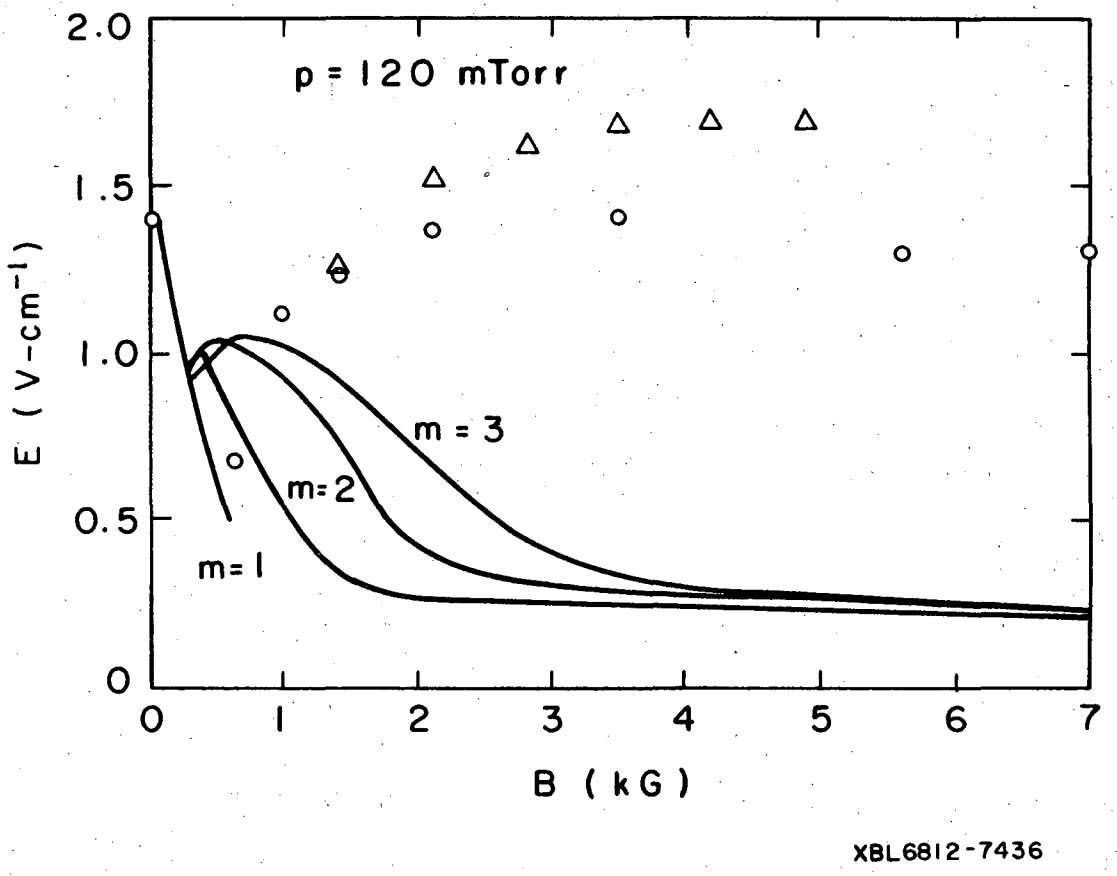

Fig. 44. Electric field vs magnetic field. p = 120 mTorr. Comparison with Kadomtsev and Nedospasov curves, Ref. 10. o, dc signal; Δ, maximum transition field.

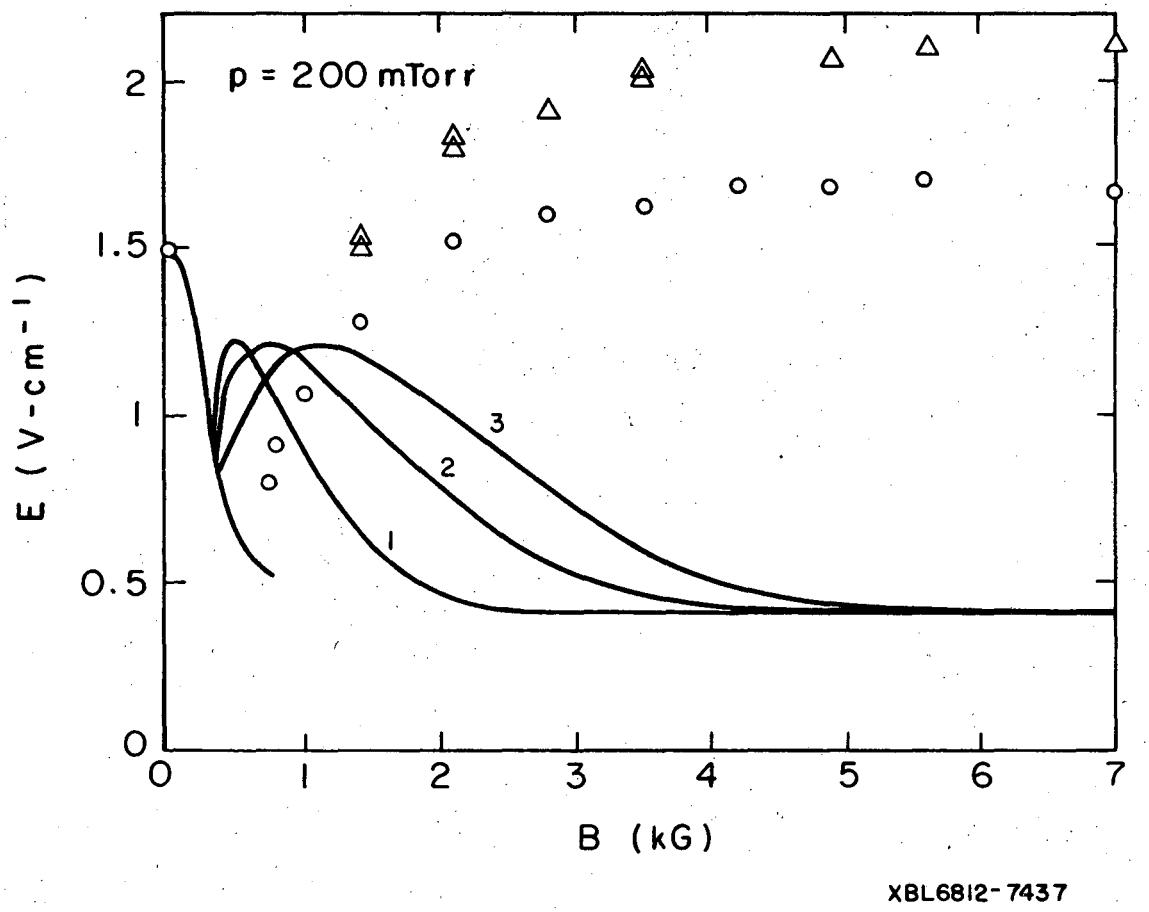

Fig. 45. Electric field vs magnetic field. p = 200 mTorr. Comparison with Kadomtsev and Nedospasov curves, Ref. 10. o, dc signal; Δ, maximum transition field.

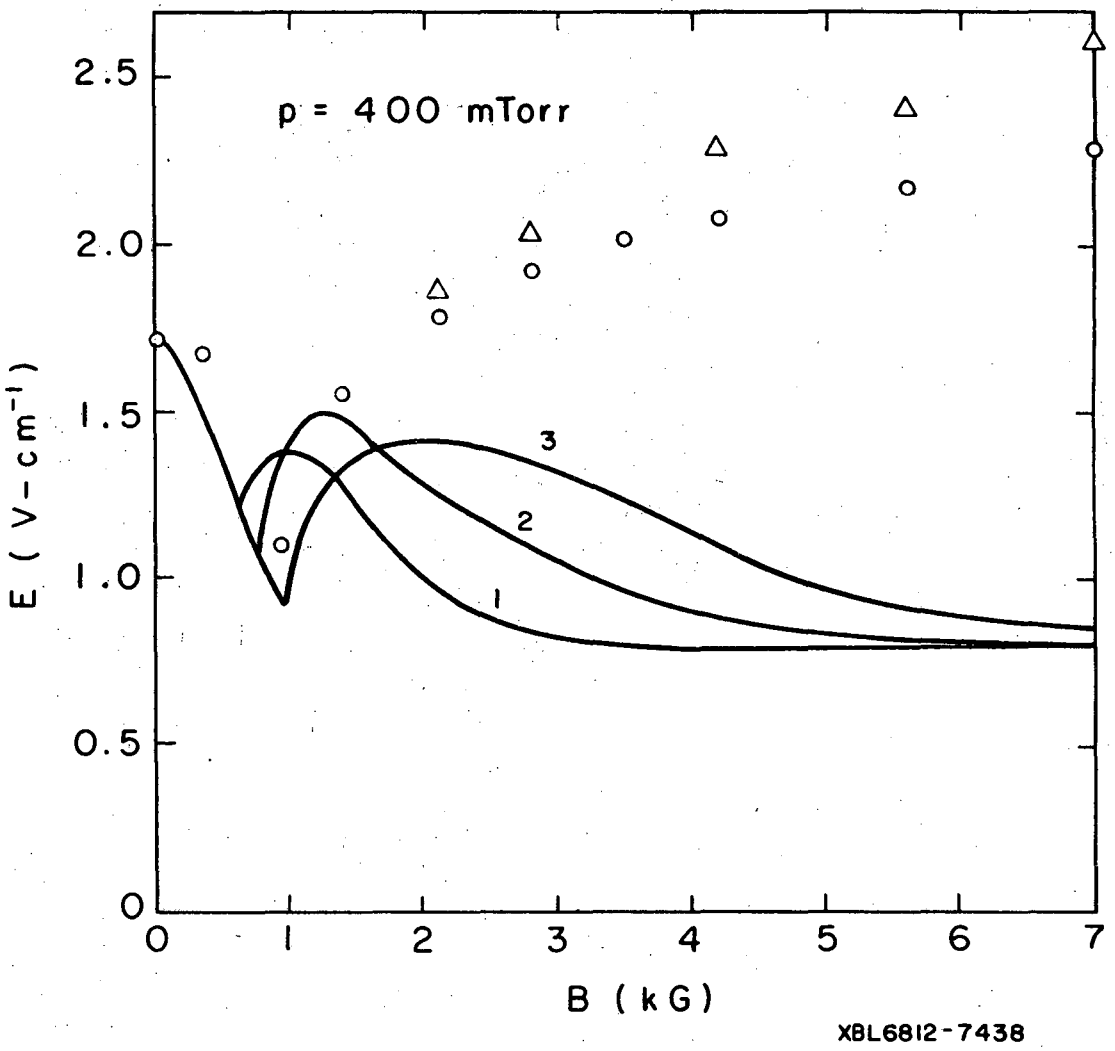

Fig. 46. Electric field vs magnetic field. p = 400 mTorr. Comparison with Kadomtsev and Nedospasov curves, Ref. 10. o, dc signal; Δ, maximum transition field.

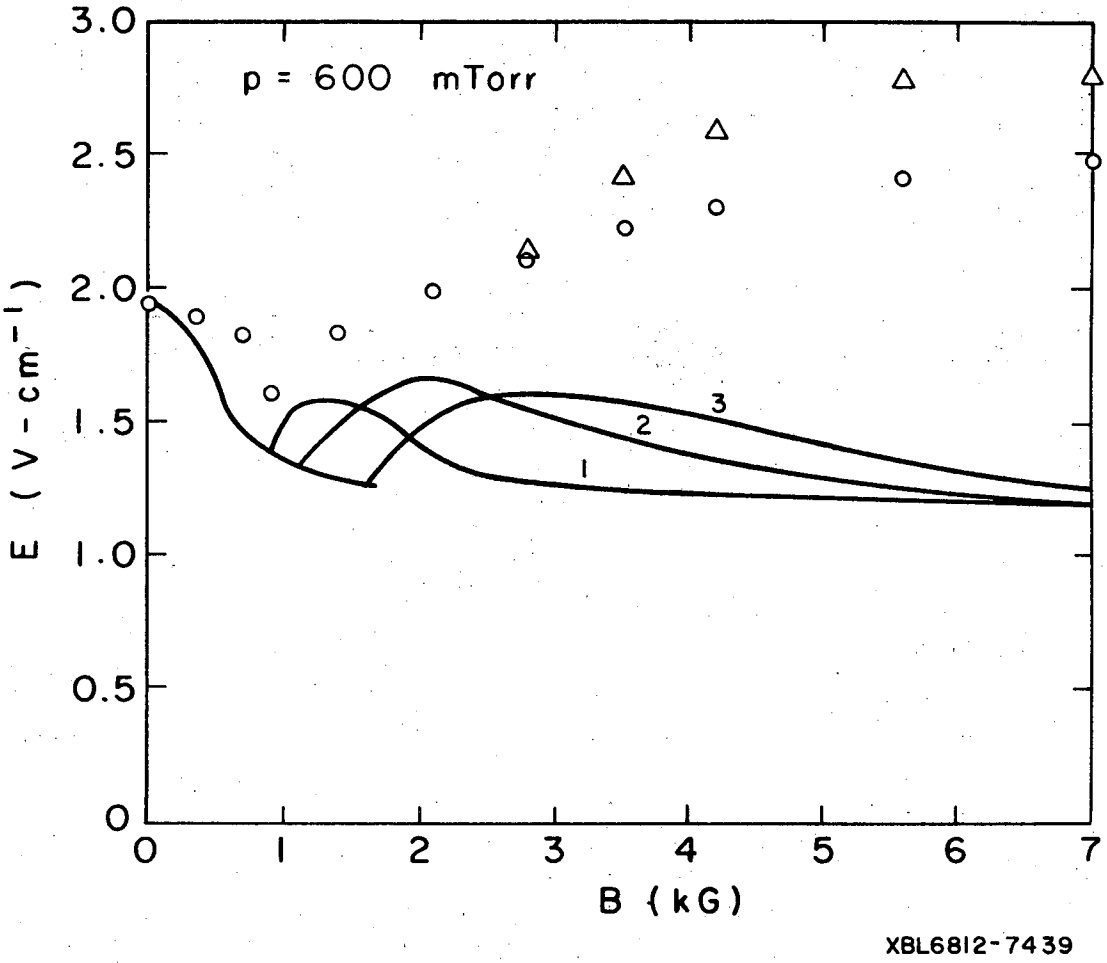

Fig. 47. Electric field vs magnetic field. p = 600 mTorr. Comparison with Kadomtsev and Nedospasov curves, Ref. 10. o, dc signal; Δ, maximum transition field.

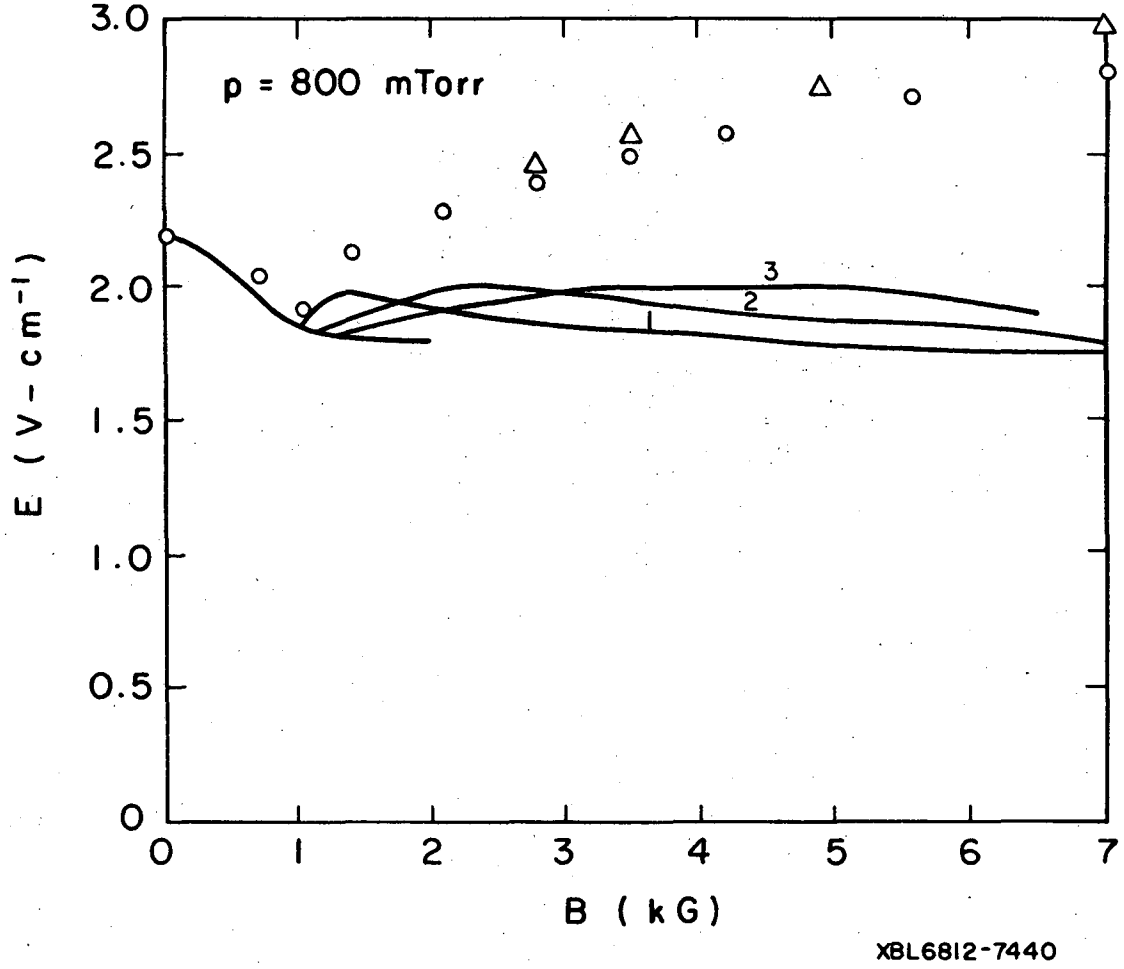

Fig. 48. Electric field vs magnetic field. p = 800 mTorr. Comparison with Kadomtsev and Nedospasov curves, Ref. 10. o, dc signal; Δ, maximum transition field.

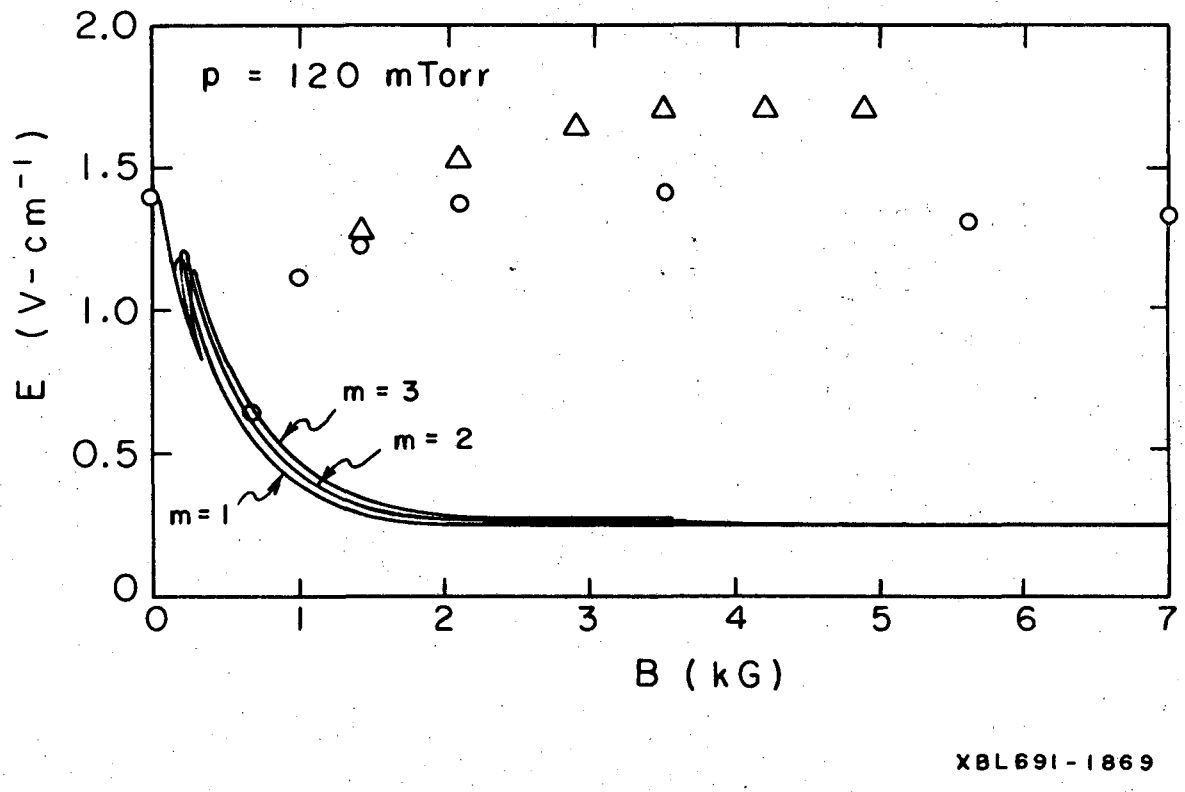

Fig. 49. Electric field vs magnetic field. p = 120 mTorr. Comparison with Johnson and Holter curves, Ref. 16. o, dc signal; Δ, maximum transition field.

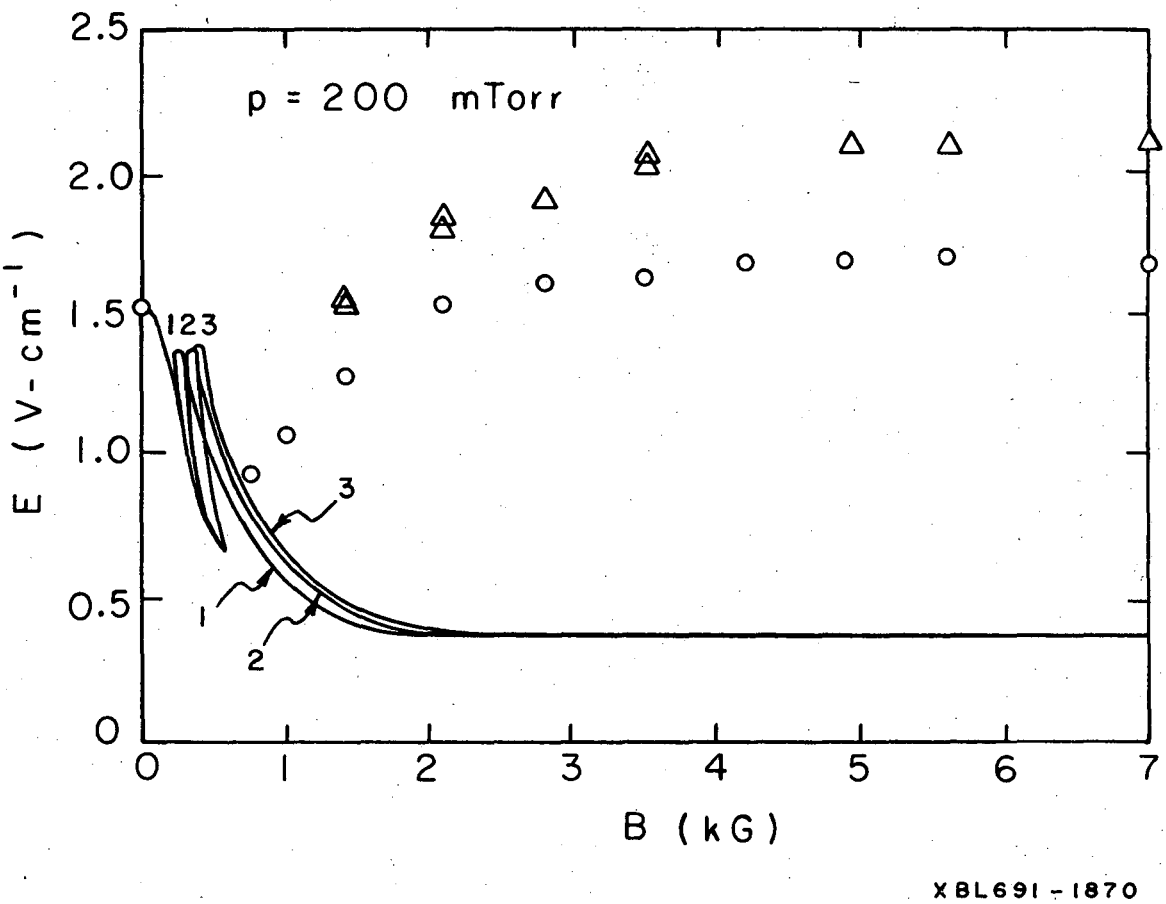

Fig. 50. Electric field vs magnetic field. p = 200 mTorr. Comparison with Johnson and Holter curves, Ref. 16. o, dc signal; Δ, maximum transition field.

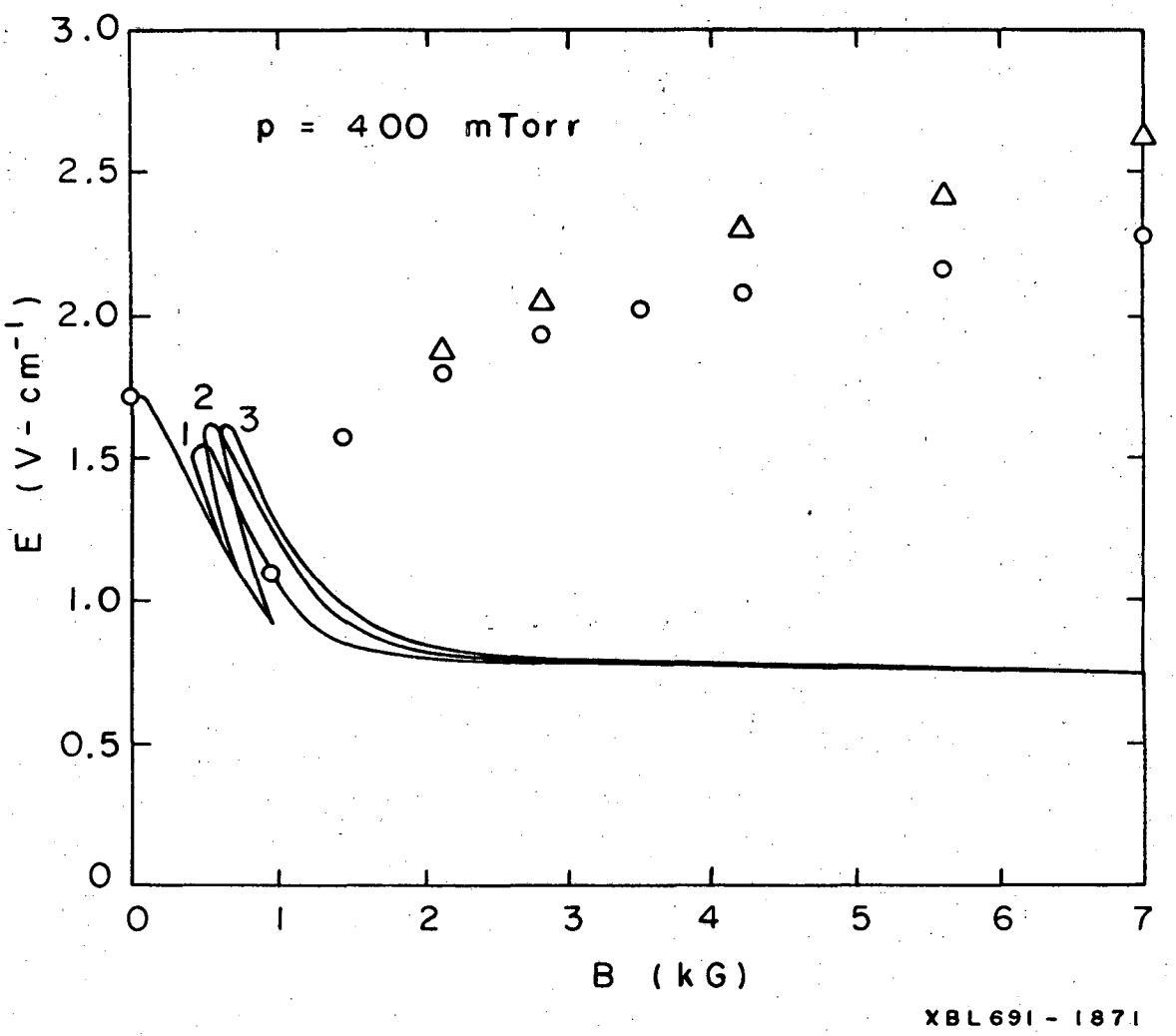

Fig. 51. Electric field vs magnetic field. p = 400 mTorr. Comparison with Johnson and Holter curves, Ref. 16. o, dc signal; Δ, maximum transition field.

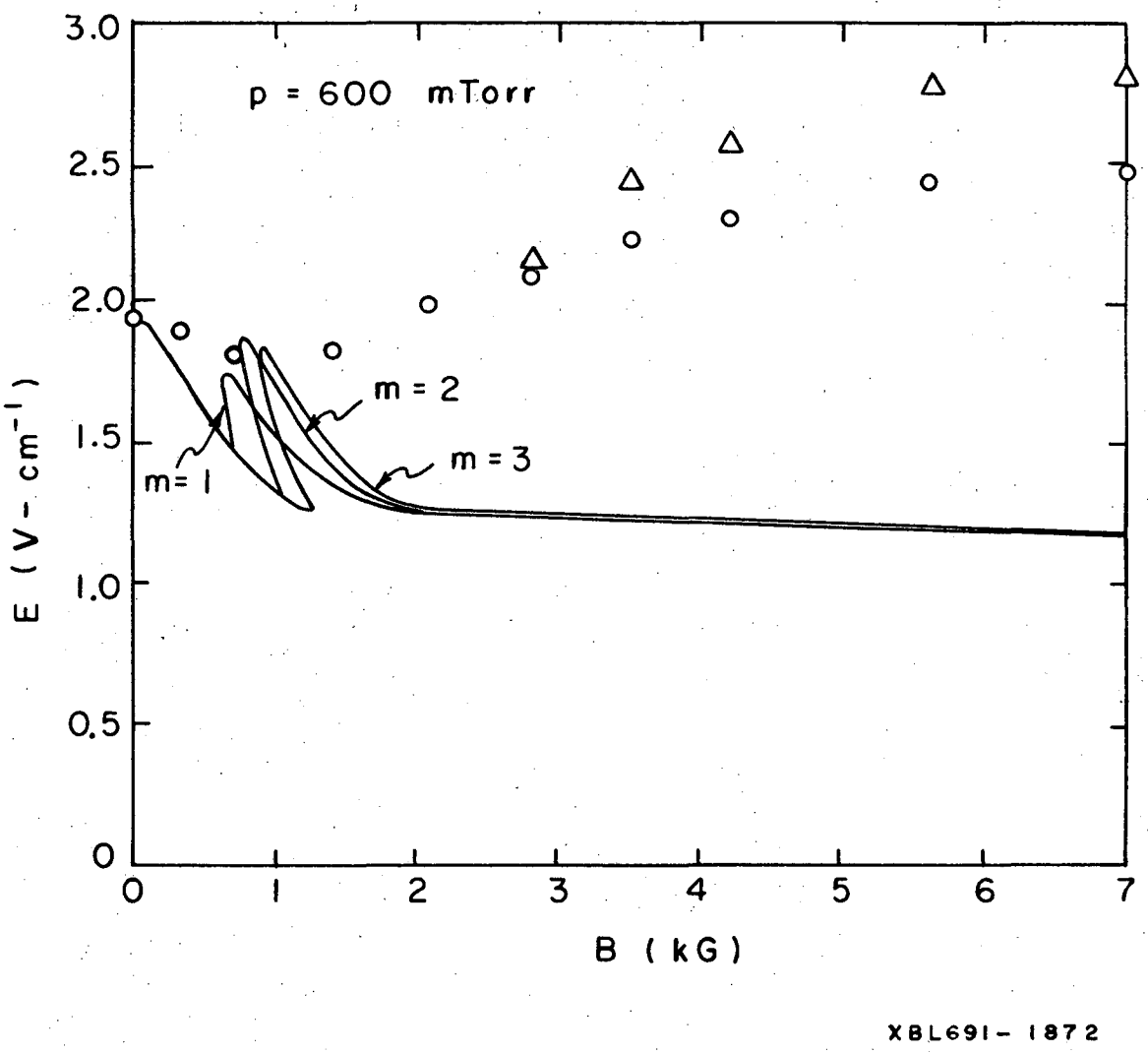

Fig. 52. Electric field vs magnetic field. p = 600 mTorr. Comparison with Johnson and Holter curves, Ref. 16. o, dc signal; Δ, maximum transition field.

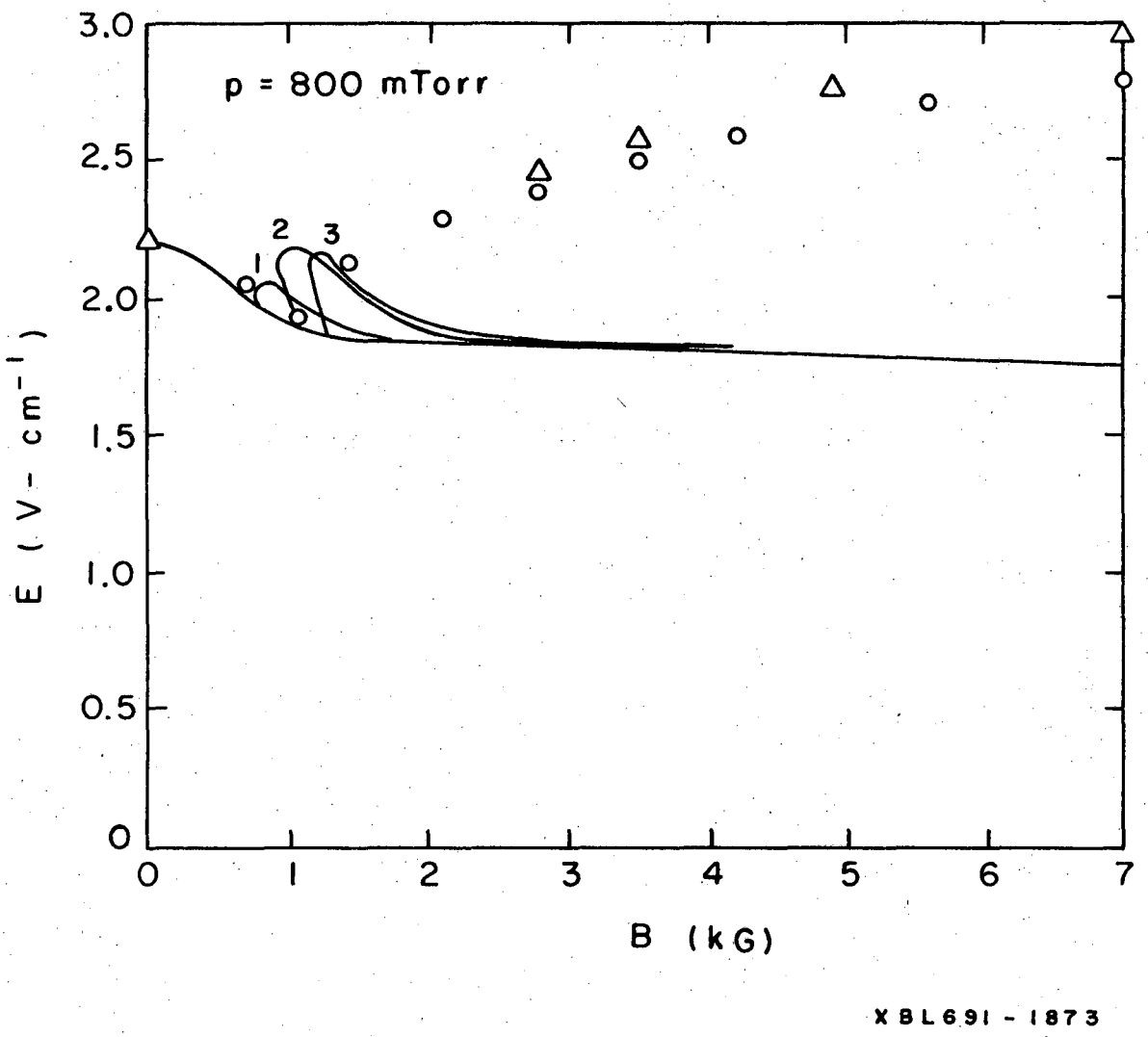

Fig. 53. Electric field vs magnetic field. p = 800 mTorr. Comparison with Johnson and Holter curves, Ref. 16. o, dc signal; Δ, maximum transition field.

range of pressures according to both experiment[41] and semi-empirical calculations using Ref. 6. Since both ϕ and the electric field are unknown in the quasi-linear equation, a last condition is necessary for the calculation of the electric field. This is determined by calculating ap^* for a given value of ϕ and comparing the value of E/p from Fig. 2 with the value from the theory. When the calculations were made no lower or higher modes were assumed to exist in the plasma. In reality, higher modes were often still present as the lower modes were growing.

Although there is qualitative agreement, the quantitative agreement between the measured and calculated dc electric fields is poor. This is a common result in dc plasma experiments in the positive column. Better agreement is found between (a) the measured increase in E during transition over the final value and (b) the differential increase in electric field calculated for higher modes over that calculated for m = 1.

The disagreement between the measured and calculated values of E may be explained by the approach used in Sheffield's paper.[15] His use of a density profile which was allowed to differ from zero at the wall and a nonzero growth rate reflecting the presence of an oscillation that is not stable, produced reasonably good agreement between predicted and measured values of ω and k.

In Figs. 45 through 57 growth rates calculated according to Ref. 41 are compared with the inverse of the time to reach the peak in electric field and the time to reach the final dc condition. The rise

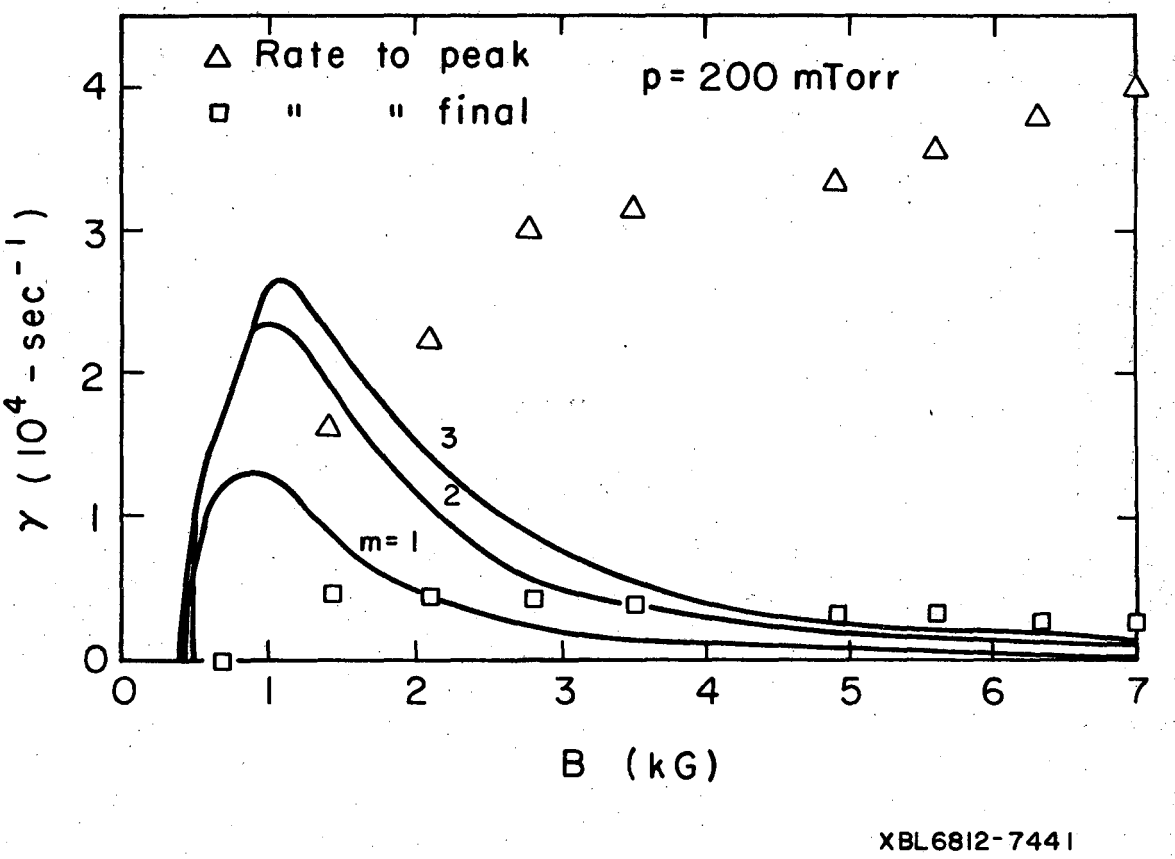

Fig. 54. Growth rate vs magnetic field: Kadomtsev and Nedospasov curves, Ref. 10. p = 200 mTorr. Δ, growth from transition to peak; □, growth from transition to final value.

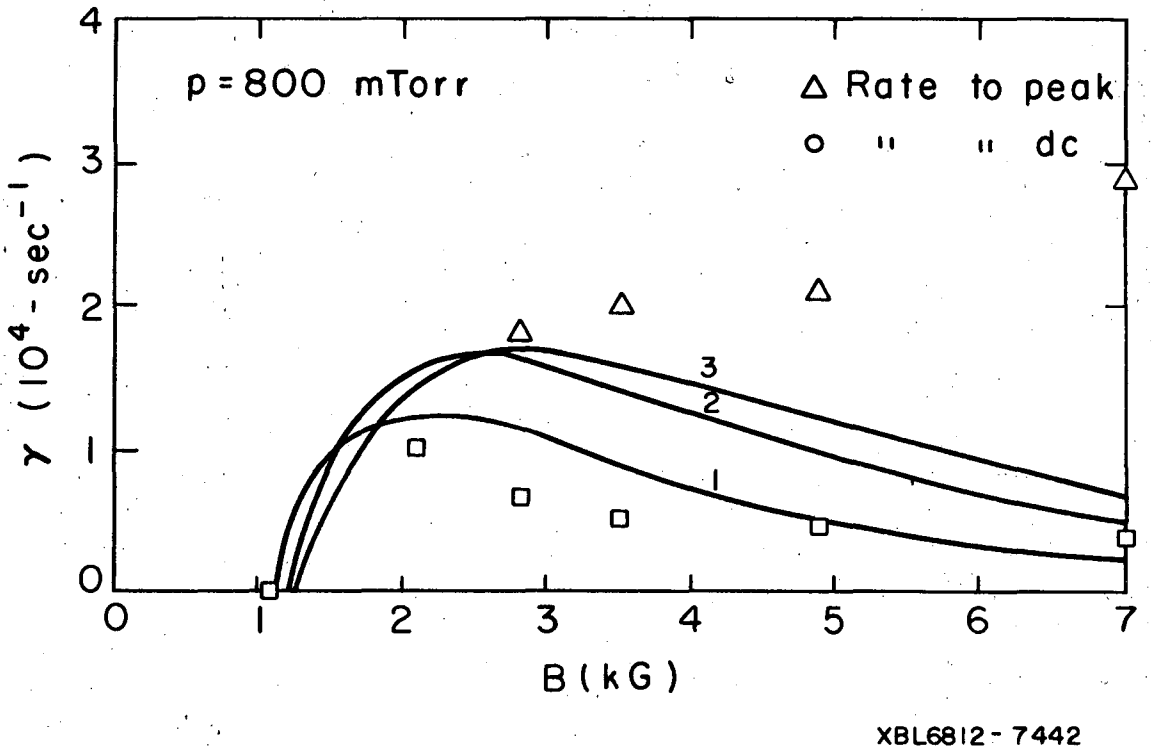

Fig. 55. Growth rate vs magnetic field: Kadomtsev and Nedospasov curves, Ref 10. p = 800 mTorr. Δ, growth from transition to peak; □, growth from transition to final value.

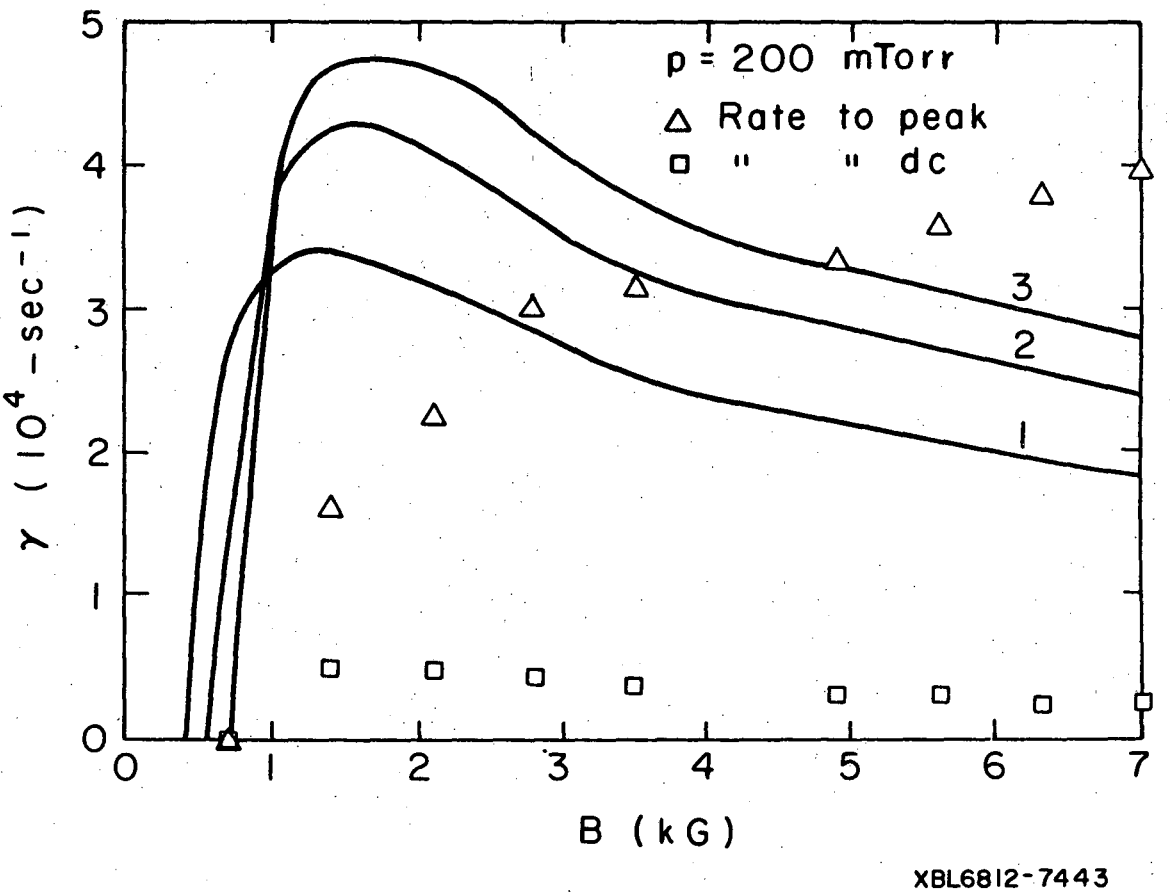

Fig. 56. Growth rate vs magnetic field: Johnson and Jerde curves, Ref. 30. p = 200 mTorr. Δ, growth from transition to peak; □, growth from transition to final value.

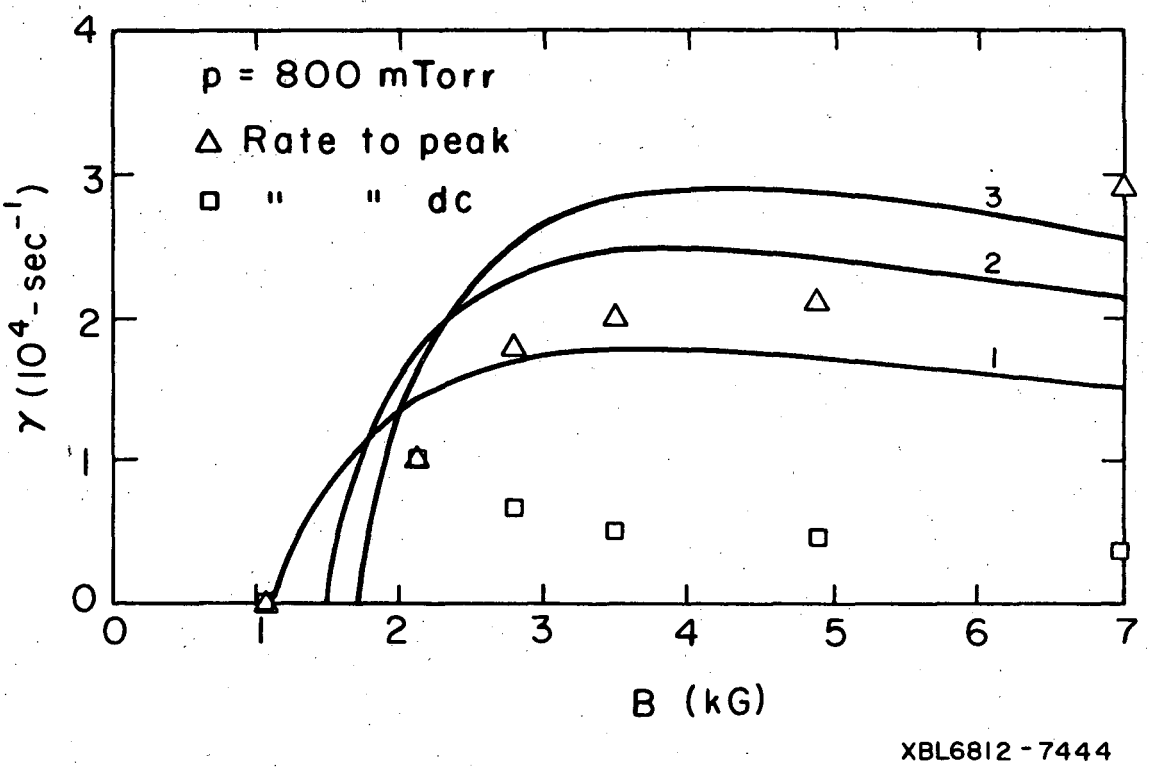

Fig. 57. Growth rate vs magnetic field: Johnson and Jerde curves, Ref. 30. p = 800 mTorr. Δ, growth from transition to peak; □, growth from transition to final value.

time should correspond to the highest mode in the plasma. The longer time should match the growth rate for the m = 1 mode. The calculations come from Kadomtsev's linear theory and from Johnson and Jerde's improvement on that theory.

F. Density Fluctuations in a Transitional Plasma

In order to classify the modes present in the transitional plasma, a frequency analysis of double Langmuir probe signals was made for the few hundred microseconds when the state of the plasma was changing. Because of the rapid growth and decay of the higher modes, only the first few modes could be observed by analyzing the saturated ion-current signals. The pressure and magnetic field ranges of observation were limited because of the interference between the modes when B was greater than 5 kG or p was greater than 200 mTorr.

Photographs of the probe current during the period spanning the alternating, transitional, and direct current portions of the discharge were taken with a 35-mm camera. The record on the film was then reduced by a system of lenses and electronics to computerized information which could be analyzed. Two sample photographs of the probe current during two different runs with the same plasma parameters are shown in Figs. 58 and 59.

The time correlations and power spectra of these curves, taken from computer curves, are shown in Figs. 58 through 60. The general theory on which the computer program was based can be found in Ref. 43. Use of the time autocovariance reduced the error introduced by the limited periods of any mode that were available on any one photograph.

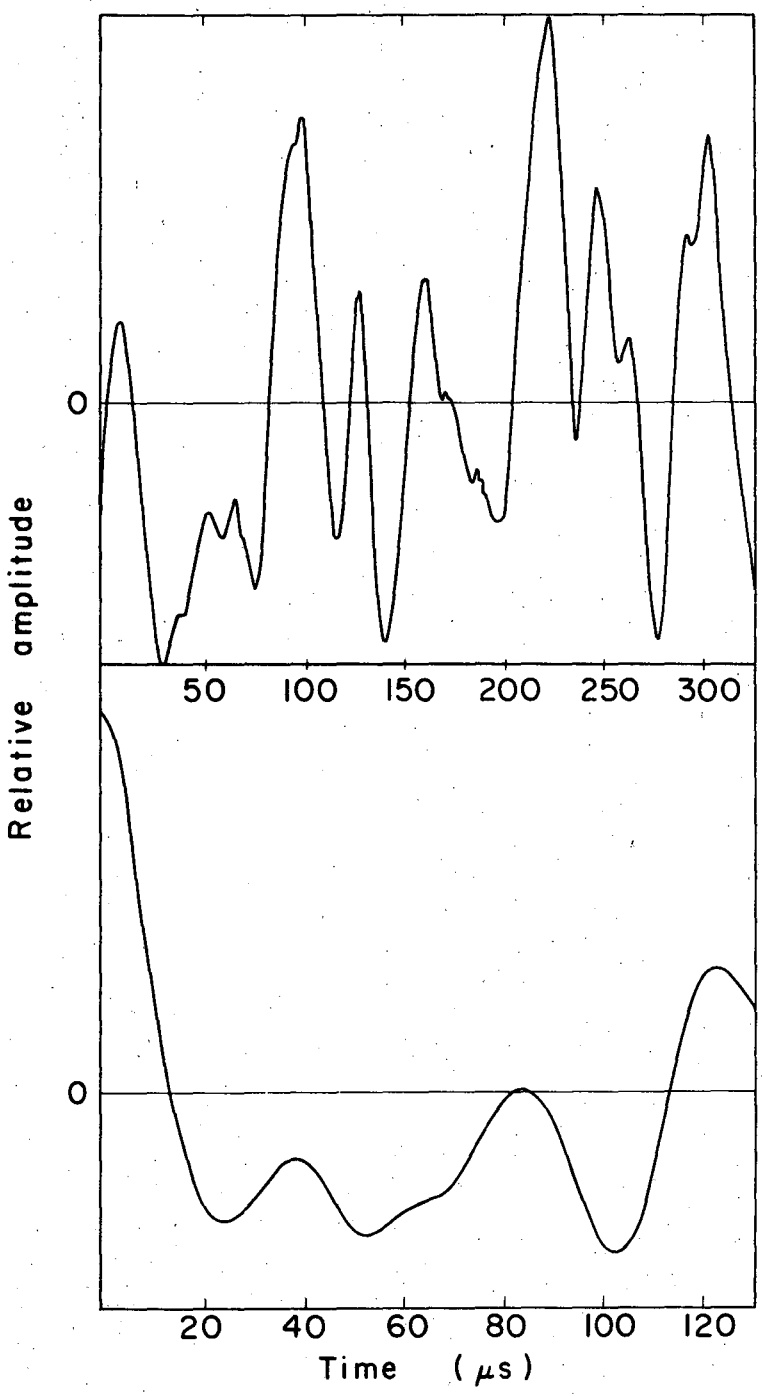

Fig. 58. The fluctuations in ion density (top) and the autocorrelation of the fluctuations (bottom) during the transition from an ac to a dc plasma. B = 4.2 kG; p = 200 mTorr.

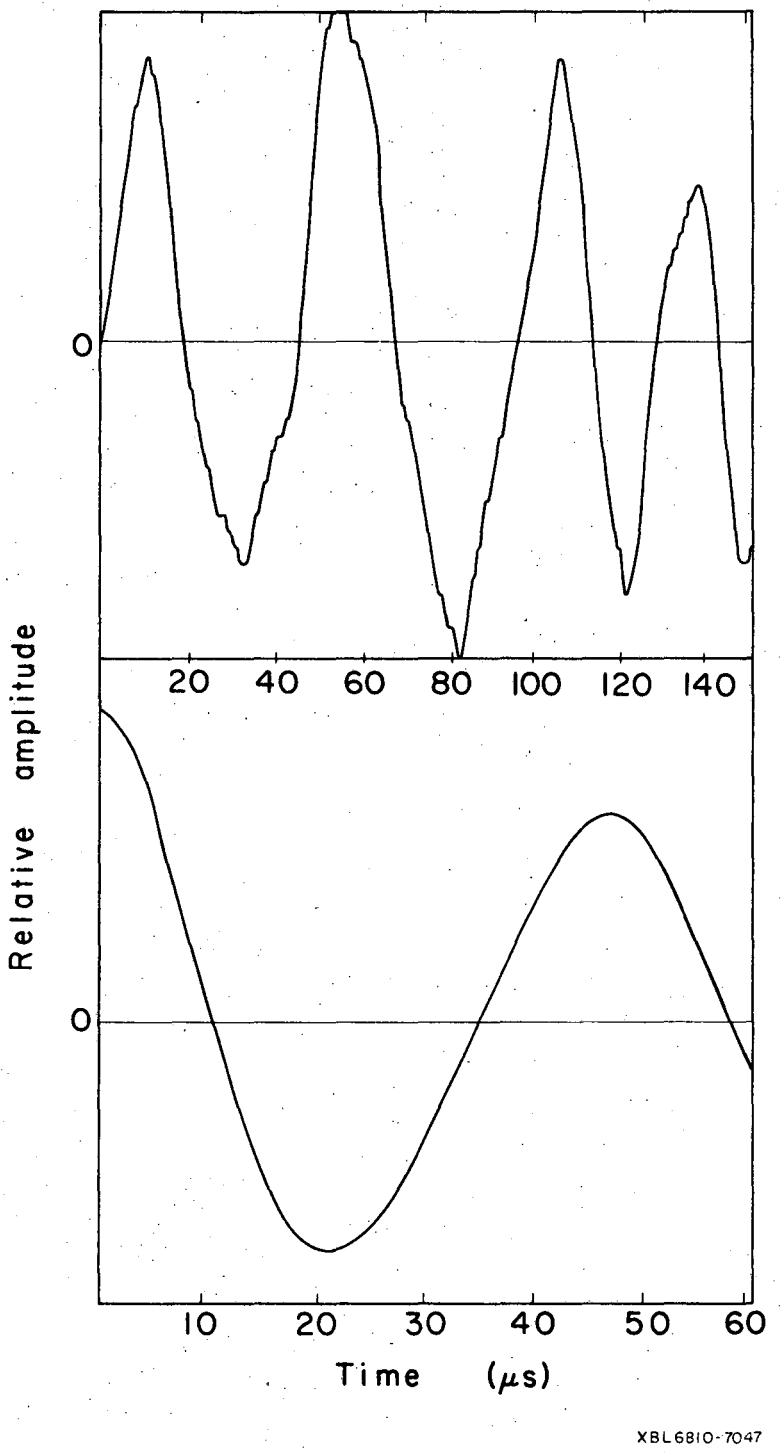

Fig. 59. Plots of fluctuations in ion density (top) and their autocorrelation (bottom) for another trial at the same conditions as Fig. 58.

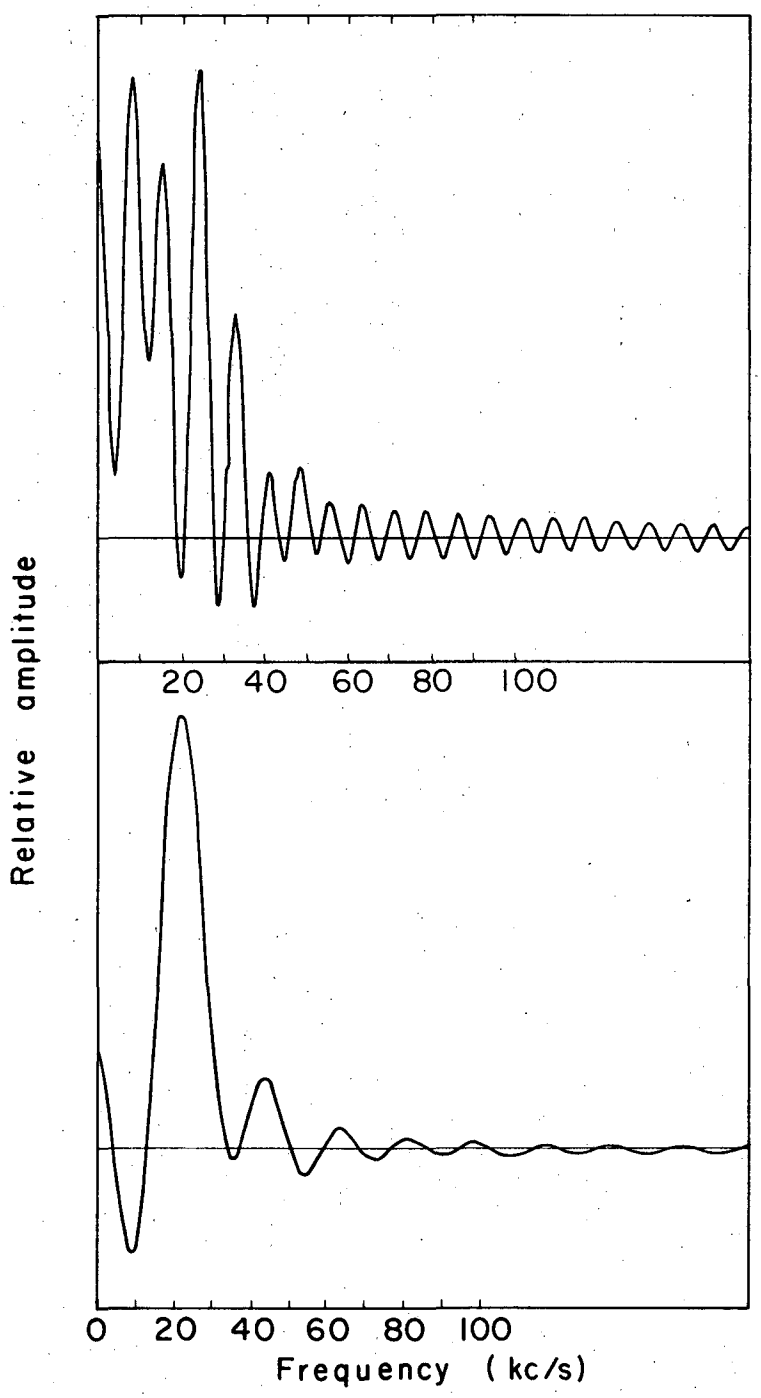

Fig. 60. Power spectrum of the fluctuations in Fig. 58 (top) and Fig. 59 (bottom). B = 4.2 kG; p = 200 mTorr.

The presence of other modes in the signal and the shortness of the record resulted in some shifting of the spectral maxima and also produced extraneous secondary maxima. As a result, only those secondary maxima which had amplitudes of greater than 50% of the dominant peak were included in the data recorded in the figures.

Figures 61 and 62 show the spectral peaks as a function of field. Frequencies calculated by using the theory of Holter and Johnson and experimentally measured electric fields are also shown. Data taken with a spectrum analyzer and data taken from computer analysis of photographs, both for a dc plasma, are included for comparison.

Ion saturation currents measured on four radial fixed probes located 90 deg from each other at the same radial and axial positions are shown in Fig. 63. They were taken in the transitional plasma to aid in mode-number identification. If a mode is correlated with itself over a cross section of the plasma, the phase relation should appear in the figure. Although there are some time segments when all the signals appear to be out of phase by 180 deg, indicating the m = 2 mode, the general phase relationship appears to be random. Apparently too many other modes intrude into the picture, and the dominant mode at one azimuthal location may not have achieved full amplitude elsewhere.

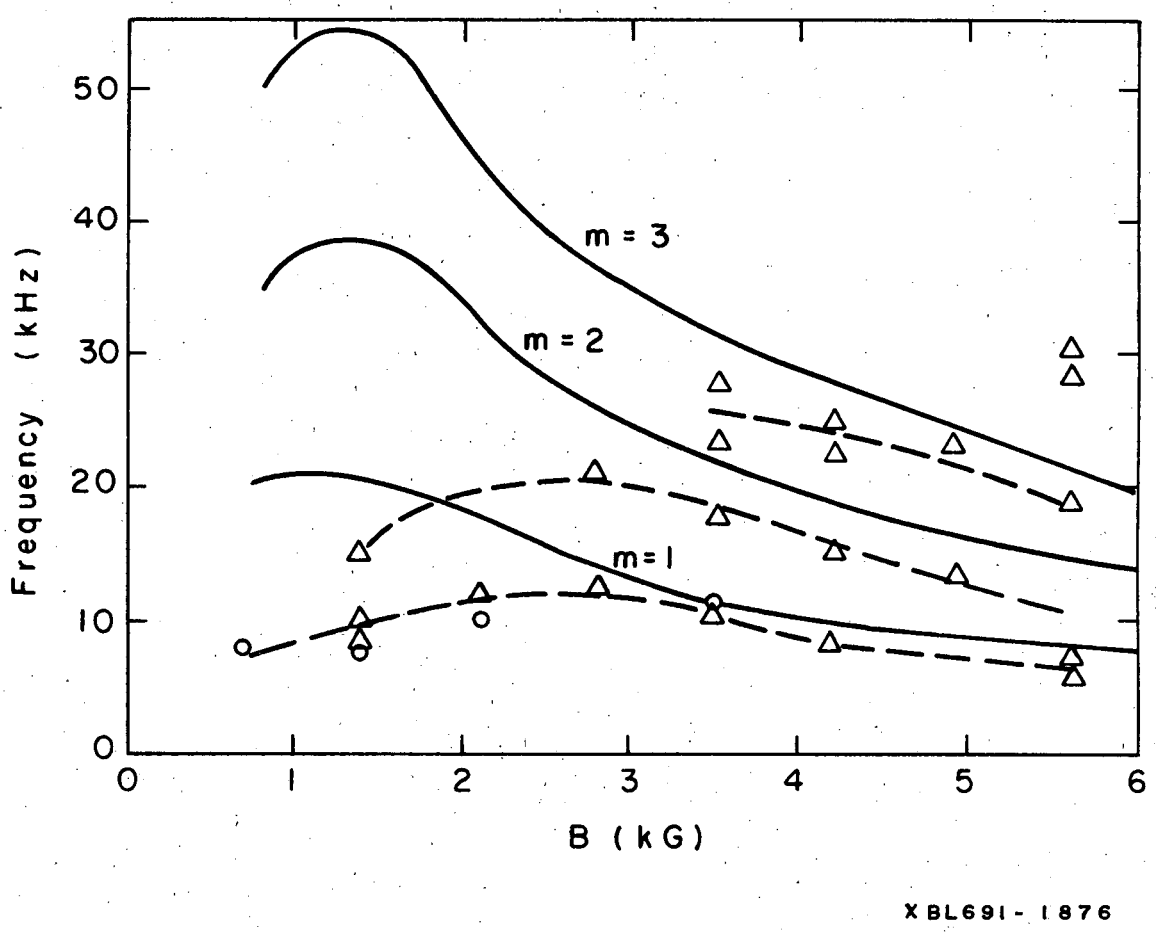

Fig. 61. Oscillation frequency vs magnetic field. Comparison with Holter and Johnson curves, Ref. 16. p = 200 mTorr. o, frequencies measured at final dc conditions; Δ, frequencies measured during transition (– – – drawn to fit data).

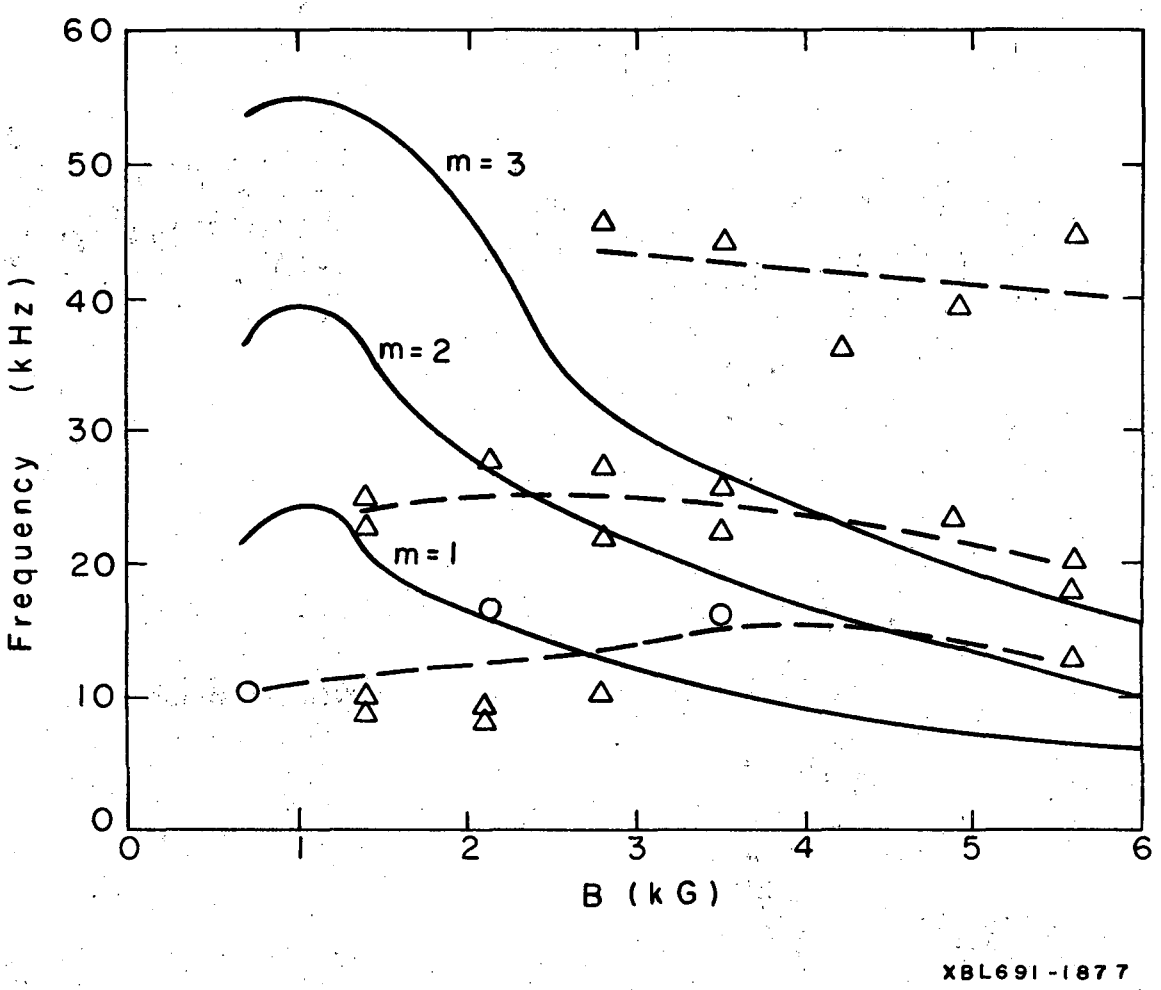

Fig. 62. Oscillation frequency vs magnetic field. Comparison with Holter and Johnson curves, Ref. 16. p = 120 mTorr. o, frequencies measured at final dc conditions; Δ, frequencies measured during transition (– – – drawn to fit data).

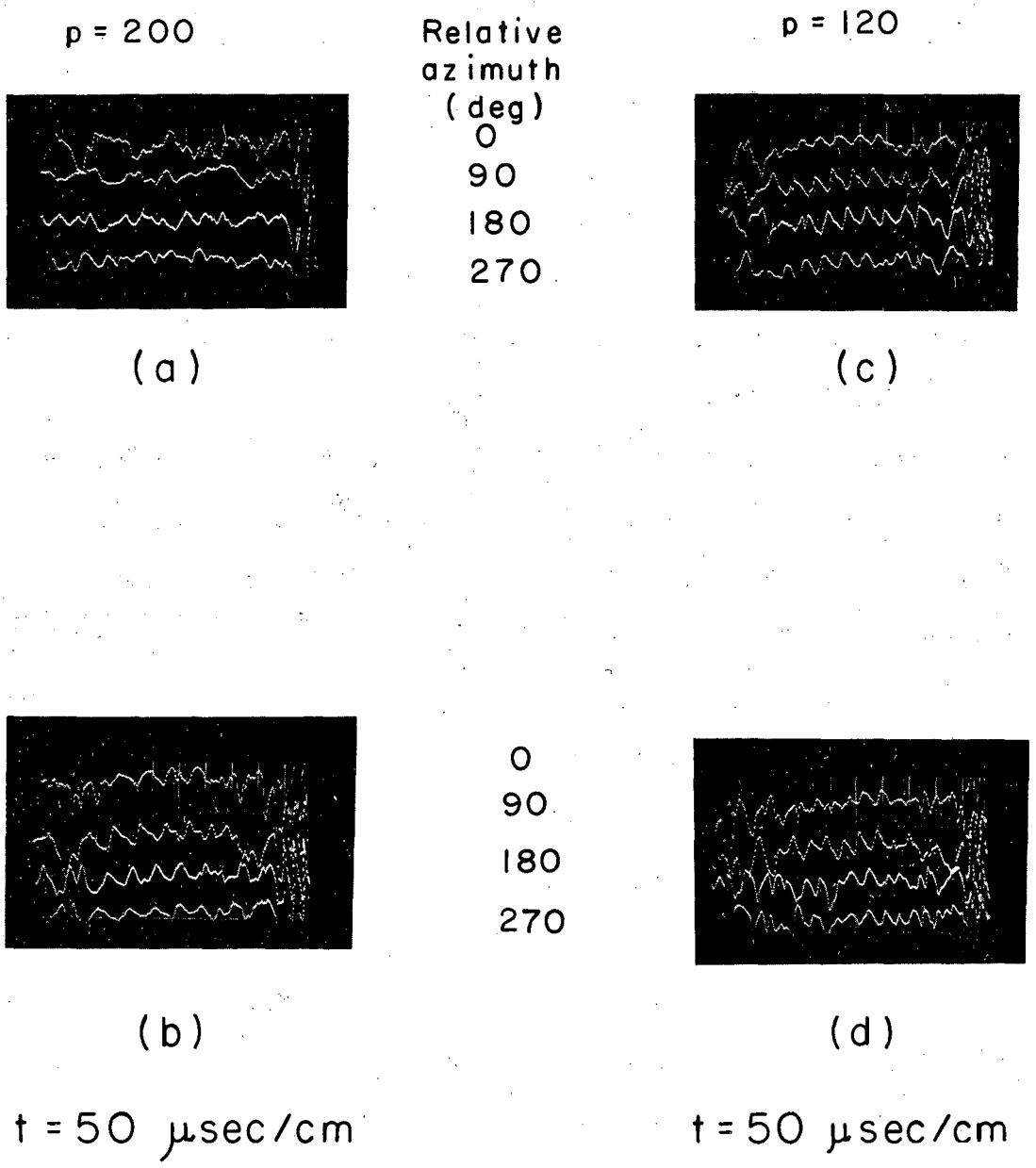

Fig. 63. Relative ion current received during transition on four equally spaced azimuthal probes. (a) B = 2.1 kG; (b) B = 4.2 kG; (c) B = 2.8 kG; (d) B = 4.2 kG.

V. DISCUSSION OF RESULTS

The results of the dc measurements show that the oscillations in the positive column can be separated into two types, according to the magnetic field strength.

The first type is the well-documented helical wave. At the critical field, this is predicted by Kadomtsev and others to be a wave with a discrete frequency and wavelength. The predicted values, as calculated by Johnson and Jerde, of these two quantities agree well with the results in Table II and Figs. 36 through 40. The critical magnetic field is larger by as much as a factor 3 than the values derived from either Kadomtsev and Nedospasov's theory or that of Johnson and Jerde, as are the fields reported in other papers.[15,34]

At higher magnetic fields than B_c, a spread in the spectra occurs, but one frequency still dominates the spectral curve. The radial correlations demonstrate the presence of a helical mode in the plasma. The frequencies and wavelengths in this intermediate region (up to 15 B_c) show rough agreement with the semi-empirical theory of Sheffield. Just as Sheffield in his paper has observed, we find that the density profile is flat in comparison with the profile measured at B = 0. In fact, all the data taken in the quasi-linear region agree with the measurements taken by Sheffield, if allowance is made for the difference in tube radius. As in other experiments, the electric field here differs quantitatively from theoretical predictions. It shows a slow rise as a function of B, and the value of E may be five times the theoretical value.

Since the theory of Kadomtsev and Nedospasov was written only for small amplitudes, it should not be expected to work for a magnetic field more than 10% above the critical field. Apparently, the quasi-linear theory of Holter and Johnson is also adequate only for oscillations of smaller amplitude than those present here, since it does not fit the experiment either.

Particle transport in a tubulent system is described by Eq. (II-22). The general form of the production term is $q_p = 1/\rho \int_0^\rho n(r)z\ r\ dr$, which, of course, must equal $q(\rho)$ theoretically. Because of the good fit between the theoretical and experimental density profiles, and the reasonably good agreement between measured and calculated mixing lengths, $q(\rho) \approx q_p(\rho)$ experimentally. Nowhere is there a term specifically dependent on the magnetic field, implying that, for a given gas, tube, and pressure the electric field and mixing length remains constant. The experimental value of E is essentially constant above 7 kG for every pressure at which measurements were made. The frequency spectrum seems to saturate, along with the electric field, at 10 B_c, as seen in Fig. 19. The radial correlation, however, shows signs of the m = 1 helix at all fields, although its contribution to the correlation steadily decreases above 7 kG as the field is raised (Figs. 27, 28).

Production terms q_p can be calculated without a detailed knowledge of the density profile by using the relationship between the axial current and the average density, $I = 2\pi\mu_- E\int_0^a r\ n(r)dr$. The production term can be written as $q_p(a) = IZ/2\pi ea\mu_- E$. As examples of the particle flux at the wall (which must equal the production term)

values were calculated at B = 3.5 kG and 12 kG. Equation (II-5) was used for Z, with T_- calculated from the experimental curve in Ref. 6. The flux rose from $4.8 \times 10^{14}/cm^2$-sec to $6.2 \times 10^{14}/cm^2$-sec when the plasma changed from the quasi-linear (B = 3.5 kG) to the turbulent (B = 12 kG) regime.

From the transitional plasma data taken at intermediate magnetic field, comparison can be made with a higher-mode extension of the Holter and Johnson theory, in which only the development of the higher mode is considered. Again, the frequencies are in much better agreement with the theoretical calculations than are the electric fields. The calculated increase in electric field for the higher modes also agrees with the hypothesis that the growth of such higher modes is respondible for the temporary increase in the observed electric field during transition. Signals from the four azimuthal probes provide some indication that an m = 2 mode was produced for a short time. The inconsistency of frequency in these signals suggests phase instability resulting from the many competing modes in the plasma. This in turn suggests that such competition can exist in the dc plasma, which can lead to turbulence if there are a sufficient number of modes.

The fit with the calculations made from the turbulence theory of Kadomtsev of the measured radial density proviles and correlation lengths provides definite evidence of the presence of the second, turbulent type of oscillation when B is 12 kG. Previous evidence of turbulence in the positive column consists of the radial density profile measured by Nedospasov and Artsimovich[36] when B was eight times the critical field.

The correlation measurements made here at 12 kG disagree with the results of Wöhler.[14] In that paper, for a comparable ratio of B to the critical field, the correlation length was found to be four or five times as large as measured here. Density profiles measured by Wöhler were very flat. However, his probes were straight, rather than bent toward the cathode, and Fig. 34 illustrates the effects of this type of probe on the radial correlation. The interference of the probe stems is sufficient to make the correlation many times the value determined by probes whose tips extended toward the cathode several centimeters from their support.

Another study of turbulence in the positive column by Nedospasov and Sobolev[44] yields frequency spectra which agree with the results of Sheffield. Their use of an enlargement at the cathode end of the tube has prevented the tube walls from charging positively near the cathode.[34] When there is a high axial field applied, the electrons are focused along the axis as they enter the field region, and radial transport cannot completely compensate for this end effect until the particles have traveled several centimeters along the axis. Increasing the tube diameter at the entrance region increases the size of the cylinder into which the electrons are swept. The enlargement used in Ref. 44 was found to be sufficient to make the electron cylinder the same size as the column diameter inside the field. Potential fluctuation correlations, made at the maximum ratio of B to B_c of 10, between a probe at the wall and a radial probe 7.5 mm from the wall, indicate the presence of an oscillation which has a frequency near

the frequency of the second helical mode in the tube with enlargement.

The radial cross-correlation in space and time is lower in the tube without an enlargement, and the peak is displaced slightly in time in comparison with the signal from the tube with enlargement. Apparently, the authors have succeeded in inhibiting the m = 0 mode and have observed a new oscillation which may be a higher mode of the helical instability or another type of azimuthally symmetric drift wave. Because of the different type of radial correlation and the lower value of B/B_c those results are not directly comparable with this experiment.

VI. SUMMARY AND CONCLUSIONS

The result of applying a magnetic field with a value greater than 15 times the critical field to a positive column is shown to be the production of a turbulent plasma with parameters which compared closely with the predictions from Kadomtsev's theory[26] of turbulence in the positive column. Transport is dominated by the radial convection of charged particles under the influence of random oscillations of the electric field in accordance with this theory. For fields with lower values, convection caused by the helical instability rather than turbulent convection appears to be the dominant transport mechanism, in agreement with other experiments. The parameters such as electric field and wavelength that are measured in this quasi-linear region do not compare well with the results predicted for this instability by Kadomtsev and Nedospasov.[10]

Considering the apparent dominance of the first helical mode at fields up to 7 kG, where one would expect other modes to be present, it is not possible to say unequivocally that the turbulence observed was a result of the presence of many competitive helical modes unless the data (correlation lengths, etc.) at 12 kG fit a theory such as that of Kadomtsev[26] which relies upon the presence of these modes. Experiments have established that higher modes grow in but are unstable when the plasma makes a transition from a steady state to a helically unstable column. It is possible--and the ac-dc experiments provide some indication of this--that higher modes do grow in the positive column at fields as low as 2 kG, in agreement with theoretical pre-

dictions, but then are destroyed, resulting in a power spectrum which is centered about the first mode. The work of Sheffield[15] indicates that the first mode becomes a relaxation oscillation at 5 B_c but that the new wave is nearly in phase with the old. In comparison, higher modes upon rebirth may be unrelated to their previous forms. This would account for their lack of effect upon the power spectrum and radial correlation, which are averaged quantities that are measured over many cycles of the oscillations' growth and destruction.

The close fit between experimental and theoretical values of the mixing length and the density profile at very high magnetic fields shows that the Kadomtsev model of turbulence in the positive column fits the conditions of this experiment. Transport is a matter of small turbulent cells convecting radially outward with an average velocity determined by their size and growth rate. A better description of transport, however, should include the effects of inhomogeneous turbulence at the boundary. Such an analysis would avoid the need to invent an extrapolation-length boundary condition such as that used by Kadomtsev. The work of Nedospasov and Sobolev[44] in the quasi-linear region suggests that it would also be worthwhile to suppress the entrance effects of the magnetic field at the cathode end and study the effects upon oscillations at all values of the magnetic field.

In the quasi-linear region, agreement between theoretical and experimental transport rates is not so good. The theories which are not empirical[10,16] yield electric fields and density profiles which

do not agree well with experiment except near the critical field. Reasonable comparison with experimental values of the frequency is obtained for the helical modes if experimental values of the electric field are used in the theory of Holter and Johnson. Experimental density profiles as well as electric field values are needed in the semi-empirical theory of Sheffield[15] in order to obtain agreement between experimental and theoretical values of the wavelength of the first mode. If the equivalence of the transport and production rates is considered, then one can make good estimates of the transport rate at the wall if one knows the electric field. Above $4\ B_c$ the electric field has essentially saturated at a value slightly larger than the value without an applied axial magnetic field, and, consequently, the transport rates have also ceased to depend upon B.

ACKNOWLEDGMENTS

I am especially grateful to Dr. Robert V. Pyle for his encouragement and guidance throughout the course of this work. I am grateful to Vincent J. Honey and Donald B. Hopkins for the design and construction of much of the electronic equipment used in this experiment; to Dr. Wulf B. Kunkel, Dr. Roy R. Johnson, and Dr. Laird Warren for valuable discussions of the theory and experiment, and to Dr. C. M. Van Atta for his support of this research. The skill and dedication of Harry Powell's glass shop, especially Ione Maxwell, and the mechanical shops of Louis Biagi and Harland Hughes were essential to the success of this work. The CDC 6600 programs were written or rewritten by Edna Williams and Esther Schroeder.

This research was performed under the auspices of the U. S. Atomic Energy Commission and, in part, under the tenure of a Nuclear Science and Engineering fellowship granted by the AEC.

REFERENCES

1. David J. Rose and Melville Clark, Jr., Plasmas and Controlled Fusion (The MIT Press, Massachusetts Institute of Technology, and J. Wiley and Sons, New York, 1961).

2. Sanford C. Brown, Basic Data of Plasma Physics (The MIT Press, Massachusetts Institute of Technology, and J. Wiley and Sons, New York, 1959).

3. S. V. Pashkin and I. Ya. Shipuk, Dokl. Akad. Nauk SSSR 176, 1278 (1967) (Russian).

4. K. W. Gentle, Phys. Fluids 9, 2212 (1966).

5. K. Takayama, H. Ikezi, and S. Miyake, A Discharge Tube Having Quiescent Positive Column, in Proceedings of the 8th Int. Conf. on Phenomena in Ionized Gases, Vienna, 1967 (Springer-Verlag, Vienna, 1967), p. 553.

6. R. J. Bickerton and A. von Engel, Proc. Phys. Soc. (London) 69, 468 (1955).

7. F. C. Hoh and B. Lehnert, in Proceedings of the 4th Int. Conf. on Ionization Phenomena in Gases, Uppsala (North-Holland Publishing Co., Amsterdam, 1960), p. 604.

8. T. K. Allen, G. A. Paulikas, and R. V. Pyle, Phys. Rev. Letters 5, 409 (1960).

9. G. A. Paulikas and R. V. Pyle, Phys. Fluids 5, 348 (1962).

10. B. B. Kadomtsev and A. V. Nedospasov, J. Nucl. Energy, Pt. C, 1, 230 (1960).

11. F. C. Hoh, Phys. Fluids 5, 22 (1962).

12. J. Polman, Plasma Phys. 9, 471 (1967).

13. D. A. Huchital and E. H. Holt, Appl. Phys. Letters 8, 321 (1966).

14. K. Wöhler, Phys. Fluids 10, 245 (1967).

15. J. Sheffield, Phys. Fluids 11, 222 (1968).

16. Ø. Holter and R. Johnson, Phys. Fluids 8, 333 (1965).

17. B. B. Kadomtsev, Plasma Turbulence (Academic Press, New York, 1965).

18. D. Bohm, E. H. S. Burhop, H. S. W. Massey, and R. M. Williams, in The Characteristics of Electrical Discharges in Magnetic Fields, A. Guthrie and R. K. Wakerling, eds. (McGraw-Hill Book Co., Inc., New York, 1949).

19. V. L. Granatstein, S. J. Buchsbaum, and D. S. Bugnolo, Phys. Rev. Letters 16, 504 (1966).

20. A. N. Kolmogorov, Compt. Rend. Acad. Sci. USSR 30, 301 (1941); 32, 16 (1941).

21. G. K. Batchelor, The Theory of Homogeneous Turbulence (Cambridge University Press, 1953).

22. R. H. Kraichnan, Phys. Fluids 7, 1717 (1964).

23. B. B. Kadomtsev, J. Nucl. Energy, Pt. C 5, 31 (1963).

24. R. Z. Sagdeev and A. A. Galeev, Lectures on the Non-Linear Theory of Plasma, IC/66/64 (1966), International Centre for Theoretical Physics, Trieste.

25. F. C. Hoh, Onset of Turbulence in the Positive Column, Boeing Scientific Research Laboratories report D-1-82 0512.

26. B. B. Kadomtsev, Soviet Phys.-Tech. Phys. 6, 927 (1962).

27. W. Schottky, Physik. Z. 25, 635 (1924).

28. A. von Engel, Ionized Gases (Clarendon Press, Oxford, 1955).

29. F. C. Hoh, Phys. Rev. Letters 4, 559 (1960).

30. R. R. Johnson and D. A. Jerde, Phys. Fluids 5, 988 (1962).

31. F. C. Hoh, Rev. Mod. Phys. 34, 267 (1962).

32. J. W. Dettman, Mathematical Methods in Physics and Engineering (McGraw-Hill Book Co., New York, 1962).

33. B. B. Kadomtsev, Soviet Phys.-Tech. Phys. 6, 882 (1962).

34. L. L. Artsimovich and A. V. Nedospasov, Doklady 7, 717 (1963).

35. M. Sato, AERE Trans. 924 of Kaku-Yugo Kenkyu 8, 563 (1962).

36. E. O. Johnson and L. Malter, Phys. Rev. 80, 58 (1950).

37. F. F. Chen, Probe Techniques for Low-Density Plasmas, Princeton University Plasma Physics Laboratory report MATT-520, March 1967.

38. A. Simon, Phys. Rev. 98, 317 (1955).

39. D. A. Huchital and E. H. Holt, Phys. Rev. Letters 16, 677 (1966).

40. L. Prandtl, The Essentials of Fluid Dynamics (Blackie, London, 1952).

41. H. F. Rugge, Instability of an Alternating-Current Positive Column in a Magnetic Field, Ph.D. Thesis, Lawrence Radiation Laboratory report UCRL-10698, April 22, 1963.

42. H. F. Rugge and R. V. Pyle, Phys. Fluids 7, 754 (1964).

43. R. B. Blackman and J. W. Tukey, The Measurement of Power Spectra (Dover Publications, New York, 1958).

44. A. V. Nedospasov and S. S. Sobolev, Soviet Phys.-Tech. Phys. 11, 1309 (1967).

LEGAL NOTICE

TECHNICAL INFORMATION DIVISION
LAWRENCE RADIATION LABORATORY
UNIVERSITY OF CALIFORNIA
BERKELEY, CALIFORNIA 94720